DEVELOPMENT OF A TWO-PHASE MICROFLUIDIC PLATFORM FOR DRUG SCREENING

THÈSE

Présentée à l'Université de Strasbourg
Ecole Doctorale des Sciences Chimiques

Pour obtenir le grade de docteur de l'Université de Strasbourg

Par
JENIFER CLAUSELL-TORMOS

Strasbourg 2010

SOUTENUE PUBLIQUEMENT LE 18 MARS 2010 DEVANT LA COMMISSION D'EXAMEN :

Directeur de Thèse: **Prof. Andrew Griffiths**
Institut de Science et d'Ingénierie Supramoléculaire, Strasbourg, France

Rapporteur: **Prof. Josep Esteve Romero**
Universitat de la UJI, Castelló, Espagne

Examinateur: **Directeur de Recherche Roland Marquet**
Institut de Biologie Moléculaire et Cellulaire, Strasbourg, France

Rapporteur: **Prof. Andrew de Mello**
Imperial College, London, Royaume-Uni

Rapporteur: **Directeur de Recherche Jean-Louis Viovy**
Institut Curie, Paris, France

Solo se que no se nada

Je sais que je ne sais rien

I know that I know nothing

Ich weiß, daß ich nichts weiß

Socrates

Dedicat als meus pares, als meus iaios i als meus abuelos.

ABSTRACT

High-throughput cell-based assays require small sample volumes to reduce assay costs and to allow for rapid sample manipulation. However, further miniaturization of conventional microtiter plate technology is problematic due to evaporation and capillary action. To overcome these limitations, we have developed a two-phase microfluidic platform in which human cells and multicellular organisms can be cultivated for several days in aqueous microcomparments separated by an inert perfluorocarbon carrier oil. Furthermore, we focussed on the automated generation of chemically-dictinct microcompartment to exploit the technology for screening purposes. In particular, we interfaced an autosampler with our microfluidic platform sequentially loading compounds from microtiter plates into a length of tubing. All compounds are loaded in form of aqueous plugs (nanoliter volumes) separated by fluorinated oil. The resulting array of plugs can be split into multiple small volume copies which can be used as replicates for the same assay as well as for different assays. Moreover, each array of plugs can be injected into a microfluidic chip for further manipulation (such as the addition of reagents or the detection of fluorescence signals). Since the order of the compounds and thus their identity is known throughout the whole screening procedure, the system does not require direct compound labelling. Furthermore, each individual plug can be monitored over time, thus allowing the recording of kinetic data. In the last part of the work we focussed on the development of a novel assay coupling a positive fluorescence signal with the inhibition of viral transduction. This should ultimately allow the screening of antivirals in the previously developed microfluidic systems.

Table of contents

1. Introduction

1.1 Current High-Throughput Screening (HTS) technologies

High-throughput screening (HTS) is a well-established procedure for the identification of novel and relevant chemical structures with desired properties. The big progress in synthesis technologies, such as combinatorial chemistry (e.g. click chemistry) and automated synthesis, together with the development in genomics have generated a huge number of new chemical compounds as well as new targets. Hence, new technology for HTS is being boosted by the need of assessing these new molecules against a variety of existing and new targets.

The throughput corresponding to the number of assays per day, and the cost of equipment and consumables are the most critical factors for promoting the development and use of novel screening technologies. One way of improving theses critical factors is miniaturization of established assays. It involves a reduction in reagents and samples volumes, and at the same time it decreases the assays cost and allows highly parallelized experiments (Hill, 1998).

1.1.1 Microtiter plate technologies

Current HTS is based on microtiter plate format, which is a well-established technique used worldwide. The liquid handling in the microplates is performed automatically. Typically, an integrated system consisting of one or more robots handles the microplates, and performs all manipulation steps of the samples and reagents, such as addition and mixing of compounds, incubation and finally detection. HTS systems can handle many plates simultaneously, allowing to assay 100,000 compounds per day (Hann and Oprea, 2004). Recently, systems capable of screening even more than 100.000 compounds per day have been introduced and were termed ultra high throughput screening (uHTS) (Weber et al., 2007).

Initially, most assays were done in 96-well plates, where the assay volume is ~100 microliters and the throughput potential is about 20,000 assays per day. However, other

microplate formats of higher density have also been used. 384-well plates allow assay volumes of 10 microliters and a throughput of up to 50,000 assays per day. The use of 1536-well plates can reduce assay volumes to 5 microliters and provide a throughput potential of 100,000 assays per day. Additionally, the surface-to-volume ratio in this well plate format does not change much compared to 96-well plates. Hence evaporation can still be well managed by controlling the humidity and by covering the plate whenever possible. Besides, many biological assays including cell-based assays can still be done in this format. It has been demonstrated that cells can grow until confluence in these wells, corresponding to ~1000 cells, which is sufficient for performing reliable assays (Burbaum, 1998). Further miniaturization of microtiter plates has been shown, with typical assay volumes of 1 microliter for 3456-well plates (Stylli, 1997) and 0.2 microliter for 9600-well plates (Oldenburg, 1997). However, the adaptation of established assay systems to microplate formats of this density requires a careful examination of the feasibility with special attention to the pipetting error as well as the reproducibility and the sensitivity. Problems like cross contamination, formation of foam, evaporation and capillary action (causing “wicking” and bridging of liquid between wells) can cause problems at this scale (Berg et al., 2001) (Dove, 1999).

Table 1. *Specifications of typical microtiter plate formats*

Well plate format	Assay volumes (µl)	Throughput / day
96	100	20.000
384	10	50.000
1534	5	100.000
3456	1	>100.000
9600	0.2	>100.000

1.1.2 Microarrays technologies

A microarray is a two dimensional (2D) array on a solid substrate (usually a glass slide, plastic or silicon chip) for assaying large samples numbers of biological material in a high-throughput fashion. Different types of microarrays include: DNA microarrays (Figure 1),

protein microarrays (Korf and Wiemann, 2005), tissue microarrays, cellular microarrays, chemical compound microarrays, antibody microarrays and carbohydrate arrays.

A microarray consists of an arrayed series of thousands of microscopic spots of biological material (e.g. DNA oligonucleotides, proteins, lipids, tissue) or chemical compounds that are used as probes to hybridize with a target (e.g. DNA, cDNA, proteins, cell). Probe-target hybridization is usually detected and quantified by the detection of fluorophore-, silver-, or chemiluminescence-labeled targets. Typical applications are the detection of DNA (Figure 1) (e.g. to detect single nucleotide polymorphisms) and RNA (using cDNA after reverse transcription), or the identification of protein-protein interactions, small molecule-protein interactions, multiplex histological analysis or multiplex interrogation of living cells (Chen and Davis, 2006).

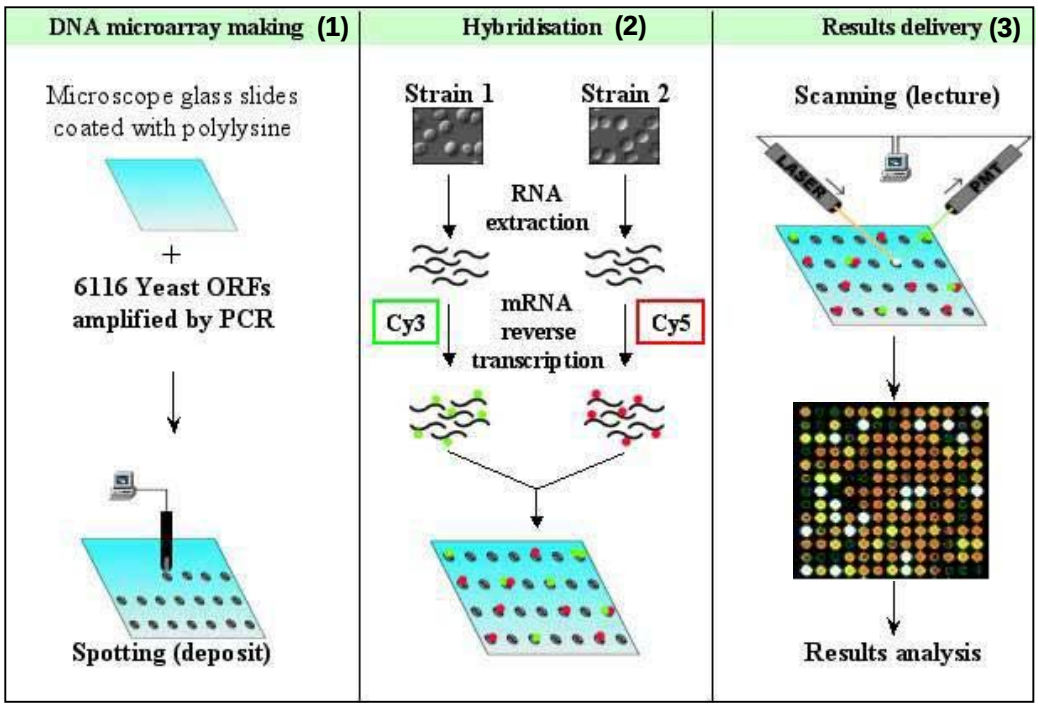

Figure 1. DNA microarray for comparative genomic hybridization. *(1) The probes are spotted on a microscopic glass slide. (2) RNA is extracted and purified from two different yeast strains. Subsequently cDNA is synthesized from mRNA by Reverse Transcription (RT), and the two different cDNAs are labelled with two different dyes (Cy3 and Cy5). Subsequently, the labelled samples are mixed with a hybridisation solution and with a blocking agent. This mix is denatured and added to a pin hole in a microarray. (3) Afterwards, the microarray chip is incubated overnight in an oven, before the nonspecific binders are washed off, and the chip is finally dried and scanned (Picture taken from the website of 'The Genomic Service from the Biology Department (SGDB), Paris').*

1.2 Novel High-Throughput Screening (HTS) technologies

1.2.1 Microfluidics

In the 1950's microtechnology was invented for developing integrated semiconductor structures for microelectronic chips; and it was in the 1960's when lithography-based technologies were applied in pressure sensor manufacturing. Ultimately, lithography-based technologies were used to generate micrometer or sub-micrometer sized mechanical structures in silicon wafers, marking the beginning of the Micro Electro Mechanical Systems (MEMS) era. In the beginning of the 1990's the development of micropumps and flowsensors started and in the mid 1990's Micro Total Analysis Systems (μTAS) for capillary electrophoresis and DNA microarrays were established.
Micro Total Analysis Systems, also referred to as Lab-on-a-chip (LOC) technology, integrate one or several laboratory functions on a single chip of only a few square centimeters in size. Performing experiments in these systems allows operating with extremely small fluid volumes down to pico or nanoliters. LOC devices are usually fabricated using photolithography (Whitesides et al., 2001), etching (Qu et al., 2008) or milling (Kummrow et al., 2009). The most important advantages of lab-on-a-chip systems compared to microtiter plate technology are: low sample and reagent volumes, compactness of the system, massive parallelization of the experiments, and finally, lower fabrication and assays costs.

Microarray technologies are high-throughput techniques, but do not give information about interaction dynamics between molecules. Methods such as affinity chromatography are used to quantify interaction dynamics (Phizicky and Fields, 1995), but are hardly compatible with high-throughput screening. However, these limitations can be overcome by microfluidic technologies which have the potential of performing many laboratory functions in a high-throughput manner. In addition, microfluidic systems allow further miniaturization of biochemical and cell-based assays compared to microtiter plate technology since they work with pico-to-nanoliter volumes in sealed devices, thus circumventing the problems of evaporation and capillary action.

One of the goals of microfluidics is the integration of multiple laboratory functions on a single chip such as fluid manipulation (e.g. pumps, valves, filters and mixers), chemical analyses (e.g electrophoresis, chromatography) and further detection techniques (e.g. fluorescence, electrochemical detection). More precisely, microfluidic systems consist of networks of channels of typically 10-100 µm diameter; where small quantities of reagents can be brought together in a specific sequence, mixed, and allowed to react for a specified time in a controlled region of the channel network by using electrokinetic and/or hydrodynamic pumping (Li and Harrison, 1997). The ability to rapidly fabricate microfluidic devices in polydimethylsiloxane (PDMS) using soft-lithography (Whitesides et al., 2001) has greatly stimulated the development of microfluidic systems.
In the past 15 years, the amount of research involving microfluidic applications in biology has increased dramatically, and it became so popular that new companies solely dedicated to microfluidics have been established. Some examples are Micronit Microfluidics (founded in 1999), Microfluidic System Inc. (founded in 2001), Aline Inc. (founded in 2003) and Raindance Technologies (founded in 2004). Other companies also making use of microfluidics are Caliper Life Sciences (founded in 1995) and Agilent technologies (founded in 1998). The big potential of integrated microfluidic circuits for biological/chemical experimentation and automation should enable microfluidics in the near future to become as widespread as common technologies such as DNA microarrays.
In general, microfluidics techniques can be classified in two different groups: continuous-flow and two-phase microfluidics.

1.2.1.1 Continuous flow-based microfluidics

1.2.1.1.1 Working principle

The flow of liquids in microfluidic channels is laminar and characterized by a low Reynolds number (*Re*). *Re* is defined as the ratio between dynamic pressure and shearing stress corresponding to the ratio between inertial forces and viscous forces:

$$Re = \frac{\rho \cdot \upsilon \cdot \ell}{\mu}$$

Where ρ is the fluid density, v is the fluid velocity, μ is the dynamic fluid viscosity and l is the characteristic channel length. Laminar flow occurs in fluidic systems when $Re < 2000$ while turbulent flow is observed when $Re > 2000$. In microfluidic systems Reynolds numbers are typically lower than 1 and thus viscous forces (shearing stress) dominate, while inertial forces (dynamic pressure) become negligible.

In laminar flow diffusive mixing is slow compared to convection flow (Song et al., 2003b). The distance that molecules diffuse between two adjacent streams depends on the size of the molecules, the viscosity of the liquids and the distance from channel edges (Figure 2). This ability to generate and sustain parallel streams of different solutions in capillaries/microchannels opens the possibility of modifying the channel surface with different adhesive molecules (e.g. poly-l-lysine, for analyzing its effect on cell growth) and allows localizing chemicals– fluorescent labels, nutrients, growth factors, toxins, enzymes, drugs–. In addition, continuous flow of a single stream is useful for molecule separation (e.g. electrophoresis). However, in the case of fast reactions in which the reagents are initially present in separate streams it is a disadvantage because the reaction does not occur uniformly throughout the whole width of the channel. Possible ways to enhance the mixing are either the use of passive mixers which are based on geometrical properties of the microchannels (like zig-zag-shaped channels (Song et al., 2003a)) or the use of active mixers which rely on fluid flow perturbations at different time points (Stroock, Dertinger et al. 2002; Hong, Choi et al. 2004).

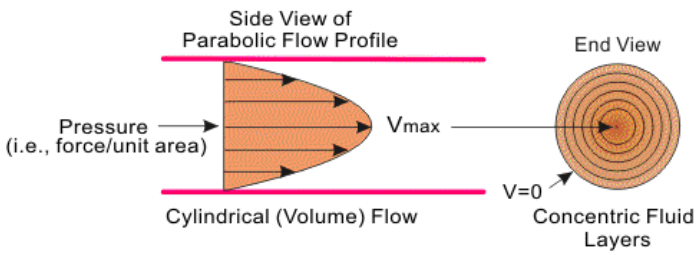

Figure 2. Representation of the parabolic flow profile in a cylindrical flow. *(Picture taken from www.cvphysiology.com/Hemodynamics/H006.htm)*

Besides the slow mixing, the dispersion of solutes along the channel is large due to a parabolic flow profile, also called Taylor-Aris dispersion (Figure 2 and Figure 3a) (Aris, 1956; Taylor, 1953) which is explained by Poiseuille's law. In Poiseuille's flow the

channel walls apply shear forces on the fluid establishing this parabolic flow profile over the cross-section of the channel; therefore, the fluid at the centre of the channel moves faster than that at the edge. In the case of microfluidics, this effect can generate cross contamination problems. However, this can be overcome by compartmentalizing the fluid in form of discrete droplets (Figure 3b) (Song et al., 2003b).

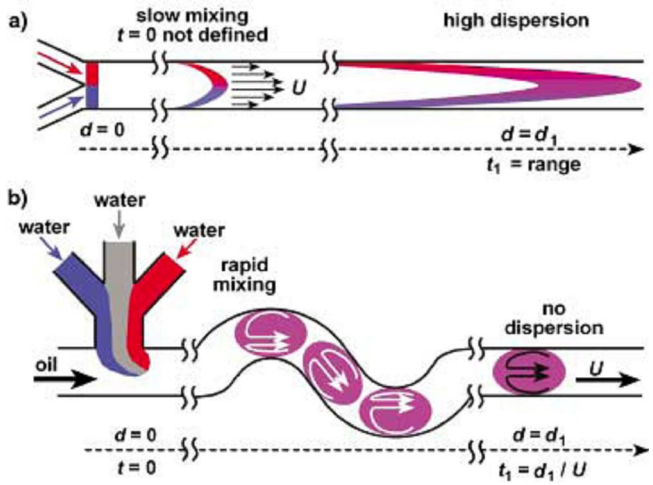

Figure 3. Schematic comparison of continuous-flow and drop-based microfluidics. (a) *In continuous-flow microfluidics mixing is slow and dispersion is high due to the parabolic flow profile.* ***(b)*** *In drop-based microfluidics mixing is rapid and no dispersion occurs due to microcompartmentalization (Song et al., 2003b).*

1.2.1.1.2 Applications

Continuous-flow microfluidic systems have been used for many applications. These include Polymerase Chain Reaction (PCR) (Kopp et al., 1998), electrophoresis (Ewing et al., 1997), generation of chemical/protein gradients (Thompson et al., 2004), cultivating cells (Ong et al., 2008), generation of spatial-temporal dynamic perturbations on cells or multicellular organism (Lucchetta et al., 2005; Takayama et al., 2001) and single molecule analysis (Brewer and Bianco, 2008). In general, assay miniaturization enables massive cost savings and the use of samples that are not available in big quantities. Furthermore, when doing cell-based assays, different conditions can be applied to individual cells or subpopulations of a culture.

Kopp et al. performed rapid Polymerase Chain Reactions (PCR) in a continuous-flow microfluidic system. The DNA sample and the corresponding buffer were hydrostatically pumped through a single channel etched into a glass chip. This channel passed repetitively through three temperature zones (denaturation (95°C), extension (77°C) and annealing (60°C) temperatures) defining the thermal cycling process (Figure 4) (Kopp et al., 1998). The product quality and quantity were comparable to standard thermal cycling methods.

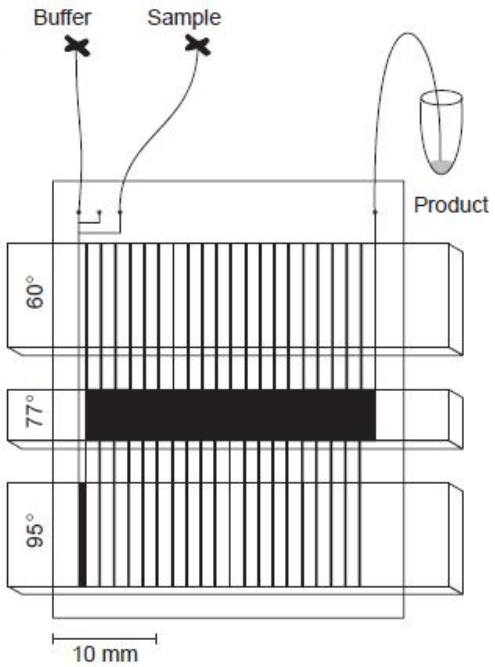

Figure 4. Continuous-flow PCR on-chip. *A DNA sample and the corresponding reaction mix are delivered through a single channel etched into a glass chip. The sample is amplified while passing repetitively (20 cycles) through 3 different temperature zones (copper blocks covered by a thin-film resistor to monitor the temperature) (Kopp et al., 1998).*

Continuous flow microfluidics show great potential for inducing molecule separation, which has been exploited for electrophoresis. In 1997, *Ewing et al*. developed the first capillary-channel electrophoresis device to dynamically study single-cell secretions. Flow from a microfluidic capillary entered a rectangular channel where it was subjected to electrophoresis as it translated across the channel (Figure 5a). The authors dynamically separated twelve different DNA samples (Figure 5b), and 4 different aminoacids.

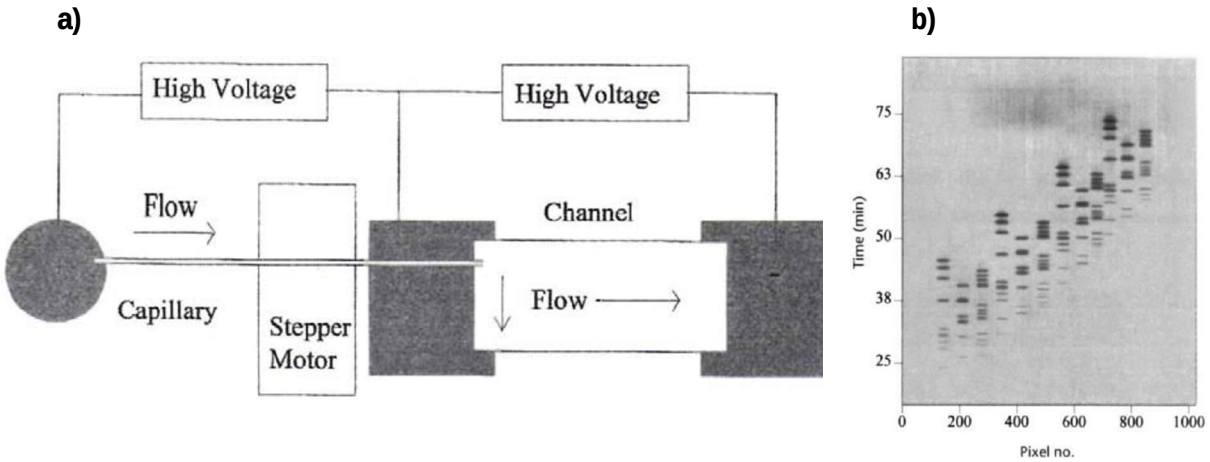

***Figure 5. Molecule separation in microfluidics**. **(a)** Schematic representation of a capillary-channel electrophoretic separation system. Samples enter the device through the microcapillary before being separated in the rectangular channel filled with polyacrilamide gel. **(b)** DNA separations are shown over time, demonstrating the continuous and dynamic monitoring capabilities of the device (Ewing et al., 1997).*

Some years later, *Li et Martin* fabricated a device for the immobilization of a variety of cell lines and the analysis of various released analytes by electrophoresis (Li and Martin, 2008). Even though this was not performed on the single-cell level, the approach allowed the on-chip stimulation of cells and the controlled valve-based injection of the released products into an electrophoresis channel. Furthermore it enabled the separation of the analytes, rendering the analytes fluorescent by a subsequent post-column derivatization (Bergquist et al., 1994); and finally fluorescence detection (Figure 6). An electric field was used to load the sample into the device and to pull the sample in the separation channel, where it was separated by electrophoresis in about 20 seconds.

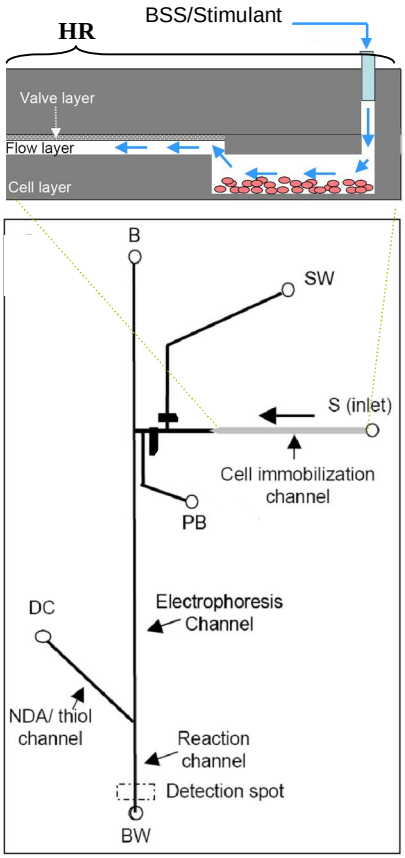

Figure 6. Multilayer cell analysis device*. Cells are immobilized within the device. Through the actuation of PDMS-based pneumatic valves, samples from the hydrodynamic region (HR) can be injected into the electrophoresis part of the microchip, where the analytes are separated based upon mass and charge. Post-separation derivatization, which is done using naphthalene-2,3-dicarboxaldehyde (NDA) and 2-β-mercaptoethanol (2ME) enables fluorescent detection of the released analytes. HR: hydrodynamic region, B: buffer reservoir, SW: sample waste outlet, S: sample, PB: pushback reservoir, DC: derivatization channel, BW: buffer waste reservoir. (Li and Martin, 2008).*

Due to the easy generation of gradients using continuous-flow, it is also possible to continuously perfuse living cells with several concentrations (Figure 7) of a soluble molecular stimulus and monitor their gene expression at the same time. *Thompson et al.* used cells expressing a green fluorescence reporter plasmid (GFP) under the control of a gene-specific promotor to study the expression dynamics of a transcription factor (NF-kB). Whenever the gene-promotor was activated by an external stimuli (cytokine TNF-α), the cells became fluorescent due to the expression of GFP. Consequently, when using different concentrations of the external stimuli different fluorescence intensities were obtained inferring the expression dynamics of the transcription factor (NF-kB) (Thompson

et al., 2004). Hence, the technology allows monitoring dynamic changes in gene expression in a time-dependent manner for multiple concentrations and not only, as in conventional approaches, using standard cell culture flasks, for a single concentration. Additionally, this microfluidic approach could be scaled-up allowing the monitoring of multiple stimulation conditions (by using an even more complex device with eight different gradient generators connected to eight cell culture chambers) (Ye et al., 2007) and the cultivation of different reporter cells at the same time (Dino Di Carlo, 2006).

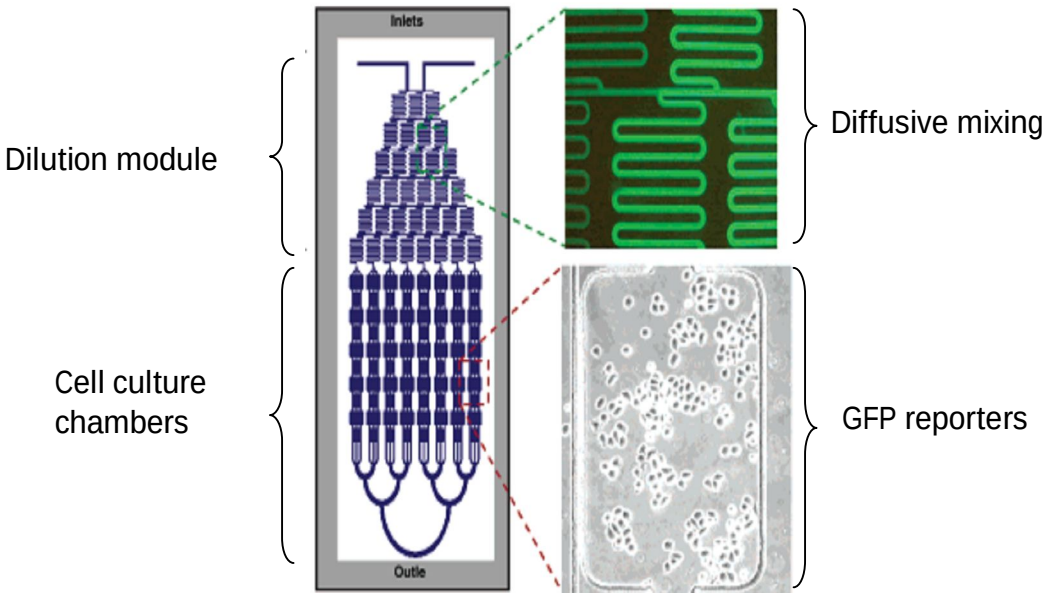

Figure 7. Living Cell Array device*. A gradient generator splits two inputs into eight different concentrations, which flow into eight columns of cell chambers. In this study the activation of the transcription factor NF-KB in HeLa S3 cells was studied in response to varying doses of the inflammatory cytokine TNF-r (Thompson et al., 2004).*

Microfluidic chips can also be used to culture cells in a three dimensional (3D) manner allowing cells to display gene expression profiles and biological activities that resemble the in vivo situation much more closely than in 2D (Pampaloni et al., 2007). Current ways to seed and culture mammalian cells in 3D are based on hydrogels. They are operationally complex, hinder mass transfer, and are incompatible with establishing cell-dense extracellular matrix (ECM)-poor constructs. However, Ong et al have recently described a gel-free 3D microfluidic cell culture system (Figure 8) which uses a combination of transient inter-cellular polymeric linkers and micro-fabricated pillar arrays to generate the 3D environment (cell clamps) (Ong et al., 2008). In combination with

perfusion systems this allows the screening for cell differentiation protocols (Ong et al., 2008).

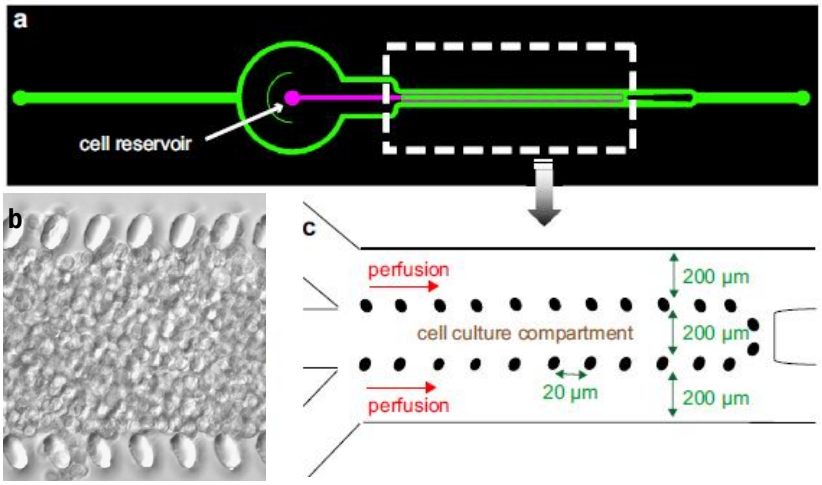

***Figure 8. Gel-free 3D microfluidic cell culture system**. **(a)** Design of the device. The gel-free 3D chip has two inlets (one for the infusion of culture medium and one as a cell reservoir) and one outlet. **(b)** Cells were mixed with transient inter-cellular polymeric linkers and seeded in between the pillar array to generate a 3D environment. Subsequently, an image of the cellular culture in the gel-free 3D environment was taken. **(c)** Micropillars (shown as black points) divide the microfluidic channel into a central cell culture compartment and two side channels for the perfusion of culture medium (Ong et al., 2008).*

Localized microfluidic flow can be used to apply precise, localized, as well as spatially and temporally dynamic perturbations. As a demonstration, *Takayama et al.* have studied the cytoskeletal structure and subcellular processes of mitochondrial movement of a cell after applying several stimuli. For that purpose, different fluorescent dyes were flowed over opposite sides of a live endothelial cell, staining two subpopulations of mitochondria. Subsequently, the cell was locally treated with latrunculin A (promoting the break up of polymeric actin filaments) and the mitochondrial response to the cellular damage could be observed (Takayama et al., 2001). Localized microfluidic flow has also been used to explore embryonic patterning compensation mechanisms against spatiotemporal perturbations applied to a *Drosophila* embryo (Lucchetta et al., 2005). The embryo was positioned between two laminar streams of different temperatures resulting in a different rate of development of each half of the embryo observed by differences in the density of nuclei in the two halves of the embryo. However, when exposing the whole embryo at room temperature after this temperature step, the embryo

did not show a defect in patterning, and it developed into normal larvae with the correct number of patterned segments. This demonstrated the existence of a compensation system counteracting the effects of harsh environmental conditions (such as a temperature step, T-step). Additionally the authors demonstrated that even-skipped patterning (genes that are expressed in striped patterns of seven bands perpendicular to the anterior-posterior axis within the syncytial bastoderm during the embryo development) remained robust in embryos exposed to the T-step (Figure 9). The even-skipped stripes resolved faster at higher temperatures (one half of the embryo), but ultimately this effect was abolished by the compensation system.

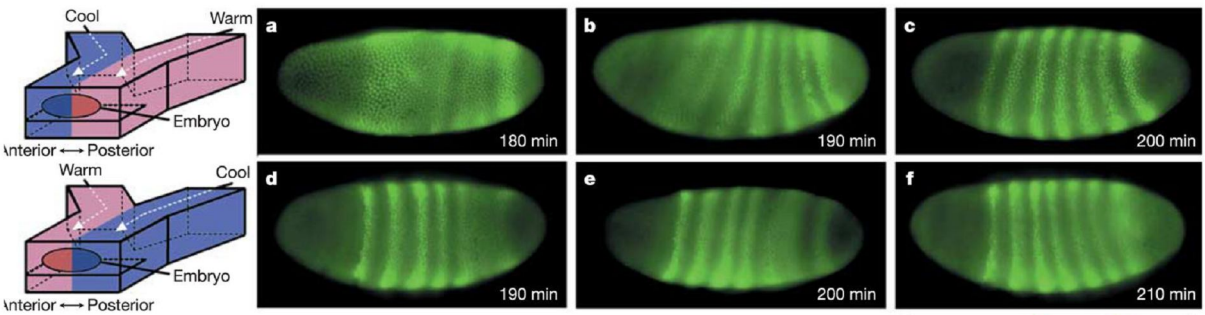

Figure 9. Study of the development of a Drosophila embryo after localized flow perturbations. *Microfluidic devices are used to apply different temperatures across the embryo (left), and to study the dynamic even-skipped gene expression response (right). The second row shows the reversed temperature-step experiment of the first row experiments (Lucchetta et al., 2005).*

The combination of continuous-flow microfluidics and optical microscopy enables dynamic monitoring of small populations of cells with single-cell resolution during long term cultivation. As a demonstration, the group of Stephen Quake has studied the dynamics of cell density and the associated morphological changes in an *E. Coli* culture. For that purpose, they have used a microfluidic device containing six independent 16-nanoliter reactors fed by peristaltic pumps through micromechanical valves (Figure 10a). Each reactor operates in two different states: continuous recirculation of media through the culture chamber (Figure 10b) and dilution of the media and cleaning of the culture chamber (Figure 10c). Using valves the culture could be provided with growth media and reagents, the cells could be washed, diluted, lysed and the waste could be removed. The cell proliferation was induced with isopropyl-b-D-thiogalactopyranoside (IPTG), and the

cell death was regulated by the expression of a suicide gene (*lacZα-ccdB*) (Balagadde et al., 2005).

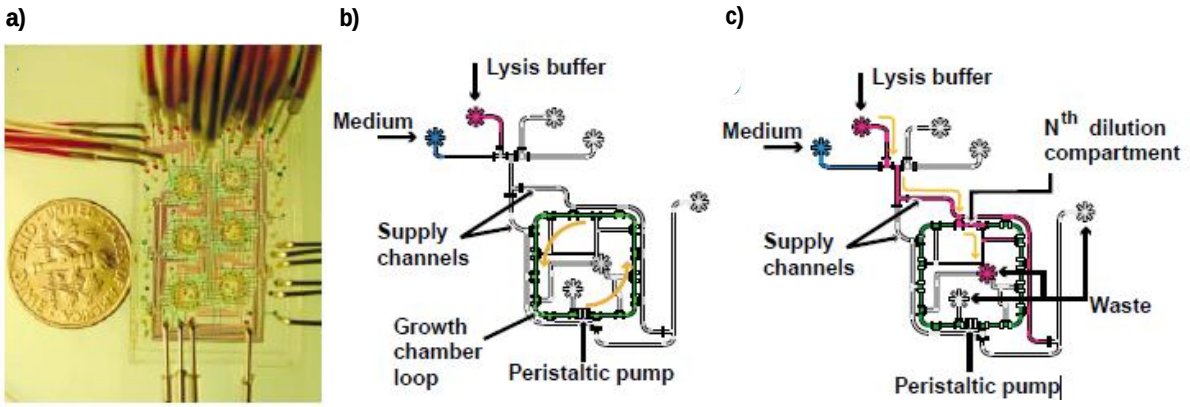

Figure 10. Microfluidic device with peristaltic pumps and micromechanical valves for the cultivation of cells. ***(a)*** *Micrograph of the device showing six microchemostats that operate in parallel on a single chip. The coin is 18 mm in diameter.* ***(b)*** *Schematic diagram of a microchemostat in continuous circulation mode. The peristaltic pump moves the microculture around the growth chamber loop.* ***(c)*** *Schematic diagram of a microchemostat during cleaning and dilution. A lysis buffer is introduced into the chip through the lysis buffer port. Integrated microvalves direct the buffer through the segment, flushing out cells, including those adhering to the chamber walls. Subsequently, the segment is rinsed and refilled with fresh sterile medium (Balagadde et al., 2005).*

1.2.1.2 Two-phase microfluidics

1.2.1.2.1 Working principle

a) Characteristics of laminar flow

As described above, for certain types of screens the laminar flow in single phase microfluidic systems creates two problems (Song et al., 2003b): first mixing is slow, the reagents mix only by diffusion and second, the dispersion of solutes along the channel is large due to the parabolic flow profile. However, this can be overcome by compartmentalizing the fluid in form of discrete droplets. Microfluidic droplet generators are based on combining two or more streams of immiscible fluids and generating a shear force on the discontinuous phase causing it to break up into discrete droplets. Droplets

can be created either by flow-focussing in a nozzle or using a T-junction (Figure 11) (Song et al., 2006; Teh et al., 2008). In the flow-focusing configuration, the continuous and the dispersed phases are forced through a nozzle in the microfluidic device, in which the continuous phase symmetrically shears the dispersed phase into droplets (Figure 11a). In the T-junction configuration, the inlet channel containing the continuous phase perpendicularly intersects the dispersed phase and shears the dispersed phase into droplets (Figure 11b). Depending on the relative flow rates of the two phases, droplets of different sizes can be generated. “Plugs” are big droplets that completely fill up the channel, while “drops” usually do not get in contact with the channel walls during their formation.

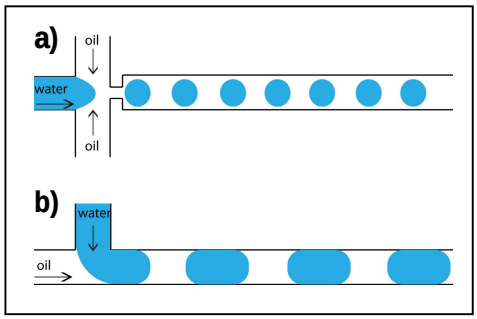

Figure 11. Droplet formation. *Droplets can be generated either using* ***(a)*** *flow-focussing or* ***(b)*** *T-junction configuration.*

b) Capillary numbers and viscosity ratios

The deformation of droplets due to external flow depends on capillary numbers (*Ca*) and on viscosity ratios (ρ) (HA, 1994; Peter Van Puyveldea, 2001) (Zheng et al., 2004).

$$Ca = \frac{\eta \cdot v}{\gamma}$$

Where η (Pa·s) is the viscosity of the liquid, v (m/s) is the total flow velocity, and γ (N/m) is the interfacial tension between two immiscible phases.

$$\rho = \frac{\eta_d}{\eta_m}$$

Where η_d is the viscosity of the droplet and η_m is the viscosity of the carrier fluid. Deformation increases with increasing *Ca* or with increasing ρ. If *Ca* exceeds a critical value (Ca_{cr}), the droplets are known to become unstable (Figure 12): they either break up by waist-thinning, $Ca>Ca_{cr}$, or they break up in a highly extended fiber into a large number of droplets, $Ca>>Ca_{cr}$. The effect of deformation and breakup due to high capillary numbers is more notable when working with plugs since they have a higher surface to volume ratio than drops.

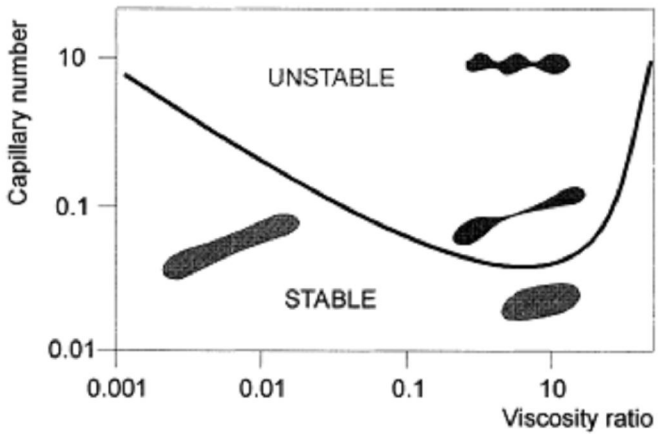

***Figure 12. Stability of drops in relation to the capillary number (Ca) and the viscosity ratio** (ρ). Ca is the viscosity of the liquid times the flow velocity divided by the interfacial tension between two immiscible phases. ρ represents the viscosity of the droplet divided by the viscosity of the carrier fluid (Briscoe, 1999).*

c) Surface tension / Surfactants

In general, water drops within a continuous oil phase tend to fuse to decrease their surface per unit of volume, thereby decreasing the energy state of the system. Surfactants are used to increase the stability of the drops, and hence avoid coalescence upon contact between drops (Stone HA, 1990). Surfactants reduce the interfacial tension between two immiscible liquids by adsorbing at the liquid-liquid interface. The interfacial tension (γ) is caused by the attraction of various intermolecular forces between the molecules of two immiscible liquids. The molecules in the interface are in a higher state of energy than those within the liquid. Molecules within the liquid undergo attractive

forces equal in all directions resulting in a net force of zero; however, the molecules at the interface undergo attractive forces mainly inwards the liquid (the attractive forces from the neighbouring liquid are weaker) resulting in a net force different of zero (Figure 13). Hence, γ is the driving force to diminish the interfacial area, and therefore to decrease the number of molecules at the interface. γ between two liquids is defined as the energy (W) used per unit of area (A): $\gamma = dW/dA$.

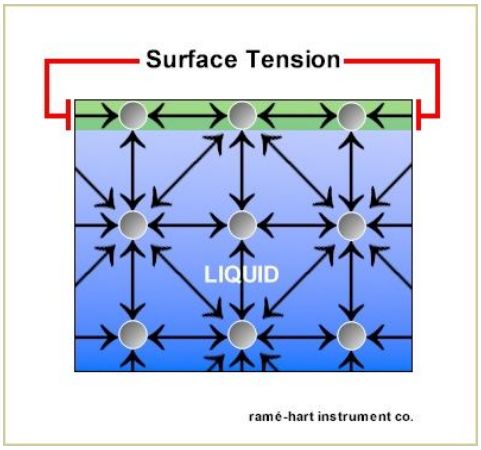

Figure 13. Representation of the forces in the interface of two immiscible liquids and within a liquid *(Picture taken from http://www.ramehart.com/goniometers/surface_tension.jpg).*

During drop production, surfactants must reach the drop interface very quickly to prevent drop coalescence, and this is easier achievable if their size and weight are not large. Besides, surfactants can be fluorinated or hydrogenated; and can be classified into non-ionic, cationic, anionic and zwitterionic (both positively and negatively charged) surfactants. Surfactants can be dissolved in both the oil and the aqueous phase depending on their hydrophile-lipophile balance (HBL) number. HLB measures the degree to which a surfactant is hydrophobic and lipophobic, thus determining the type of emulsion formed; $HLB = 20 * M_h / M$ where M_h is the molecular mass of the hydrophilic portion of the molecule, and M is the molecular mass of the whole molecule, giving a result on an arbitrary scale of 0 to 20 (Griffin, 1949). Surfactants with low HLB (<6) are more lipophilic and thus tend to generate a water-in-oil (w/o) emulsion; in contrast, surfactants with high HLB (8 – 18) are more hydrophilic and tend to make an oil-in-water (o/w) emulsion. When the concentration of surfactant is below the critical micelle

concentration (CMC), all surfactant molecules are dissolved in the oil phase (unimers); but when the concentration of surfactant is above the CMC, additional surfactant molecules assemble into micelles (molecules associate placing their heads in a core and the tails in contact with oil) (Piirma, 1992; Tadros, 2005). These micelles can carry molecules dissolved in the water phase and transport them from one drop to another, thus generating cross contamination. Besides, if the surfactant concentration is too high, an increased drop polydispersity or jetting (generation of a continuous aqueous stream instead of drops due to a very low surface tension) can be observed during the production of drops.

For drug screening assays in two phase microfluidics, reliable drop stability is required and exchange of small molecules between drops must be prevented. These requirements can be fulfilled using fluorocarbon oil as the continuous phase for the production of drops, due to its insolubility in aqueous and organic solutions (Scott, 1948; Studer et al., 1997), in which most drugs and biological compounds are assayed. However, this does not overcome the possible cross contamination between drops generated by the presence of micelles when surfactants are used. Besides, fluorocarbon oils are advantageous because do not swell PDMS and are gas permeable, which is an important feature for the cell viability in cell-based assays (Love et al., 2005; Lowe et al., 1998). Furthermore, for drug screening full biocompatibility of the oil mixture with the samples is necessary. Therefore, since most proteins, cell walls and DNA are charged and could thus possibly interact strongly with an oppositely charged interface; non-ionic surfactants are preferable. In contrast to hydrocarbon surfactants, fluorinated surfactants are more stable and fit for harsh conditions due to the high stability of their carbone-fluorine bond (bond dissociation energy of C-F (BDE_{C-F}) is 130 kcal/mol compared to 104,9 kcal/mol for BDE_{C-H}).

As opposed to drops, plugs do not require the presence of surfactant to increase their stability and avoid coalescence. While drops are usually incubated either in delay-lines or in reservoirs (e.g. eppendorf tubes) where they continuously get in direct contact, plugs are generally stored in a holding cartridge (e.g. a tubing or capillary) and separated by spacers of oil, hence preventing the fusion of two consecutive plugs without the need of any surfactant. Thereby micellar transport between plugs can be circumvented. However

the lacking of surfactant increases the wettability of the channels thus requiring special coatings of the devices (Stone HA, 1990). Aquapel (rain repellent (Mazutis et al., 2009a)) or/and perfluorinated silanes (Sagiv, 1980) are the most common coating treatments for PDMS/glass devices.

Non-microfluidic systems based on the compartmentalization of reactions in aqueous microdroplets of water-in-oil emulsions (in vitro compartmentalization, IVC) have been used for directed evolution (Tawfik and Griffiths, 1998). Typically, an aqueous solution of genes and an *in vitro* transcription-translation (IVT) system was stirred into an oil-surfactant mixture to create a water-in-oil (w/o) emulsion resulting in ~10^{10} highly polydisperse aqueous droplets per milliliter of emulsion.

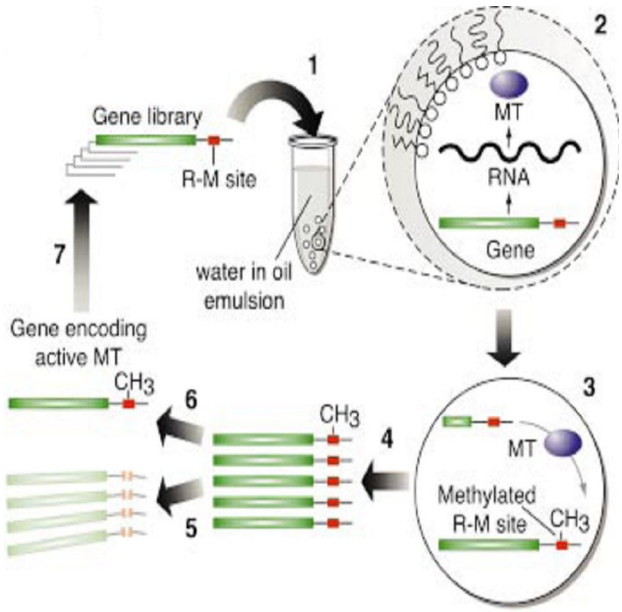

Figure 14. Schematic representation of in vitro compartmentalization*: (1) An in vitro transcription/translation mixture containing a library of genes is stirred to form water-in-oil emulsions. (2) The genes undergo transcription and translation within the microcompartments. (3) The resulting proteins, if active, methylate the substrate (gene). (4) The emulsion is broken, all the reactions are stopped and the aqueous compartments are combined. (5) Genes encoding the methylation activity are amplified by PCR since methylation gives protection to the gene to digestion by restriction endonucleases, and subsequently they are characterized. (6) Selected genes are compartmentalized again for further rounds of selection (Cohen et al., 2004).*

The genes encoded a library of methyltransferase DNA variants which after IVT within the drop (if active) methylate the substrate (their encoding gene) resulting in resistance to digestion by the HaeIII restriction endonuclease. The methylated (and thus non-digested) genes were subsequently amplified by PCR and thus enriched (Cohen et al., 2004). Since phenotype (methylation activity) and genotype (encoded mutant) were coupled *in vitro*, it was possible to select large libraries of protein variants (10^8–10^{11} genes) for catalytic activity (Figure 14). In addition to the selection of methyltransferase variants, IVC has been applied in a number of areas, including ultra-high-throughput sequencing (Margulies et al., 2005).

Generating droplets conventionally (e.g. using a homogenizer) results in highly polydisperse drops making quantitative readouts and further manipulations (e.g. splitting and addition of further compounds) difficult. In contrast, two-phase microfluidic systems allow for a level of control that was hitherto impossible. Thereby, biochemical assays can be miniaturized down to picoliter volumes. Highly monodisperse (<3% polydispersity) w/o drops can be generated at frequencies greater than 10 kHz (P. B. Umbanhowar, 2000).

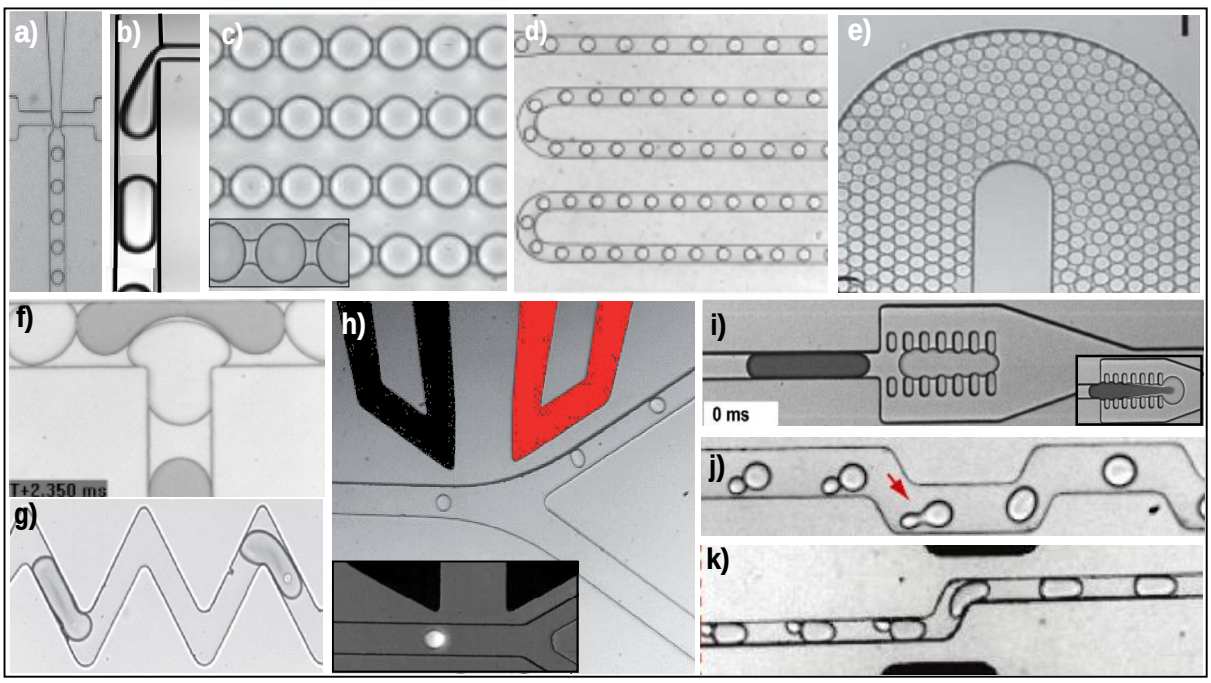

Figure 15. Drop manipulation. *Drops can be generated* ***(a)*** *by flow-focussing (Baret et al., 2009) or* ***(b)*** *in a T-junction configuration (Thorsen et al., 2001). Drops can be* ***(c-e)*** *stored in delay-lines (Koster et al., 2008; Schmitz et al., 2009) and* ***(f)*** *splited (Link et al., 2004).* ***(g)*** *Their content can*

*be mixed (Song et al., 2003a), and in addition drops can be **(h)** sorted (Baret et al., 2009) and **(i-k)** fused (Niu et al., 2008) (Mazutis et al., 2009b) (Frenz et al., 2008).*

The aqueous microdroplets can be fused or subdivided (Link et al., 2004; Link et al., 2006; Mazutis et al., 2009b), the contents of microdroplets can be mixed rapidly, and sorting modules allow for the specific enrichment of microdroplets (Baret et al., 2009; Link et al., 2006; Song et al., 2003b) (Figure 15).

1.2.1.2.2 Applications

Two-phase microfluidic systems have been used for a range of different applications, including single-molecule PCR (Schaerli et al., 2009), proteome analysis, clinical diagnosis on human physiological fluids, protein crystallization, titration of anticoagulants (Beer et al., 2007; Chen and Ismagilov, 2006; Srinivasan et al., 2004; Wheeler et al., 2005), synthesis of molecules (Hatakeyama et al., 2006) and the synthesis of nanoparticles (Frenz et al., 2008). They have also been used to encapsulate prokaryotic and eukaryotic cells (Grodrian et al., 2004; He et al., 2005; Martin et al., 2003), and even the embryos of multicellular organisms (Funfak et al., 2007).

Schaerli et al have recently developed a system for single molecule-PCR in droplets, which is an attractive tool for directed evolution experiments in drops (Tawfik and Griffiths, 1998). Usually, directed evolution requires single-gene variants in each droplet; however for efficient in vitro expression (IVT) several copies of the same gene are required. Hence, the integration of PCR in droplets would allow amplifying the single-gene variants resulting in higher yields of protein, and thus in the increase of the detection sensitivity. The authors used a device containing different zones with alternating temperatures (Figure 16) (corresponding to denaturation, annealing and extension) thus avoiding temperature cycling of the entire device, and therefore allowing quicker heat transfer and higher throughput (Schaerli et al., 2009).

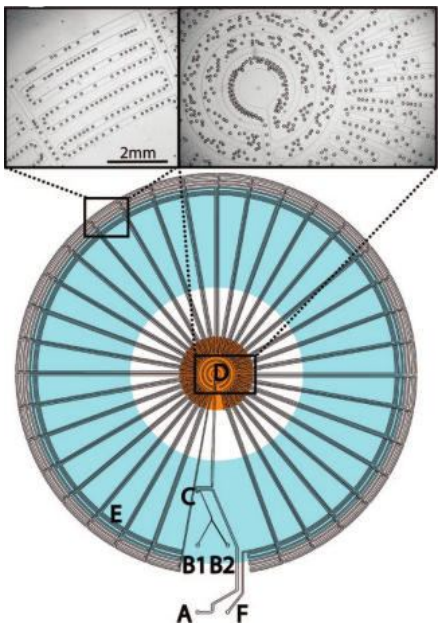

Figure 16. Design of a micro PCR device*. The device has an oil inlet (A) and two aqueous inlets (B). Droplets are formed using a t-junction (C). The DNA within the droplets undergoes amplification while passing through the channels: denaturation takes place in the inner circles (D) heated by a copper rod (orange zone) and primer annealing and template extension occurs in the exterior circles (E). Heating from the center establishes a natural temperature gradient across the device, which can be increased or diminished by an annular Peltier module (blue zone). Droplets flow back and forth from the exterior circles to the center to undergo the different cycles, and ultimately they exit the device (F) (Schaerli et al., 2009).*

The group of Ismagilov has demonstrated protein crystallization in plug-based microfluidics. This is interesting for both, the determination of three dimensional protein structures and the understanding of protein aggregation in a high throughput fashion (Kreutz et al., 2009; Meier et al., 2009). In contrast to current crystallization methods (such as 2D lipid- and self-assembled monolayers (SAMs)-based methods) (Darst and Edwards, 1995; Love et al., 2005) this system allows the generation of protein crystals from samples that are only available in small volumes (e.g. cerebrospinal fluid from mice) and the parallelization of thousands of crystallization trials resulting in the rapid improvement of crystallization conditions (like nucleation and growth of the crystals). *Kreutz et al*. have shown that plugs can be used as mobile and functionalized SAMs and that the precipitation degree of a protein in plugs was proportional to the adsorption of proteins at the interface. For that purpose, they designed a complex of RFNTA (nitriloatriacetate headgroup coupled to an oligoethylene glycol) with Ni^{2+} which introduced specific interactions with his-tagged proteins at the plug interface and allowed

protein precipitation. However, when adding only Ni^{2+} to the his-tagged protein, all nucleation was suppressed indicating that crystal formation was inhibited; and with only RfNTA, the precipitation degree was similar to that under standard conditions (Figure 17) (Kreutz et al., 2009; Meier et al., 2009) .

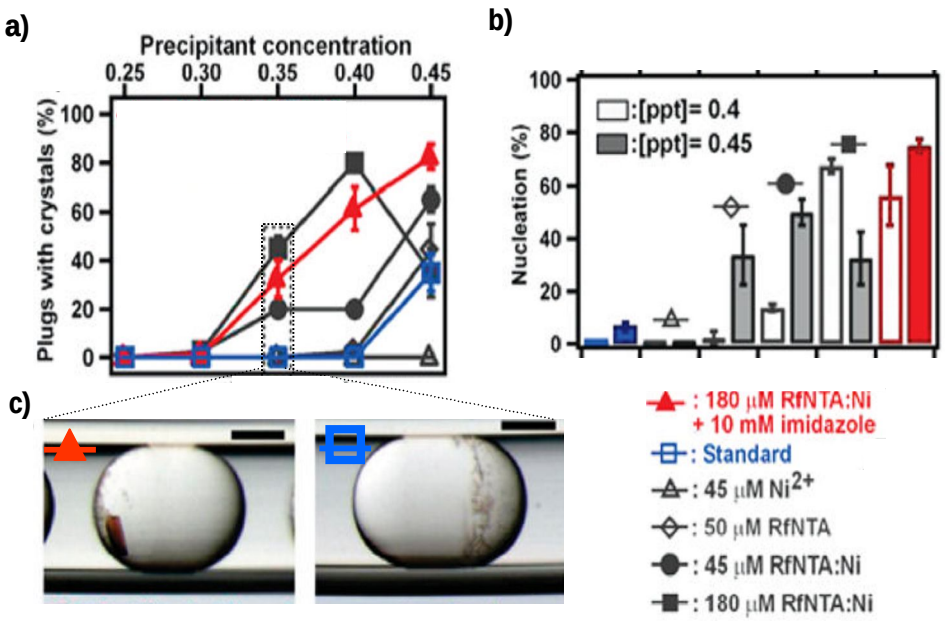

Figure 17. Protein crystallization in aqueous microcompartments. *Different additives were used in the solution phase of the drops to study* ***(a)*** *the precipitation rate and efficiency and* ***(b)*** *the nucleation rate.* ***(c)*** *Microphotographs of plugs after precipitation with RfNTA:Ni and imidazol (left) and under standard conditions (right). Scale bar = 100 µm (Kreutz et al., 2009).*

Synthetic chemistry has been performed in drop-based microfluidics too. Conventional bulk synthesis strategies or continuous-flow microfluidics provide only poor spatial and temporal control of the reactions. In contrast, compounds encapsulated into drops of specific volumes can be merged and their contents can be mixed rapidly (milliseconds), thus preventing uncontrolled progression of the reaction. As an example, *Frenz et al.* have synthesized iron oxide nanoparticles (Figure 18), for which controlling the synthesis conditions is absolutely crucial since the product precipitates rapidly (within milliseconds). While this causes problems in bulk, the microfluidic approach allowed the controlled generation of nanoparticles with desired properties (Frenz et al., 2008).

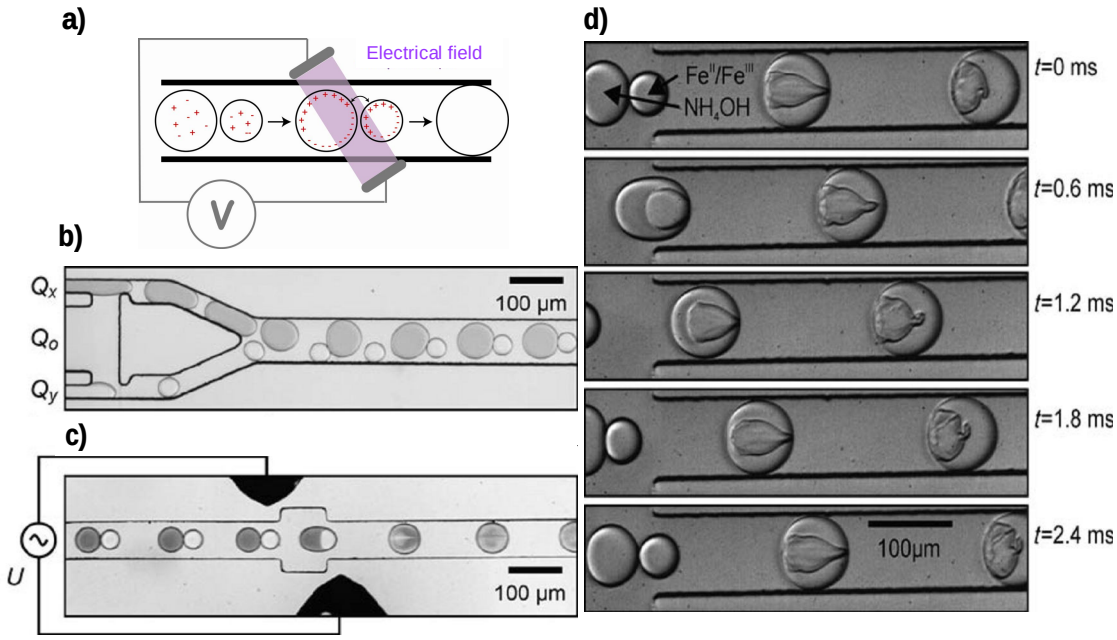

***Figure 18. Synthesis of iron oxide nanoparticles in droplets**. **(a)** Schematic representation of drop fusion: drops containing Fe^{II}/Fe^{III} (small drops) and NH_4OH (big drops) were **(b)** paired synchronously on-chip and subsequently **(c)** fused using electrocoalescence, resulting in **(d)** the formation of iron oxide precipitates (Frenz et al., 2008).*

The present study investigated two-phase microfluidic platforms for cell-based HTS. When this project was started, neither incubation and/or recovery of viable mammalian cells, nor a full life cycle of an encapsulated multicellular organism had been demonstrated. Furthermore, none of the existing systems allowed for an automated analysis of individual compartments subsequent to an incubation period as required for high-throughput, cell based-assays.

Martin et al. demonstrated first the encapsulation of single cells and small cell populations into drops in an automated manner (using syringe pumps and microchips). GFPuv-expressing bacteria were encapsulated into droplets at a rate of 30 Hz using a T-junction configuration and subsequently incubated in a length of Teflon tubing. After several days of incubation, cell growth was confirmed by fluorescent measurements directly in the tubing and by determining the cell number in a counting chamber after different incubation times (Martin et al., 2003).

Two years later, *Sakai et al*. encapsulated small mammalian cell populations in droplets (Sakai et al., 2005). They generated drops using a droplet breakup technique, in which an

aqueous solution is injected by a needle into a stream of liquid paraffin within a coaxial glass tubule (Figure 19). However, the cells were not incubated in the drops; immediately after their encapsulation they were cultured in cell dishes to confirm their viability.

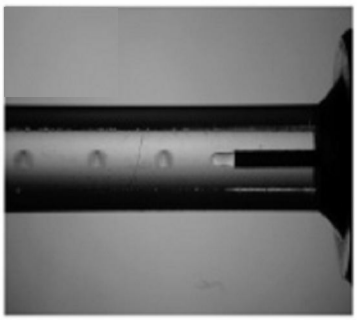

Figure 19. Generation of droplets containing cells using a breakup technique, *picture from (Sakai et al., 2005).*

He et al. encapsulated individual mammalian cells and subcellular organelles into drops. Drops were generated using a T-junction configuration in which the oil phase was controlled with a syringe pump and the aqueous phase was manually pressure pulse driven (using a syringe). The authors performed an enzymatic assay on-chip: cells expressing β-galactosidase were encapsulated together with a fluorogenic substrate. Subsequently they were lysed by a laser-beam on-chip to bring the intracellular enzyme and the substrate into close contact, resulting in the generation of a fluorescent product (He et al., 2005).

In contrast to the previous cell studies, *Huebner et al.* generated drops at a rate of 60 Hz with less than 5 % polydispersity and with controlled cell-drop occupancy. Cell dilution was performed on-chip by varying the ratio between the cell and LB media streams. The resulting cell occupancy was in good agreement with a Poisson distribution. The purpose was the monitoring of bacterial cell growth by continuously measuring the signal of a fluorescent protein expressed by the cells. To do so, bacterial cells were cultivated off-chip, encapsulated at different time points and injected into the device to perform fluorescent measurements, thus counting the cells (Huebner et al., 2007).

In another study, *Funfak et al.* analysized the embryonic development of a multicellular organism in drops (Figure 20). For this purpose, they encapsulated eggs from zebrafish (*Danio rerio*) into plugs by alternately aspirating aqueous samples and immisicible oil using a syringe-pump. After 3 days of incubation, embryos hatched from eggs. To increase the stability of the drops, the applied oil contained a surfactant (sodium dodecyl sulphate (SDS)) which at high concentrations unfortunately led to negative impacts on the development of the embryo (Funfak et al., 2007).

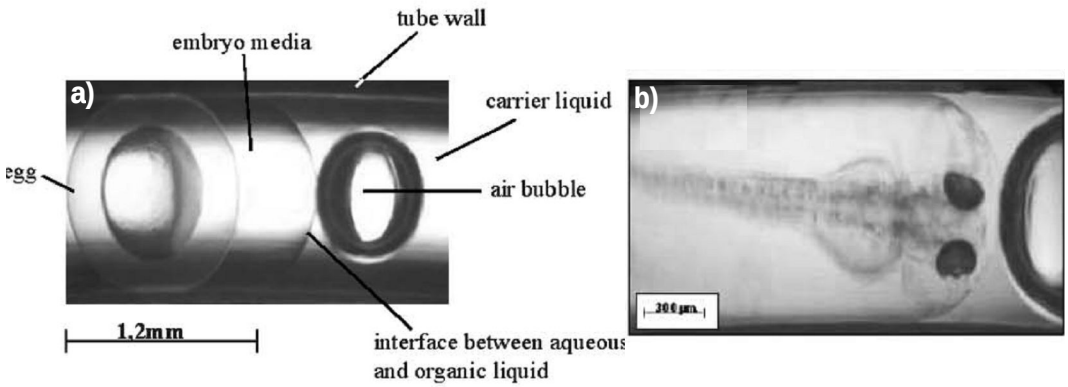

Figure 20. Zebrafish embryos encapsulated into aqueous plugs stored in Teflon tubing. (a) *Multicell stage of a Danio rerio embryo.* ***(b)*** *Hatched embryo with an age of 75h (Funfak et al., 2007).*

Our studies also investigated the development of a two-phase microfluidic platform for the screening of synthetic small molecules. Hence, the generation of chemically-distinct drops was required. This can, in theory, be achieved by either encapsulating cells expressing different variants of genetically-encoded entities (e.g. peptides, antibodies, enzymes) on the single-cell level (Figure 21a), or by encapsulating different small molecules (e.g. libraries of drugs candidates) into each drop (Figure 21b, 21c). Moreover, to detect hits in a rapid manner, a desired effect must be coupled to an easily detectable readout signal (e.g. fluorescence). In the case of genetically-encoded entities, droplets containing molecules with desired properties can be sorted. Subsequently, the identity of these hits can be revealed by sequencing the gene variant (e.g. antibody) expressed by the encapsulated cell. However, the screening of synthetic molecules in two-phase microfluidic systems still remains challenging. One possible approach might be the application of individually labelled beads displaying variants of a small molecule library

(one-bead-one-compound libraries) (Figure 21b). Beads could be individually encapsulated and after the screen, depending on the labelling method, hits could be identified either on chip (e.g. optical tags) or after sorting (e.g. mass spectroscopy tags). Possible problems of this approach could be the manipulation of beads in drops due to their size since standard library synthesis is done on beads of 90 to 300 µm in diameter (Brown et al., ; Liu et al., 2002), as well as the generation of large libraries of tags compatible with the screening assay (Liu et al., 2002; Pregibon et al., 2007).

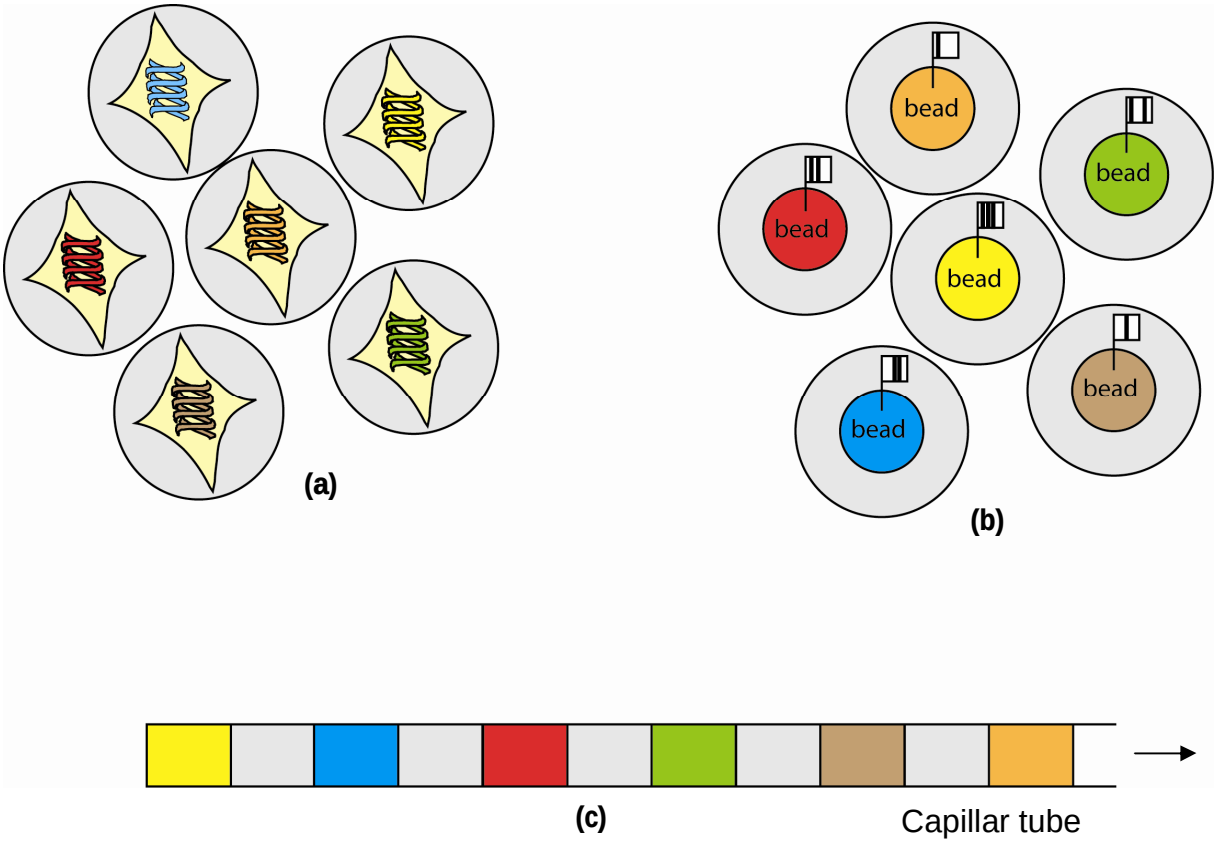

***Figure 21. Different approaches for the screening of chemically distinct droplets**. **(a)** Droplets of different composition can be obtained by either encapsulating cells expressing different variants of genetically-encoded entities or, **(b)** individually labelled beads displaying a library of small molecules (OBOC), or **(c)** by sequentially loading compounds into a capillary tube in form of aqueous plugs spaced by oil (spatial encoding).*

A second approach is the encapsulation of compounds sequentially in a fixed order, thus abolishing the need for labelling and decoding (Figure 21c). Hovewer this approach is currently limited by a lack of automation, the time required to generate thousands of

chemically-distinct drops and problems resulting from interfacing the compound array with the microfluidic world.

Whitesides and coworkers have described the generation of chemically distinct plugs loaded into a length of tubing. They used two approaches to generate the array of plugs based on a liquid/air two-phase flow system. One was based on a syringe connected to a length of tubing manually operated to withdraw volumes from different wells (Figure 22a). The other was based on several cartridges (pieces of tubing) connected at one end to the vacuum via an array of computer-controlled valves and at the other end immersed into the reagent well (Figure 22b). To deliver the sequence of reagents into the microchip, the cartridge was connected to a microfluidic device and subsequently vacuum was applied to the outlet using a simple hand-operated pump (Linder et al., 2005). In both cases the cartridges were manually dipped into the different wells and high cross-contamination levels (14 %) were observed between consecutive reagent plugs, most probably due to a thin film of reagents on the wall of the cartridge. Consequently, this approach resulted in a slow non-automated low-throughput process (each cartridge contained only 10 plugs and the cartridges had to be moved manually between the wells).

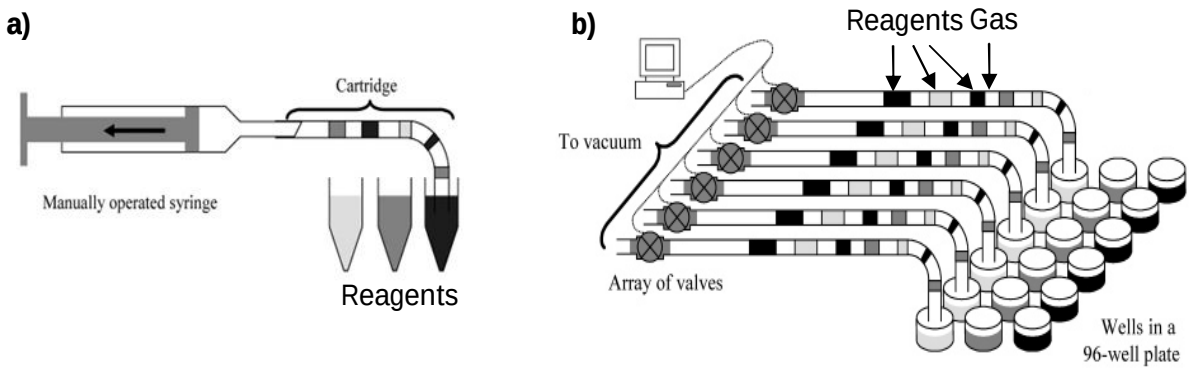

Figure 22. Preparation of an array of plugs. (a) *Liquid/air is aspirated into a cartridge using a manually operated syringe, or* ***(b)*** *using computer-operated valves connected to a vacuum source (Linder et al., 2005).*

Ismagilov and coworkers have implemented another approach based on immersing the end of the target tubing into the sample solutions and an oil reservoir (two- (liquid/liquid) and three- (liquid/liquid/air) phase flow systems) in an alternating fashion (manually or by

using an X-Y-Z micromanipulator) while aspirating the desired volumes (Figure 23) (Chen et al., 2008; Chen and Ismagilov, 2006; Chen et al., 2007; Hatakeyama et al., 2006). On-chip manipulations, such as the splitting of samples into small-volume subunits and the addition of further compounds to each plug have been shown (Adamson et al., 2006; Li et al., 2007). However, no data about cross contamination and throughput was published for the automated system, though it can be assumed that there are certain limitations. For example, this approach neither allowed any washing steps, nor could it be parallelized.

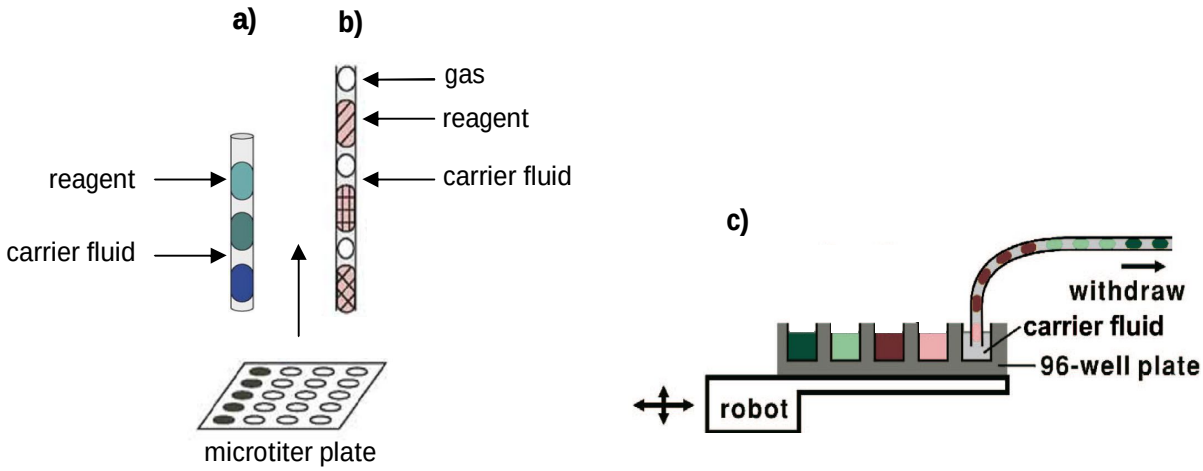

Figure 23. Different approaches of compound separation. *Manually generated* ***(a)*** *two- (liquid/liquid) and* ***(b)*** *three- (liquid/liquid/gas) phase flow systems (Chen and Ismagilov, 2006; Hatakeyama et al., 2006).* ***(c)*** *Automatically generated two-phase flow systems using a robotic x,y,z displacement stage (Chen et al., 2008).*

In an alternative system, all samples of a microtiter plate have been covered with two additional fluid layers (oil and washing buffer). Thereby, plugs were formed by first aspirating the aqueous solution from the well and subsequently aspirating oil. Finally the tip was washed in the washing buffer layer before aspirating the next sample (Figure 24a). Fluid transport was provided by two synchronized syringe pumps interfaced with a customized X-Y-Z displacement stage. One pump ensured a continuous fluidic circulation into the target tubing, while the other was aspirating new samples sequentially from different wells of the microtiter plate. The two pumps switched their function by a two-state loop (Figure 24b) to continuously generate plugs without increasing the pressure of the system, thus increasing the throughput. In this way, plugs with negligible cross-

contamination were generated. However, no on-chip manipulations such as the splitting of samples into small-volume subunits (e.g. to generate replicates), nor the addition of further compounds to the initially generated plugs (e.g. by droplet fusion) were integrated into the system. (Chabert et al., 2006).

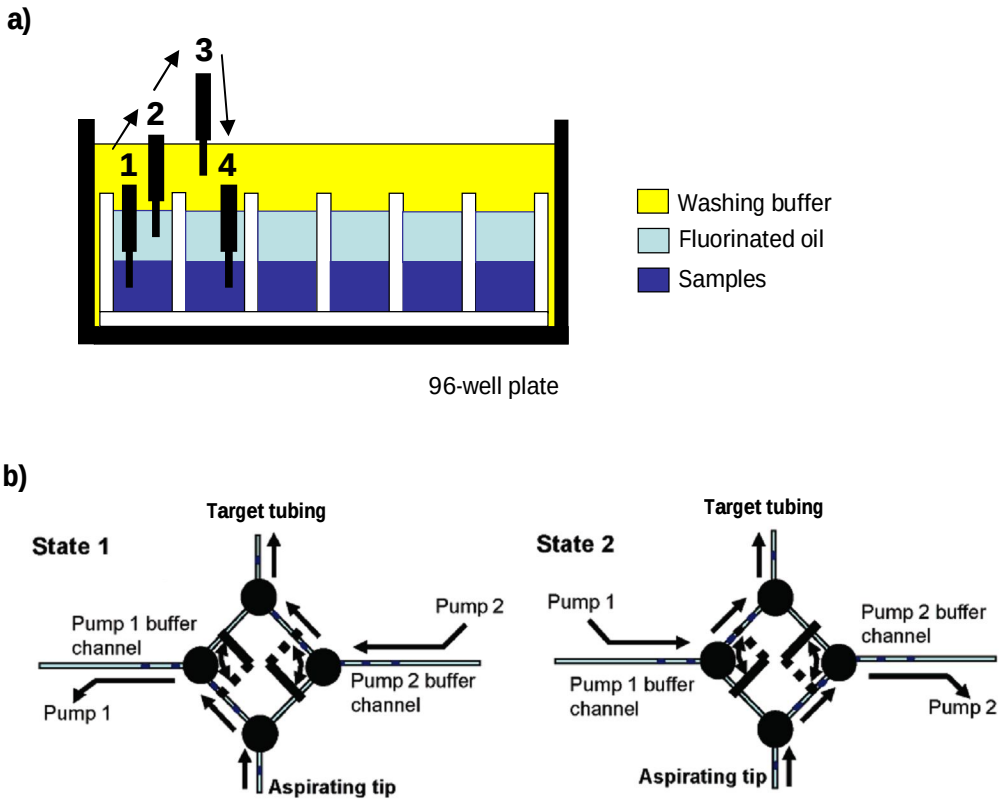

***Figure 24. Technical set up for the generation of chemically distinct plugs for PCR reactions**. **(a)** The generation of plugs consists of different steps. First, a certain aqueous volume is aspirated from a well in a microtiter plate (1); second, the tip is lifted and aspirates oil from the same well (2); third, the tip moves into the cleaning buffer (3); and finally into the next well (4). **(b)** A two-state loop with two synchronized syringe pumps controls the fluidic pathway. In state 1 pump 1 sequentially forms samples from the aspirating tip, while pump 2 pushes continuously the plugs formed in state 2 of the previous cycle into a target tubing. In state 2 pump 2 sequentially forms the plugs, while pump 1 pushes the plugs formed in state 1 of the previous cycle into a collecting tube. The fluorinated oil is fixed in between the two aqueous layers due to a special hydrophobic/fluorophilic treatment of the wells (Chabert et al., 2006).*

1.2.2 Viral-inhibition assays compatible with on-chip readouts systems

HTS of compound libraries is a key element in drug discovery. Typically assays are performed by coupling a specific biomolecular event with a detectable readout signal. This can be achieved using measurements of radioactivity, photon absorption or photon emission. Radioactive methods have been successfully applied in HTS, but became unpopular due to problems related with the handling of radioactive materials and improved non-radioactive techniques. Assays based on photon absorption impose limits on assay design and miniaturization since they typically provide low sensitivity. In contrast, photon emission is a good readout signal perfectly suited for HTS since it can be coupled to many different biological events and can be detected at high speed and high sensitivity. Photon emission is achieved primarily through fluorescence and chemiluminescence. Although both processes create photons through energy transitions from excited states to their corresponding ground states, they differ in how the excited states are generated. This has major consequences on the brightness and the background level of an assay. In fluorescence, the energy needed for exciting the molecule is gained by the absorption of light, whereas in chemiluminescence it is gained by exotermic chemical reactions. In consequence, the signal in fluorescent assays tends to be much brighter since the samples can be excited at very high rates (nanoseconds to milliseconds) (Fan and Wood, 2007). Even though high influx of photons also leads to higher background activity, fluorescence is preferred over chemiluminesce for microfluidics systems since the readout can be performed at very high rates (chemiluminescence assays typically require exposure times of several seconds).

In our study we were focusing on viral inhibition assays that could be performed inside the drops. For this purpose we established a series of fluorescence assays coupling a positive fluorescence signal with the inhibition of viral transduction. Most commonly, cell-based assays for the inhibition of viral infections couple a positive readout signal (e.g. an increase in fluorescence) to the infection itself and not to its inhibition. These systems are based on the expression of a reporter gene (e.g. *GFP, YFP*) within the host cell upon viral cell-entry (Daelemans et al., 2005; Siegert et al., 2005; Westby et al., 2005). When

screening for potential inhibitors of viral infection, viral particles and host cells are incubated in the presence of the compound to be tested. Subsequently, the reporter signal is determined (e.g. by measuring fluorescence). A decreased signal of a given sample (in comparison to the control sample without any test compound) should hence result from a potent inhibitor of viral cell-entry. However, a drug candidate that inhibits the reporter gene expression (e.g. by killing the host cell) instead of the viral cell-entry will inevitably be selected as a false positive. Therefore, coupling a positive signal with the inhibition of viral infection seems to be much more desirable. When using viral species mediating severe cytopathic effects (CPEs), this can be achieved by determining cell survival subsequent to the co-incubation of host cells, virus and the drug candidate (Sidwell and Huffman, 1971; Sidwell and Smee, 2000). However, these approaches are not well suited for high-throughput screening since they usually require time-consuming microscopic analysis of the samples and the use of replication competent viruses. This not only results in the need for high containment level laboratories but also makes it impossible to distinguish between inhibition of cell-entry and replication. Furthermore, many viruses do not show detectable CPEs in cell culture experiments (Dorner and Coffin, 1986).

Since parts of this work deal with the use of pseudotyped retroviral particles, the following subchapters provide a brief introduction into the field of retrovirology.

1.2.2.1 Retroviruses

1.2.2.1.1 Structure of retroviruses

Retroviruses are enveloped viruses with a diploid genome packaged as single stranded RNA of about 7-12kb. The genome is linear and has positive polarity.
The viral genome includes the structural genes gag, pol and env. These viral genes are flanked by so called long terminal repeats (LTRs) which are required for their integration into the host cell genome and efficient transcription. The LTRs can be divided into three elements: U3 forms the 5' end of the provirus after reverse transcription and it contains

the promoter elements responsible for the initiation of transcription; R is a sequence which forms a direct repeat at both ends of the genome; and U5 is the first part of the genome to be reverse transcribed, forming the 3' end of the provirus genome. During reverse transcription the enzymes “jumps” from one end of the template to the other. The psi-site (Ψ) is the sequence that ensures efficient packaging of the viral RNA into the particles (Figure 25a).

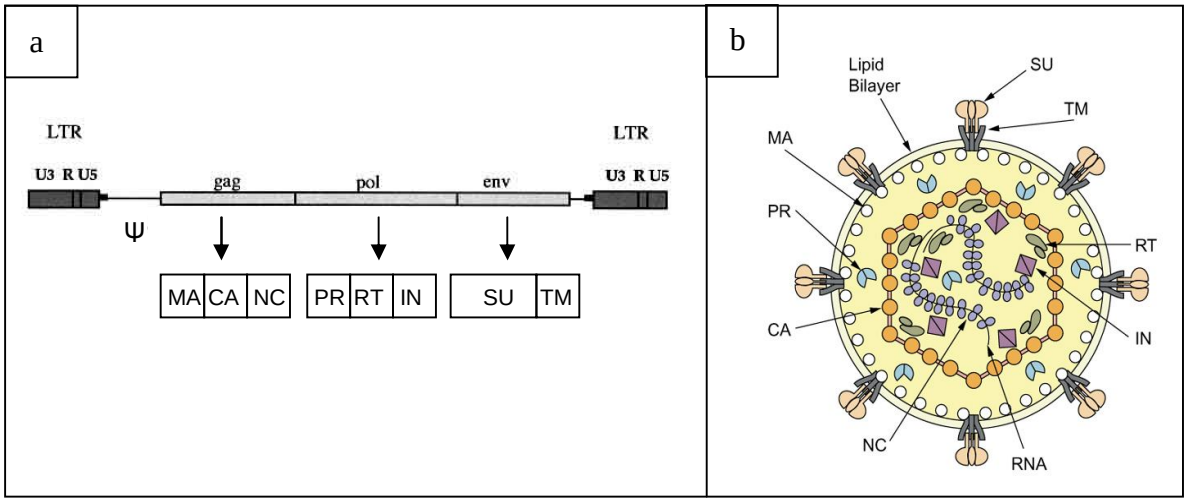

***Figure 25. Genome and structure of C-type retroviruses**. **(a)** Schematic structure of a C-type retroviral genome. The viral genome comprises the genes gag, pol and env. LTRs are long terminal repeats situated at both ends of the genome. They consist of three elements: U3 (promoter of the transcription process), R (terminal repeated sequence) and U5 (enhancing integration and the reverse transcription process). The Psi-site sequence (Ψ) ensures packaging of the viral RNA into the particles (Picture taken from: http://www.bioscience.org/2003/v8/d/967/figures.htm). **(b)** Schematic structure of a C-type retroviral particle. The viral genome (RNA) is encapsulated by the nucleocapsid protein (NC). The core structure of the virus is formed by capsid proteins (CAs) which surround the NC and the enzymes reverse transcriptase (RT) and integrase (IN). The core structure and the enzyme protease (PR) are enveloped by a lipid membrane from the host cell. The Env proteins formed by the transmembrane domain (TM) and the surface unit (SU) are embedded within the membrane and the matrix proteins (MAs) are attached to the inside of this lipid bilayer (Picture taken from the book Retroviruses by John M. Coffin, Stephen H. Hughes and Harold E. Varmus, 1997).*

All viral proteins are synthesized as precursor proteins, which are posttranslationally cleaved by viral and cellular proteases into single functional proteins. The gag gene encodes the internal structural protein of the virus. Gag is proteolytically processed into the mature proteins MA (matrix), CA (capsid), NC (nucleocapsid) (Figure 25b). The pol gene encodes the enzymes reverse transcriptase (RT), which contains both DNA polymerase and associated RNase H activities; integrase (IN) mediating integration of the

viral genome in the host cell genome and protease (PR) acting late in the assembly of the particle (Figure 25b). The env protein is proteolytically cleaved into the Env protein consisting of two non-covalently linked polypeptides: the surface unit (SU) glycoprotein and the transmembrane domain (TM) of the virion (Figure 25b). The SU of the Env protein determines the tropism of the viral particle.

1.2.2.1.2 Replication cycle of retroviruses

Since retroviral RNA molecules are not able to replicate autonomously, they need to be integrated in the host cell genome; even though there are some RNA viruses that do not integrate but still replicate. Integration is also important for transcription of viral DNA into mRNAs encoding viral proteins. The sequences that determine the integration of the viral DNA in to the host DNA are found both at the termini and at the internal edges of the LTRs. These bases are crucial for recognition of the viral DNA ends by IN.

The first step of the retroviral replication cycle is viral cell-entry (Figure 26), which is subdivided into three major events: adsorption, penetration and uncoating. During adsorption the virus attaches to the surface of its host cell, in particular to specific cellular receptors, such as glycoproteins, phospholipids or glycolipids. Penetration rapidly follows adsorption; the virus enters the host cell through receptor-mediated endocytosis (endocytosis is not the main path entry for HIV) and subsequent membrane fusion. Then, the viral capsid is degraded by viral enzymes or host enzymes thus releasing the viral nucleic acid. In a second step, the viral (+) ssRNA is reverse transcribed in the cytosol into double stranded DNA by the reverse transcriptase (RT) (Figure 26) (recent studies say that uncoating takes places after RT and the signal is the synthesis of falp DNA). Subsequently it enters the host cell nucleus where it is integrated in the host cell genome by the integrase (IN) (Figure 26). The resulting so called provirus is transcribed by the host cell machinery in the same way as endogenous genes. Expression is promoted by the viral LTR which serves as efficient promotor.

All retroviral proteins except Env are translated as polyprotein precursors, which are cleaved by the viral protease into functional elements. These posttranscriptional modifications occur during budding or maturation of already released particles. The

polyprotein synthesized at the earliest stage of replication is Gag, which is believed to initiate the budding process. Pol is also synthesized as a polyprotein, but never independent of Gag expression. The Pol-encoded proteins are then directed by Gag to the site of assembly, close to the host cell membrane (Figure 26). In contrast to all other viral proteins, the Env polyprotein is a translational product of spliced viral mRNA. It includes the SU and TM subunits and an additional N-terminal signal peptide, which ensures routing to the secretory pathway. During translocation across the membrane of the endoplasmic reticulum (ER) it is cotranslationally cleaved off and a hydrophobic region located within TM serves as membrane anchor. Within the ER, the Env precursor protein is heavily glycosylated at Asn residues and oligomerizes into trimers. Then, upon passage through the Golgi apparatus, cleavage between SU and TM is performed by furin, a cellular protease.

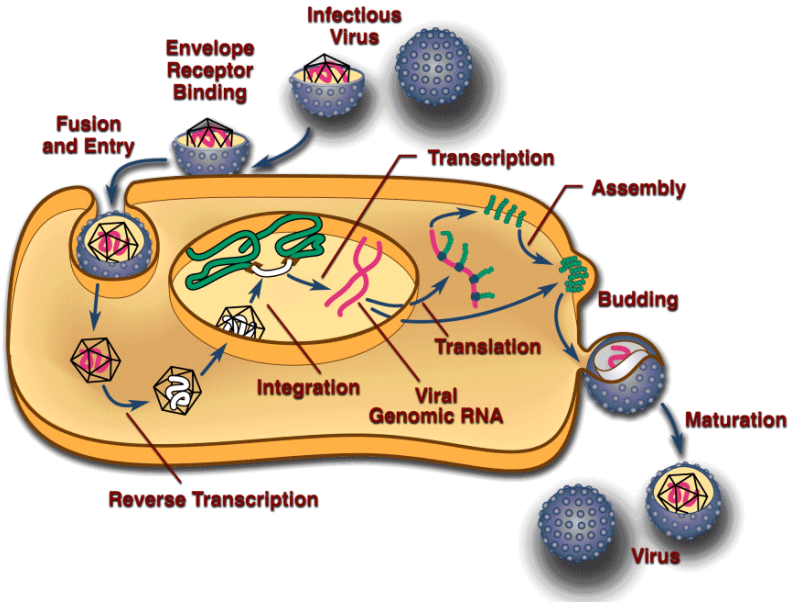

Figure 26. Replication cycle of retroviruses. *After binding to the cellular receptor, the envelope protein mediates the fusion of the particle and the cell membrane. The viral capsid is degraded and the viral genome is released into the cytosol. (+)ssRNA is reverse transcribed by RT into dsDNA, before it is integrated into the host cell genome by IN within the nucleus. Subsequently, the viral genome is transcribed by the host cell machinery in the nucleus and translated in the cytoplasm. All viral glycoproteins are transported through the cytosol to the side of budding, except the Env protein, which is routed to the cell surface. After the particles are assembled and released from the cell, a further maturation step takes place: proteolytical cleavage of the gag/pol polyprotein renders the virus infectious (Picture taken from http://www.ncbi.nlm.nih.gov/retroviruses/files/retroviral_lifecycle.gif*

Subsequently, the Env trimers are guided to the cell surface by vesicular transport, where they diffuse laterally to the site of budding. Finally, particles are released and undergo a further maturation step (Gag/Pol proteins are proteolytically cleaved by a protease) (Figure 26). For most retroviruses the budding site is a distinct region of specific composition rather than an arbitrary location on the cell surface. Lipid rafts which are rich of cholesterol and glycosphingolipids have been identified as primary sites of budding in case of HIV (Holm et al., 2003).

1.2.2.1.3 Retroviral pseudotyped vectors

A pseudotyped vector is a viral particle in which the envelope protein and the structural proteins (e.g. matrix, capsid, nucleocapsid) originate from different viral species. Pseudotyped vectors have several experimental and clinical applications.

The envelope protein of a virus determines its host cell tropism; therefore, pseudotyping a viral vector can mediate the ability of either transducing several cell-lines or just a specific cell-line (Figure 27). For example, retroviral pseudotypes bearing the Hepatitis B virus (HBV) surface antigens transduce solely human primary hepatocytes (Sung and Lai, 2002). In contrast, MLV particles pseudotyped with the Env protein of the Gibbon ape Leukemia Virus (GaLV) are able of transducing cells of human, simian, feline, canine, bovine, avian and rodent origin via the GLVR1 receptor (von Kalle *et al*. 1994). Lentiviral vectors, in contrast to C-type retroviral vectors, are able to transduce non-dividing cells. Besides, they are frequently pseudotyped with VSV-G (most human cells have cellular receptors for this G protein) on their surface to allow transduction of different human tissues.

Moreover, a pseudotyped virus can have an altered stability and/or interaction with the host immune system that increases its efficacy. For example, some pseudotyped viruses can be produced and concentrated more efficiently than the viral vector with its homologous envelope. It turned out that HIV particles concentrated by ultracentrifugation present low transduction efficiencies due to the high sensitivity of the envelope to the centrifugal forces (SU and TM dissociate resulting in non-infective particles; a phenomenon termed “shedding”). Besides, MLV(GalV Env) pseudotyped particles enable

higher transduction efficiencies on hematopoetic stem cells (HSCs) in comparison to MLV vector particles carrying the MLV Env protein (von Kalle et al., 1994).
Additionally, pseudotyping allows separating the entry process from other steps during viral replication and therefore the screening for viral cell-entry inhibitors or viral receptors (Sanders, 2002).

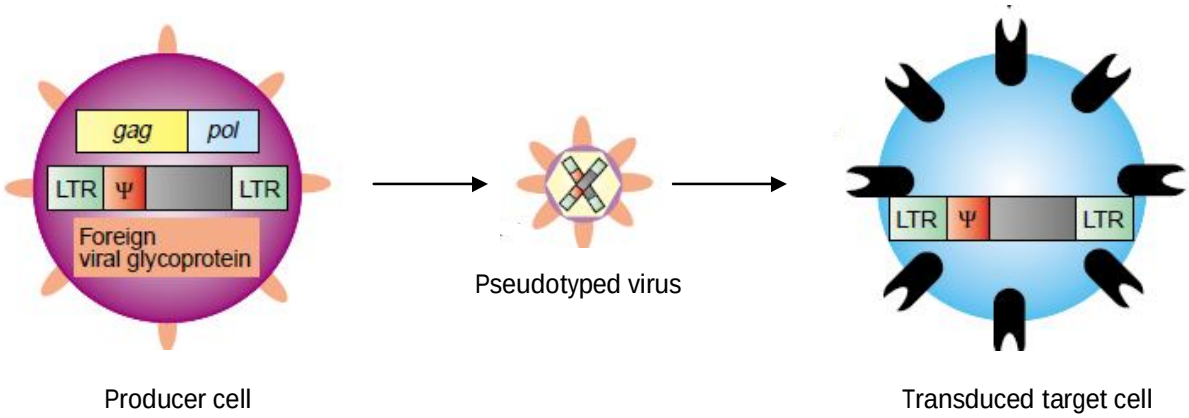

Figure 27. Schematic representation of virus production and cell transduction using replication-defective pseudotyped viruses. *Gag/pol, transfer and env genes are expressed in the producer cells from three different DNA plasmids. Gag/pol encodes the retroviral core structural proteins, reverse transcriptase and replication enzymes. The transfer gene is flanked by LTRs containing the signals for its integration and transcription. The psi-site (Ψ) signal ensures efficient packaging of the transfer gene into the recombinant particle. The envelope protein determines the viral tropism, therefore different Env-plasmids can be used to generate particles with different tropism (Sanders, 2002).*

Replication-defective retroviral vectors (DRVs) are viruses that can only deliver their transfer gene (TG) to a single target cell; they are unable to replicate and spread within a culture and can therefore be used for a single transduction round only. Instead of the wild-type genome, therapeutic or marker genes are packaged into the particles. Their coding genes and *cis*-acting sequences (which increase the transcription efficiency of genes) are separated on distinct nucleic acid molecules to avoid the reconstitution of replication-competent viral particles (Figure 28) by recombination of all viral genes on a single packagable vector. In contrast to replication-competent retroviral vectors (RRVs), the use of DRVs prevents the need for high containment level laboratories, increasing the safety conditions.

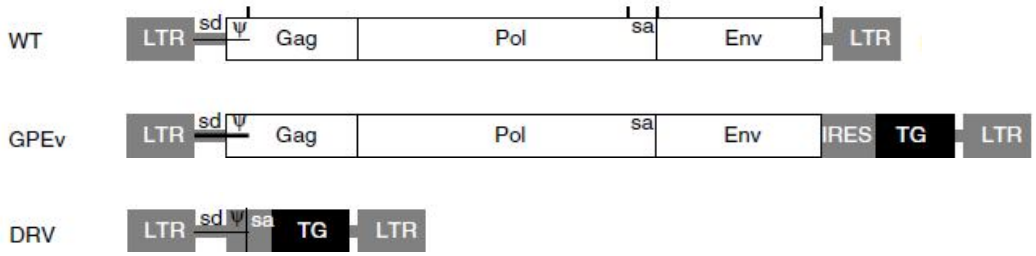

Figure 28. Schematic representation of vector genome structures*. The wild-type (WT) genome encodes all viral genes (gag, pol and env) as required for replication. For therapeutic purposes, a transfer gene (TG) can be additionally introduced in the wild type genome resulting in GPEv (gag/pol/env) particles. In contrast, defective replication viruses (DRV) package a vector solely encoding the transfer gene and are therefore not replication competent (Trajcevski et al., 2005).*

1.2.2.1.4 RNAi systems

Silencing of gene expression by RNA interference (RNAi) has become a powerful tool for specific gene silencing in mammalian systems as well as in worms, flies or plants. This system can be used to study specific gene functions by downregulating the expression of a gene of interest at the posttranscriptional level (Meister and Tuschl, 2004; Sandy et al., 2005).

RNAi sequences are double-stranded RNA molecules (dsRNA). According to their length and shape they can be divided into long RNAi molecules (500 bp), small interfering RNA (siRNA, <30 bp) and short hairpin RNAs (shRNA, <30 bp). The most effective approach to knockdown a particular gene in a transient way is to transfect synthetic siRNA. However if the goal is long-lasting gene silencing, stable expression of short hairpin RNAs is preferable. Usually, dsRNAs cannot be generated by the cell machinery. Hence the only way of obtaining continuously complementary RNA strands with high probability of binding is the integration of a gene encoding two complementary sequences (target sense sequence and target antisense sequence) separated by a hairpin loop (shRNA) into the cell genome (Figure 29). The binding reaction between sequences inside the same molecule, like in a hairpin loop, are always more efficient than intermolecular reactions

such as the binding between two independent mRNA each encoding a different complementary sequence.

During the silencing process, dsRNAs (complementary to the gene of interest) are first digested into siRNA duplexes by the action of ribonuclease III, also known as Dicer, in an ATP-dependent manner. Second, these siRNAs bind to a nuclease complex and form the RNA-induced silencing complex (RISC). Subsequently, RISC is activated by ATP before unwinding of the siRNA duplexes occurs. Finally, the active RISC targets the native, homologous transcripts by base pairing and subsequent cleavage of the mRNA, thus downregulating the expression of the gene of interest (Figure 29).
Long (about 500 bp) dsRNAs can induce efficient and highly specific gene silencing when introduced into worms, flies or plants.

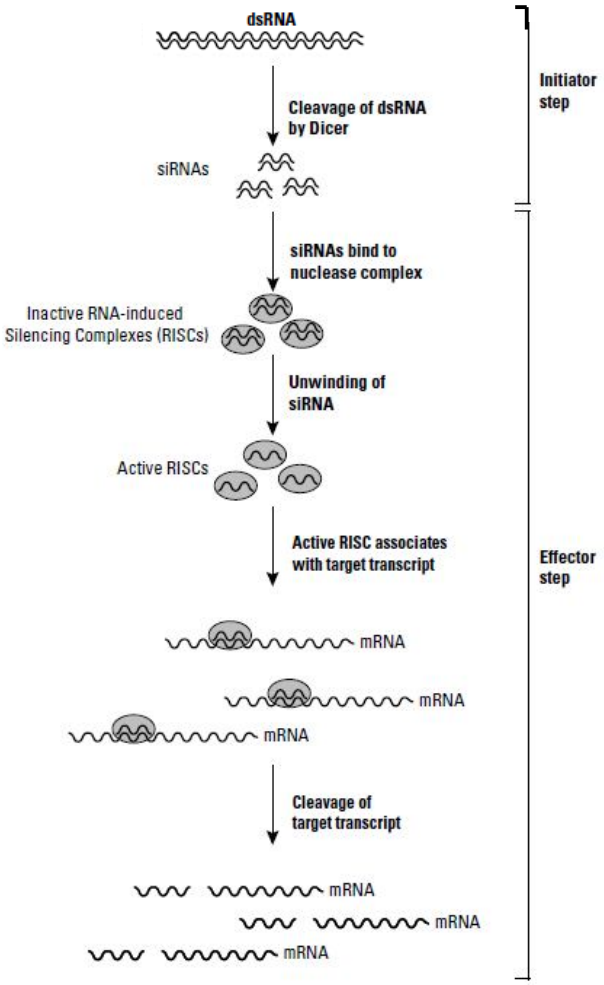

Figure 29. Mechanism of RNA interference (RNAi). *dsRNA is cleaved into several siRNAs by a cytoplasmic ribonuclease called Dicer. The antisense strand of the siRNA serves as a template for the RNA-induced silencing complex (RISC) to recognize and cleave a complementary messenger RNA (mRNA), which is then rapidly degraded, entailing the downregulation of the expression of the gene of interest (Scheme taken from BD™ Knockout RNAi Systems User Manual).*

The design of an shRNA (Paddison et al., 2002) requires the selection of the target sequence within a gene of interest. Some selecting properties are: the GC content should be between 30 % and 70 % (50 % is ideal) and secondary structure and long base runs should be avoided since they might interfere with a further annealing step. Moreover the number of nucleotides should be 19, and they should be situated immediately after an AA dimer but not within the 5' and 3' untranslated regions (UTRs) and neither near the start codon (within 100bp) as these may be richer in regulatory protein binding sites.

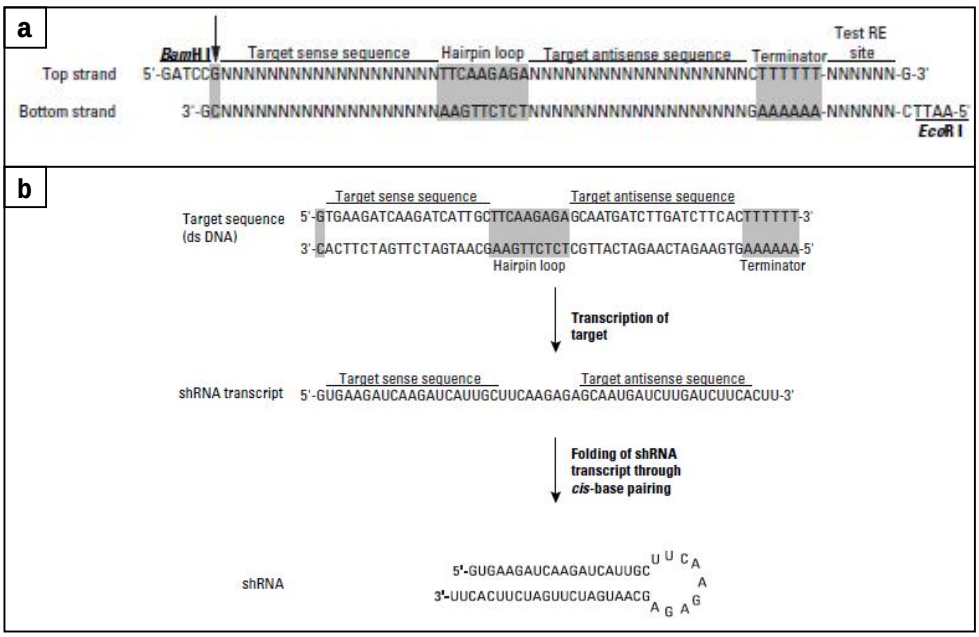

Figure 30. Cloning and expression of short hairpin RNA (shRNA). (a) *On the DNA level, the sequence of interest should have two restriction site overhangs to facilitate cloning,, a purine residue required for RNA Pol III to initiate transcription (denoted with an arrow) and a target sense sequence corresponding to the target gene. Moreover, it should have a target antisense sequence to ensure proper orientation for correct formation of the hairpin structure, a poly(T) sequence to mark termination and a unique restriction site (Test RE site) for analytical purposes.* ***(b)*** *Transcription of DNA into shRNA (Scheme taken from BD™ Knockout RNAi Systems User Manual).*

After knowing the target sequence, a second step is the design of the two complementary oligonucleotides to be inserted into the expression vector. The oligonucleotides should

include: an RNA Pol III initiator sequence for efficient transcription based on a purine, an RNA Pol III terminator sequence consisting of a 5-6 nucleotide (nt) poly(T) and a 7-9 nt hairpin loop sequence. Additionally it should include two restriction sites (e.g. 5'-*BamHI* and 5'-*EcoR* in the commercially available pSIREN vector) overhang to enable directional cloning of the annealed oligonucleotides into a vector, the target sense and antisense sequence and a unique restriction site immediately downstream of the terminator sequence for restriction digest analysis to confirm the presence of the cloned insert (Figure 30). The antisense sequence ensures proper orientation for correct formation of the hairpin structure.

1.3 Aim of the thesis

The aim of this work was the development of novel screening technologies for the identification of drug candidates; in particular the development of two-phase microfluidics systems for cell-based assays. In these systems aqueous microdroplets within a continuous oil phase serve as miniaturized reaction vessels (volumes of pico- to nanolitres). Two main challenges that had to be addressed were the cultivation of cells within droplets and the generation of chemically-distinct drops as required for screening purposes.

2. Material and methods

2.1 Molecular biology

2.1.1 Plasmids and vectors

The plasmid pMD-G encodes the vesicular stomatitis virus G-protein (VSV-G) (Randow and Sale, 2006).

The plasmid pOGP3 encodes the murine leukemia virus gag/pol genes (Randow and Sale, 2006).

The MLV-packagable vector pCMVnls-lacZ, encodes the β-galactosidase reporter gene (Merten et al., 2006) and was used to determine the viral titers and perform the fluorescein di-β-D-galactopyranoside (FDG) assay.

The MLV-packagable vector pSIREN-puro encodes an shRNA with the sequence 5'−GATCCGCTGCAAGAACTCTTCCTCATTCAAGAGATGAGGAAGAGTTCTTGCAGTTTTTTACGCGT G-3' targeting the puromycin N-acetyltransferase expression. The cloning procedure is described in the chapter *2.1.3.*

The MLV-packagable vector pSIREN-MRCI encodes an shRNA with the sequence 5'−GATCCGGCCACACTCCTTGCCCTTTTTCAAGAGAAAAGGGCAAGGAGTGTGGCTTTTTTACGCG TG −3' targeting the expression of a membrane-anchored form of tissue plasminogen activator (tpA) (Granieri et al., 2009).

The MLV-packagable vector MP71 encodes the herpes simplex virus thimidine kinase fused to the N-terminus of CD34 (HSV-TK-CD34). It was kindly provided by Christopher Baum (Fehse et al., 2002).

2.1.2 Oligonucleotides

The following oligonucleotides were used for the cloning of plasmids encoding shRNAs for gene silencing purposes.

shPuro(+):
5'−GATCCGCTGCAAGAACTCTTCCTCATTCAAGAGATGAGGAAGAGTTCTTGCAGTTTTTTACGCGT
G-3'

shPuro(−):
5'−AATTCACGCGTAAAAAACTGCAAGAACTCTTCCTCATCTCTTGAATGAGGAAGAGTTCTTGCAGC
G −3'

shtPA(+):
5'−GATCCGGCCACACTCCTTGCCCTTTTTCAAGAGAAAAGGGCAAGGAGTGTGGCTTTTTTACGCG
TG −3'

shtPA(−):
5'−AATTCACGCGTAAAAAAGCCACACTCCTTGCCCTTTTCTCTTGAAAAAGGGCAAGGAGTGTGGCC
G −3'

2.1.3 Cloning of the vector pSIREN-puro

To achieve long-lasting silencing of the puromycin gene, an shRNA-enconding vector was generated. For that purpose, the vector pSIREN-RetroQ (Figure 1) was double digested with BamHI and EcoRI in a sequential order to avoid star activity of BamHI in the EcoRI buffer. In parallel, the insert shRNA-puro was generated by annealing two oligonucleotides with BamHI/EcoRI-compatible overhangs (see chapter *2.1.2*). Then, the insert and the backbone vector were ligated. Subsequently, the puromycin N-acetyltransferase gene in the backbone of the vector pSIREN-puro was inactivated by

digestion with BsiWI, generation of blunt ends using the Klenow polymerase and subsequent relegation (out of frame).

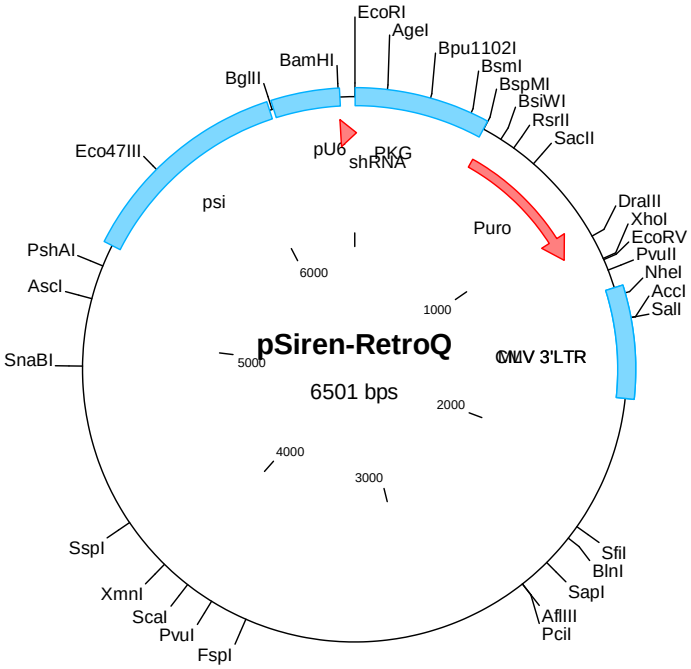

Figure 1. Restriction site map of the vector pSiren-RetroQ.

a) Standard restriction reactions for preparative purposes

6 µg DNA

10 µL 10x enzyme buffer (Fermentas)

50 U enzyme (Fermentas)

H_2O to a final volume of 100 µL

b) Standard restriction reactions for analytical purposes

0.6 µg DNA

2 µL 10x enzyme buffer (Fermentas)

10 U enzyme (Fermentas)

H_2O to a final volume of 20 µL

All restriction reaction mixtures were incubated for 3 h at 37°C while shaking at 500 rpm. A sample of 5 µL of each digestion was taken and applied to gel electrophoresis for analytical purposes. All DNA restrictions were performed using commercially available restriction endonucleases from Fermentas according to the manufacturer's instructions.

In case of double digestion with two different buffers, DNA was purified after the first digestion using the Promega kit 'PCR clean up system'. Afterwards, the purified DNA sample was incubated with the new reaction mixture for the second digest. For analytical and preparative purposes the digested samples were applied to gel electrophoresis. Finally, the DNA was extracted using the 'Gel Extraction Kit Genomics' from Millipore (see chapter *2.1.5* for details).

c) Annealing of oligonucletoides

For cloning vectors encoding short interfering RNAs, double-stranded oligonucleotides were directly cloned into the vector pSIREN (Clontech).
The oligonucleotides (VWR) were first resuspended in TE buffer at a concentration of 100 µM. As the next step, the oligonucleotides of the positive and the negative strand were mixed at a 1:1 ratio, obtaining a final concentration of 50 µM each. Subsequently, the annealing process was done in a thermal cycler (EngineTetrad2, MJ Research) using the following programme:

95°C for 30 sec
72°C for 2 min
37°C for 2 min
25°C for 2 min

Heating to 95°C ensured dissociation of the internal hairpin of each oligonucleotide, thus promoting intermolecular annealing. Finally, after a subsequent stepwise-decrease in temperature, the annealed oligonucleotides were stored at -20°C

d) Ligation of digested fragments

Recombination of DNA is usually performed by ligation of two double stranded nucleic acid molecules exhibiting complementary overhangs or blunt ends. This reaction can be accomplished using T4 DNA ligase (NEB) which catalyzes the formation of phosphodiester bonds between the fragments under consumption of ATP. The following protocol was used routinely:

0.7 µg DNA (molar ratio of backbone to insert = 1: 3)
2 µL 10x T4 DNA ligase buffer
100 U T4 DNA ligase
H_2O to a final volume of 20 µL

The reaction mixture was incubated for 12 h at 4 °C.
As a negative control, the backbone was incubated with the reagents described above but without insert.

e) Klenow fill-in of digested fragments

For deactivating the puromycin resistance gene in the vector pSIREN, the vector was first digested with a restriction enzyme, BsiWI (Fermentas). Afterwards, the newly generated sticky ends were treated with klenow polymerase to obtain blunt ends with a redundant sequence and a subsequent religation resulted in a frame-shift within the puromycing N-acetyltransferase gene. The following protocol was used for klenow fill-in:

0.1 µg digested DNA
2 µL 10x reaction buffer
0.5 µL 4 dNTP (0.05 mM)
2.5 U klenow fragment
H_2O to a final volume of 20 µL

The mixture was incubated for 10 min at 37°C, and subsequently the reaction was stopped by heating at 70°C for 10 min. Finally, the DNA was put at -20°C.

To avoid the loss of DNA, religation was done without purifying the product after klenow fill-in. For religation, the compounds of the klenow buffer that differ from the ligase buffer were added to the sample. The klenow buffer contained: 500mM Tris HCl, 50mM $MgCl_2$, 10mM DTT; and the ligase buffer contained: 400mM Tris HCl, 100mM $MgCl_2$, 100mM DTT, 5mM ATP. The following protocol was used for religation:

10 µL DNA (after klenow fill-in)
1.9 µL DTT 1M
1 µL ATP 100 mM
0.2 µL BSA
100 U T4 DNA ligase (NEB)
H_2O to a final volume of 20 µL

The reaction mixture was incubated for 4h at 16°C.
As a negative control, the BsiWI-digested pSIREN backbone was applied to the procedure described above, but without performing the klenow fill-in step.

2.1.4 Agarose gel electrophoresis and DNA extraction from gels

Agarose gel electrophoresis allows to separate DNA molecules according to their size. The principle is based on the properties of polymerized agarose, which acts like a molecular sieve. Since DNA is negatively charged, it migrates through such gels upon application of an electric current in a size-dependent manner.

For purifying DNA fragments between 1 kb to 10 kb size, agarose gels containing 1 % agarose (Invitrogen, ultrapure) in Tris-Acetat EDTA (TAE) buffer (Invitrogen) and 1 µg/mL of ethidium bromide (Eth-Br) (Promega) were generated. For this purpose, agarose was added to TAE buffer and heated in a microwave for dissolving. After cooling down to 50°C (before solidification) Eth-Br was added. Prior to electrophoresis, DNA samples were

mixed with loading buffer (Novagen) and pipetted into the wells. The 1 kb ladder (Novagen) was used as a size standard.

After electrophoretic separation the DNA band of interest was cut out of the gel and transferred into an eppendorf tube. Subsequently, it was purified using the 'Gel Extraction Kit' from Millipore, followed by ethanol precipitation. The following protocol was used:

1. Excision of the gel slice and transfer onto the Millipore spin column
2. Centrifugation at 5000 rpm for 10 min
3. Centrifugation at 14000 rpm for 10 min
4. Ethanol precipitation:
   - 4.1 10 % (v/v) of 3 M NaAc, 80 % (v/v) of isopropanol, glicogen to a final concentration of 0.2 µg/µL and the DNA sample were mixed
   - 4.2 The sample was kept for 30 min at -20°C and centrifuged afterwards at 14000 rpm for 20 min at 4°C
   - 4.3 The supernatant was discarded and subsequently 200 µL of 70 % ethanol were added
   - 4.4 The sample was centrifuged at 14000 rpm for 5 min
   - 4.5 The supernatant was discarded and subsequently the tube was left opened on the table to let the remaining ethanol evaporate.
   - 4.6 The DNA was eluted using Millipore water and the concentration was determined in the Nanodrop system. Finally, the DNA was kept at -20°C

2.1.5 Generation of competent bacteria and transformation thereof

a) Generation of competent bacteria cells

Transformation of *E. coli* is used to amplify plasmid DNA through cellular replication. For this purpose, bacteria have to be pretreated in a special manner to become competent, thus allowing introduction of foreign DNA.

2.5 mL of an overnight culture of *E. coli* were used to inoculate 100 mL of fresh LB-media which was subsequently incubated at 37°C in a bacteria shaker at 200 rpm. Cells were allowed to grow to an OD_{600} of about 0.3-0.4, hence reaching the logarithmic growth phase. Then the culture was incubated on ice for 5 min, divided into two portions and pelleted at 6000 rpm for 10 min at 4°C. Subsequently, the cells were resuspended in 1 mL of 1 M $CaCl_2$ (chilled) and water was added to a final volume of 20 mL (final concentration of $CaCl_2$ = 50 mM). Afterwards 100 µL of the suspension were aliquoted into eppendorf tubes and frozen at -80°C.

b) Transformation procedure

For the transformation of chemically-competent bacteria, an aliquot of cells was thawed on ice and 100 ng DNA were added. After incubating the mixture on ice for 30 min, a heat shock at 42°C for 45 s was performed in a prewarmed water bath. Afterwards, the mixture was put on ice for 2 min. Subsequently, 900 µL of LB-media (Sigma) was added, and the mixture was incubated for 45 min at 37°C. Ultimately, 100 µL of the suspension was plated onto an LB agar-AMP-plate (1 % w/v Bacto-Trypton, 0.5 % w/v yeast extract, 1 % NaCl, 50 µg/mL ampicilin and 1.5 % agar; MP Biomedicals) and grown overnight at 37°C.

2.1.6 Plasmid preparation

Preparation of plasmids from bacteria was performed using the Qiagen plasmid kits according to the manufacturer's instructions. The basic principle of this method is the binding of DNA to anion-exchange columns under low-salt and pH conditions. RNA, proteins, dyes, and low-molecular-weight impurities are removed by a medium-salt wash. Plasmid DNA is eluted in a high salt buffer and then concentrated and desalted by isopropanol precipitation.

For purification of low amounts of DNA (miniprep), 5 mL culture were inoculated overnight in LB-AMP medium (1 % w/v Bacto-Trypton, 0.5 % w/v yeast extract, 1 % NaCl, 50 µg/mL ampicilin and 1.5 % agar; MP Biomedicals) at 37°C and 200 rpm. The next day, bacteria were centrifuged at 4000 rpm for 10 min (Eppendorf centrifuge 5810R) and the resulting pellet was purified using the Qiagen plasmid kit.
For purification of big amounts of DNA (maxiprep), 400 mL culture were inoculated overnight in LB-AMP medium (MP Biomedicals) at 37°C and 200 rpm. The next day, bacteria were centrifuged at 4000 rpm for 30 min (Eppendorf centrifuge 5810R), and the resulting pellet was purified using the Qiagen plasmid kit.

2.1.7 Nucleic acid sequencing

Nucleic acid sequencing was performed at MWG Biotech. For this purpose, DNA samples containing 2 µg of plasmid DNA were vacuum dried using a speed-vacuum centrifuge (Eppendorf concentrator 5301) and sent to the company via regular mail.
For sequencing the plasmids pSIREN-puro and pSIREN-MRCI the primer shRNA-seq3 with the sequence 5'- TTGGCTTTATATATCTTGTGG -3' was used, while for sequencing the puromycin gene within the vector pSIREN the primer shRNA-seq1 with the sequence 5'-GTAATAATTTCTTGGGTAGTTTG-3' was used.

2.2 Cell biology

2.2.1 Cells

HEK293T cells and HEK293T-tPA cells expressing a membrane-bound and HA-tagged form of tissue plasminogen activator (Granieri et al., 2009) were grown in Dulbecco's Modified Eagles Medium, DMEM (GIBCO). Jurkat cells were grown in Roswell Park Memorial Institute, RPMI medium (GIBCO). The media of the three cell-lines was supplemented with 10 % Fetal Bovine Serum, FBS (GIBCO) and 1 % penicillin (10 U/µL) /

streptomycin (10^4 µg/mL) (GIBCO). Cells were incubated at 37°C under a 5 % CO_2 atmosphere saturated with water.

For continuous cultivation, cells were split twice a week. HEK293T cells were trypsinized (0.25 % trypsin in PBS, GIBCO), resuspended in media and then centrifuged (at 1300 rpm for 6 min at 4°C using an Eppendorff 5810R tabletop centrifuge) to remove the trypsin. Subsequently, cells were resuspended in fresh medium and a fraction of the resulting suspension was seeded into new culture flasks. When cultivating Jurkat cells, a fraction of the cell suspension was directly seeded into new culture flasks and fresh medium was added.

2.2.2 Freezing and thawing of cultured cells

For short- and long-term storage, cells were kept at -80°C.

a) Freezing procedure

Cells were trypsinized (0.25 % trypsin in PBS, GIBCO) and resuspended in DMEM. Subsequently, a centrifugation step (1300 rpm for 6 min at 4°C) was carried out to pellet the cells. The resulting pellet was then resuspended in freezing medium (90 % FBS, 10 % DMSO), and divided into cryotube (Nunc) aliquots of 1.5 x 10^6 cells. These aliquots were frozen overnight at -20°C and then transferred to -80°C.

b) Thawing procedure

Cryotubes containing-cells were incubated in a water bath at 37°C until the samples were thawed completely. Then the cell suspension was immediately transferred into a falcon tube containing 15 mL of pre-warmed medium. Subsequently, cells were centrifuged (1300 rpm for 6 min at room temperature) to exclude the cytotoxic DMSO.

The resulting pellet was resuspended in fresh medium supplemented with an additional 20 % FBS and the cells were seeded into culture flasks.

2.2.3 Generation and purification of viral pseudotype particles

To express plasmids within eukaryotic cells, transfection was performed using calcium phosphate (Gavrilescu and Van Etten, 2007; Graham and van der Eb, 1973). This method is based on the formation of DNA-calcium phosphate prepicipitates that, upon addition to cell cultures become adsorbed by the cells. In particular, the insoluble precipitates attach to the cell surface and are taken up by endocytosis. This uptake is achieved during incubation at 37°C for 24 h in presence of excess of calcium ions.
24 h prior to transfection, 9 x 10^6 cells were seeded into a 175 cm^2 flask. 3 h before transfection the media of the flask was removed and 31.5 mL of new media were added. Then the transfection was initiated as follows: 10.5 µg of the plasmid encoding env, 10.5 µg of the plasmid encoding gag/pol and 21 µg of the plasmid encoding the transfer gene were mixed with 1.75 mL of 250 mM $CaCl_2$ (when using VSV-G env, the ratio of the plasmids was altered due to cytotoxic effects, env:gag/pol:transfer vector = 6:18:18 µg). The resulting mixture was added to 1.75 mL of hepes-buffered saline solution (HBS) containing 280 mM NaCl, 10 mM KCl, 1.5 mM $Na_2HPO_4{\cdot}2H_20$, 12 mM D-glucose, 20 mM HEPES at pH 7.5. After incubating this mixture for 20 min at room temperature it was added to the flask. Subsequent to 24 h of incubation at 37°C, the media was exchanged against 12 mL of fresh DMEM containing 1 % lipid concentrate (GIBCO), 0.01 mM cholesterol (Sigma), 0.01 mM lecithin (Calbiochem), 2 % FBS and 1 % penicillin (10 U/µL) / streptomycin (10^4 µg/mL) (GIBCO). 24 h later, the supernatant was collected, centrifuged at 1300 rpm for 6 min at 4°C and filtered using 0.45 µm filters (to remove dead cells). The filtered supernatant (containing the particles released from the producer cells) was then concentrated by ultracentrifugation at 30000 rpm for 2 h at 4°C (Optima L-100 XP, Beckman-Coulter) using an SW41 rotor. Each sample (9.5 mL of the supernatant) was pelleted through a 2 mL 25 % sucrose cushion. Subsequently, the supernatant was discarded and the pellet was resuspended in 300 µL of fresh media. 24 h later (72 h post transfection), the cell culture supernatants were harvested a second time and the same procedure was repeated.

2.2.4 Viral transduction

Transfection allows only transient expression of the genetic material since the plasmids are not replicated during cell-division (mitosis). This limitation can be overcome by retrovirus-mediated DNA transfer, since retroviral transductions entail the integration of the genetic material into the cellular genome. Consequently the genetic material is stably expressed by the host cell.
In this study transductions were carried out either to generate stable cell-lines (*described* in chapter *2.2.4.1*) or during viral inhibition assays (described in chapter *2.3*).

2.2.4.1 Generation of stable cell lines

To generate HEK293T cells expressing the β-galactosidase encoding reporter gene (*lacZ*), murine leukemia virus-derived particles (pseudotyped with the G protein of the vesicular stomatitis virus) having packaged a vector encoding *lacZ* were produced as described in chapter *2.2.3*. Subsequently, HEK293T cells were transduced with these viruses. For that purpose, 2 x 10^4 cells were seeded in a 96-well plate and the next day 63 µL of concentrated virus sample (~2,5 x 10^7 i.U./ml) were added and incubated for 1 h. Finally, cells were cultivated for two weeks before performing further experiments.

2.2.4.2 Determination of viral titers

X-Gal assays were performed to calculate the transduction efficiency of MLV(VSV-G) particles having packaged *lacZ*. To do so, 72 h post transduction, cells were fixed with a solution containing 2 % formaldehyde and 0.5 % glutaraldehyde. After washing with PBS, cells were incubated with a staining solution (4 mM potassium ferricyanide, 4 mM potassium ferrocyanide, 2 mM $MgCl_2$ and 80 µg/ml X-Gal (Sigma), in PBS) at 37 °C overnight. The next day blue colonies were counted under the light microscope. Titers were calculated using the following equation:

$$\textbf{Viral titers} = \bar{x} \cdot \frac{V_{virus}}{V_{total}} \cdot \frac{A_{microscope\ field\ of\ view}}{A_{well\ plate}} \cdot \frac{1}{2}$$

Where $\bar{x}$ is the average number of blue colonies per field of view under the microscope, $\frac{V_{virus}}{V_{total}}$ is the dilution factor of the particles (*V* = volume and *A* = area) and $\frac{1}{2}$ is the correction factor due to replication.

2.3 Assays

2.3.1 Fluorescence analysis of single cells on-chip

HEK293T cells stably expressing β-galactosidase were encapsulated into 660 pL drops. During droplet generation, a fluorogenic substrate for β-galactosidase (1.7 mM fluorescein di-β-D-Galactopyranoside, FDG (Euromedex)) was co-encapsulated and subsequently converted into fluorescein by the enzyme (Figure 2) (Berg, 1999).

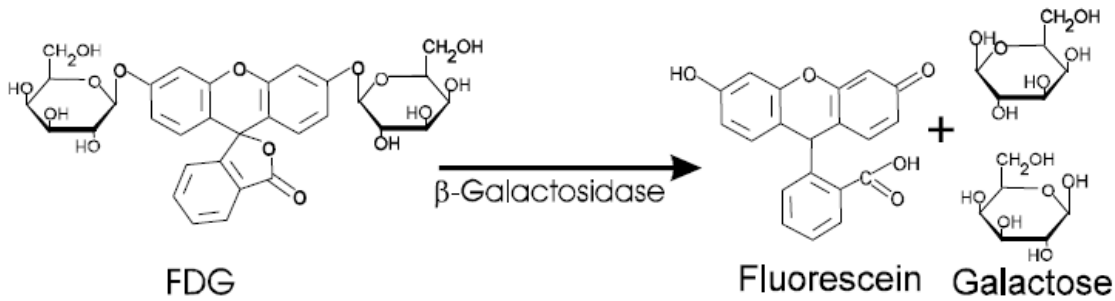

Figure 2. Fluorescence assay for β-galactosidase activity. *Fluorescein di-β-D-Galactopyranoside (FDG) is first hydrolyzed into fluorescein-monogalactopyranoside (FMG) and finally into fluorescein and two galactose residues.*

The emulsions were collected in open syringes (without the plunger being inserted) and incubated within a water-saturated atmosphere (37°C, 5 % CO_2). During the

encapsulation step, a laser beam (488 nm wavelength) was focused onto the channel by using an objective with a 40-fold magnification to excite the fluorophor. Emitted light was diverted by a dichroic mirror (488 nm notch filter), filtered (510 nm ± 10 nm) and collected in a photomultiplier tube to record the first fluorescence measurement (t_0) (See *2.8*). After the desired incubation time, mineral oil was added to fill the syringe completely before inserting the plunger and reinjecting the emulsion together with 0.5 % w/w DMP-PFPE surfactant in FC40 (3M) (injected into the oil inlet to space out the drops) into a chip with the same design as for the encapsulation step. To avoid fragmentation of the drops before the second fluorescence measurement (at t_i), the flow direction was reversed compared to the encapsulation step (the emulsion was injected into the outlet to avoid branching channels). All signals from the photomultiplier were recorded using Labview (National Instruments) and an in-house program for the data analysis.

2.3.2 Fluorescence analysis of plugs on chip

Plugs were generated from a 96-well plate (see chapter *2.7.1*) which contained the inhibitor 2-phenylethyl β-D-thiogalactoside (PETG, Sigma) in increasing concentrations (160 nM - 80 µM). Subsequently, plugs were splitted to a volume of 625 nL (see chapter *2.7.3*) and β-Galactosidase (Sigma) and the fluorogenic substrate FDG (Euromedex) in final concentrations of 1 nM and 500 µM respectively were added to each plug (see chapter *2.7.4*). Subsequently the fluorescence intensities of each plug were determined (t_0) before the plugs were collected in another length of tubing and reinjected/analyzed/recollected at multiple time points (t_x) (after 0.5, 1, 2, 4, 6 and 8 hours). The fluorescence of each plug was measured using a 488 nm laser focussed on the microfluidic channel. The emitted light of each plug (approximately 25 measurements, each) was collected with a photomultiplier tube using a 510 nm ± 10 nm Semrock filter (see chapter *2.8*). The fluorescence data (indicating the enzyme activity) was plotted against the inhibitor concentrations and the IC_{50} value was determined using non-linear regression to fit the four parameter Hill Equation using GraphPad Prism (Huang, 1991).

2.3.3 Cell-based fluorescence assays in bulk

For all assays HEK293T-tPA cells were seeded in 96 well plates ($2x10^4$ cells/well) pre-treated with poly-L-lysine (Becton Dickinson) and incubated for 24 h at 37°C.
4 h prior to the transduction with viral particles, cultures were pre-incubated with azidothymidine (a reverse transcriptase inhibitor, also called AZT or zidovudine) (Sigma) at different concentrations (0.01, 0.1, 1, 25, 100, 1000 µM). Subsequently, the transduction step was performed using concentrated virus samples (~$2,5x10^7$ i.U./ml). After 2 h of incubation, the medium was replaced by fresh DMEM supplemented with AZT at the indicated concentrations. Compounds inducing cell death (35 µg/ml puromycin (Sigma) for α-Puro effector particles or 40 µM Ganciclovir (Sigma) for TK effector particles) were added to the medium on day 1 and on day 3 post transfection. On day 4 post transfection the fluorescence readout was performed. For assays based on α-tPA effector particles, the readout was performed on day 2 post transfection without prior addition of any toxic compound.
For the assays coupling a positive fluorescence signal with the transduction itself (instead of its inhibition) effector particles having packaged a vector encoding *lacZ* were used. In this case, the fluorescence readout was initiated on day 4 post transfection.

To perform the assay readout the media was removed from each microtiter well. Subsequently, 100 µL of a mixture containing 1.67 µM plasminogen (Roche) and 1 mM His-Asp-Val-Leu-Lys-(amnio-4-methylcoumarin) (HDVLK-AMC, Bachem) in PBS was added to each well (Figure 3). All measurements were performed with excitation and emission wavelengths of 370 nm and 450 nm, respectively, using a Spectramax M5 microplate reader (Molecular Devices). For the assays coupling a positive signal with the viral infection itself, 100 µL of 100 µM fluorescein di-ß-D-Galactopyranoside (FDG; Sigma) were added to each well (Figure 2). All measurements were performed using excitation and emission wavelengths of 571 nm and 590 nm, respectively.

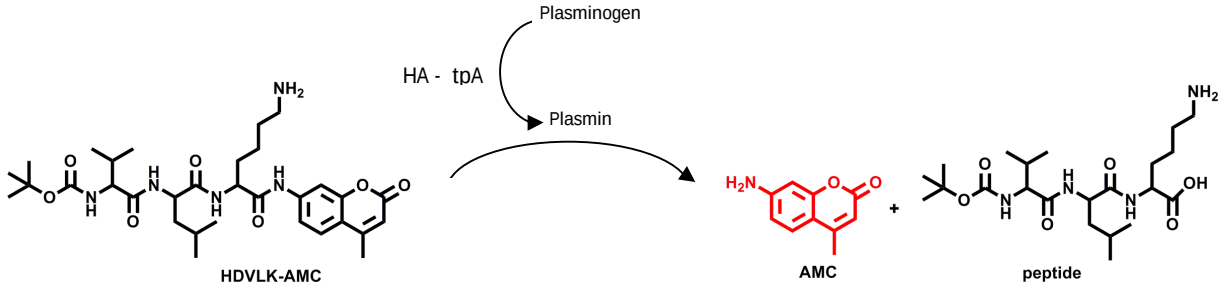

***Figure 3**. **Fluorescence assay for tpA activity**. A membrane-anchored form of tissue plasminogen activator (tpA), expressed on the surface of HEK293T cells, converts plasminogen into plasmin. Subsequently, plasmin converts a non-fluorescent substrate, His–Asp–Val–Leu–Lys–(amino–4–methylcoumarin) (HDVLK-AMC) into a fluorescent product, 7-amino-4-methylcoumarin (AMC).*

2.3.4 Determination of *Z factors*

The Z factor assesses the quality of an assay for use in high-throughput screens. Z-Factors were calculated for samples in 96-well plates using the following equation (Zhang et al., 1999):

$$Z - factor = 1 - \frac{3x(\sigma_p + \sigma_n)}{|\mu_p - \mu_n|}$$

Where σ is the standard deviation, μ is the mean signal, $x_{(p)}$ is the parameter of the positive control, and $x_{(n)}$ is the parameter of the negative control. Z-factors can never exceed 1. For values between 0.5 and 1.0 the assay is considered as an excellent assay and for values below 0.5 the assay is considered a bad assay.

2.4 Surfactants

2.4.1 Synthesis of the surfactans

Surfactants were synthesized according to the following scheme:

1-2)

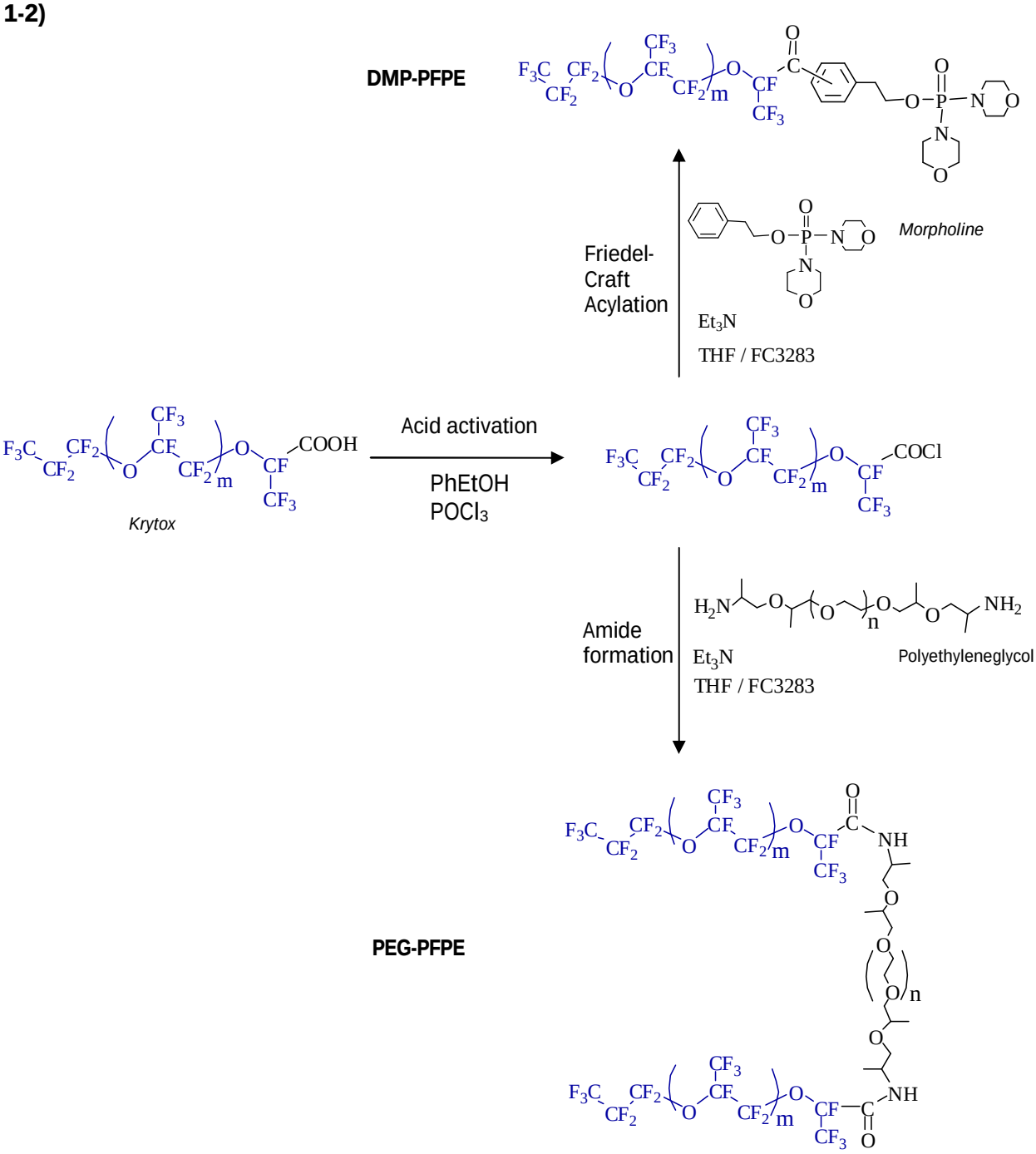

3)

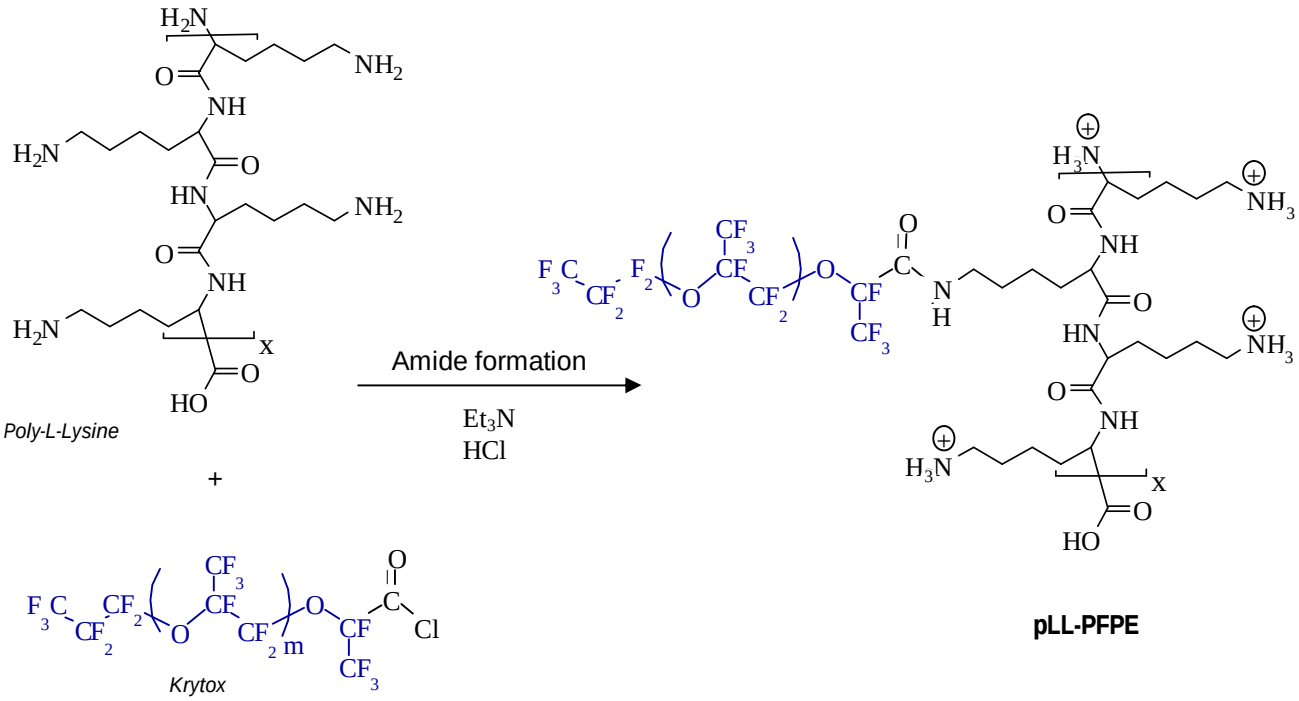
Poly-L-Lysine
+
Krytox
Amide formation
Et3N
HCl
pLL-PFPE

4)

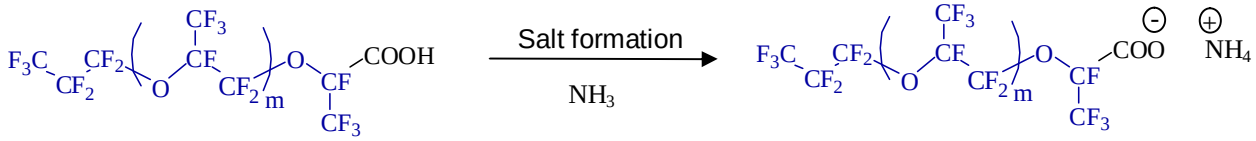
Krytox
Salt formation
NH3
Ammonium salt of carbonyl-PFPE

2.4.2 Assay for the biocompatibility of surfactants

A 100 µL suspension of HEK293T cells (1.5 x 10^6 cells/mL in fresh media) was seeded on top of a layer of perfluorocarbon oil (FC40, 3M) in the presence (0.5 % w/w) and absence of the tested surfactants. After incubation at 37°C for 48 h, bright-light images were taken with a Leica DMIRB microscope.

2.5 Encapsulation and cultivation of cells and multicellular organisms

2.5.1 Droplet-based systems

2.5.1.1 Cell encapsulation

For determining the viability and cell recovery in drops cells were initially adjusted to a density of 2.5 x 10^6 cells/mL (determined with a Neubauer counting chamber), stirred at 200 rpm using an 8 mm magnetic stir-bar (Roth) in a 5 mL polyethylene syringe (Fisher Bioblock) and injected via PTFE tubing (0.56 mm x 1.07 mm internal/external diameter, Fisher Bioblock) into the microfluidic device using a syringe pump (PHD 2000, Harvard Apparatus) at a flow rate of 1000 µL/h. The cell suspension was diluted on-chip with sterile media to 1.25 x 10^6 cells/mL (1000 µL/h if not otherwise stated), and drops were generated by flow focusing of the resulting stream with perfluorinated oil (FC40, 3M), containing 0.5 % (w/w) DMP-PFPE (4000 µL/h) (Figure 4).
The resulting drop volume was 660 pL (corresponding to a spherical diameter of 100 µm ± 1.7 %), as calculated by dividing the flow rate by the drop frequency (determined using a Phantom V4.2 high-speed camera). Experimental variations in the drop frequency (at constant flow rates) were defined as the degree of polydispersity in terms of the volume (corresponding to the third power of the polydispersity in terms of the diameter when considering a perfect sphere).

Figure 4. Cell encapsulation. *Drops are formed by co-flow of the oil and the aqueous phase, and cells are encapsulated on the single cell level (cells are highlighted with a red circle). White bar = 100 µm.*

2.5.1.2 Live/dead staining of cells recovered from drops

Subsequent to the encapsulation of cells, 500 µL of the resulting emulsion were collected within a 15 mL centrifuge tube and incubated at 37°C in a CO_2 incubator (5 % CO_2 atmosphere, saturated with H_2O). After incubation, 250 µL of the emulsion was transferred into a new centrifuge tube and broken by the addition of 15 % 1H,1H,2H,2H-perfluorooctanol (ABCR Gmb & H) in 10 mL live/dead staining solution (LIVE/DEAD Viability/Cytotoxicity kit for animal cells, Invitrogen Kit L-3224) and subsequent mixing. After incubation for 3 min (to allow sedimentation of the oil phase), 8.5 mL (containing most of the cells due to the slow sedimentation) of the supernatant were transferred into a 25 cm^2 tissue-culture flask and incubated for 1 h at room temperature.

The LIVE/DEAD Viability/Cytotoxicity solution contains on 1 µM calcein AM and 1 µM Ethidium homodimer-1 (EthD-1) in Dulbecco's Phosphate-Buffered Saline (DPBS). Calcein AM (calcein (fluorescein) acetomethoxy) is a green fluorescent marker; it is non-charged and hydrophobic (cell membrane-permeant) and thus can be introduced into cells during incubation. Once inside the cells, calcein AM is hydrolyzed by endogenous esterases (the lipophilic groups are cleaved off) into the more hydrophilic green fluorescent calcein, thus being retained in the cytoplasm (the molecule chelates calcium once the lipophilic groups are cleaved off and thus becomes fluorescent) (Figure 5a). In contrast dead cells lack active esterases, hence only live cells are labeled. EthD-1 is a red fluorescent marker; it has a high affinity for nucleic acids and binds to both DNA and RNA (Figure 5b). The DNA binding of each ethidium homodimer covers four base pairs upon intercalation, and since

the dye is highly positively charged it cannot cross cell membranes and thus does not stain living cells.

a)

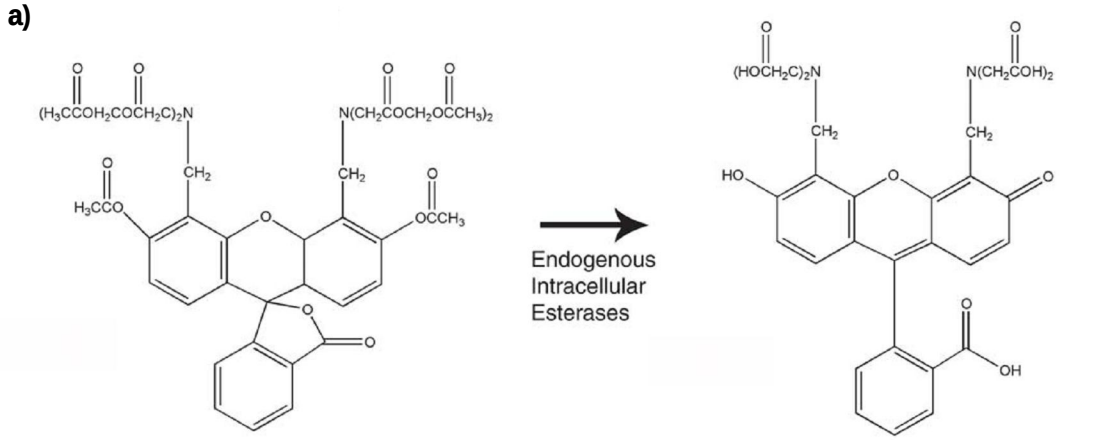

Calcein AM (non fluorescent/hydrophobic) Calcein (fluorescent/hydrophilic)

b)

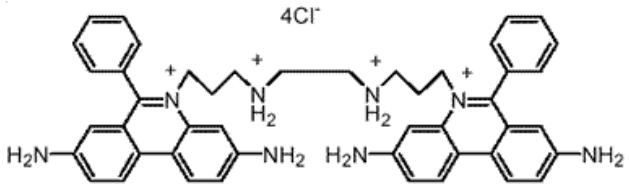

Ethidium Homodimer

Figure 5. Dyes used in the viability/cytotoxicity assay. (a) *Calcein AM. Calcein AM is hydrolyzed by endogenous esterases into the highly hydrophilic green fluorescent calcein.* ***(b)*** *Ethidium Homodimer (EthD-1) is a red fluorescent marker and has high affinity for nucleic acids (binding to both DNA and RNA).*

2.5.1.3 Determination of the cell recovery

After staining, live and dead cells were counted manually under a microscope (Leica DMIRB) with a UV-light source (LEJ ebp 100). For each sample within a 25 cm^2 tissue-culture flask, 30 fields of view (each corresponding to ~4.2 mm^2) were evaluated to calculate the total number of living (fluorescence green stain) and dead (fluorescence red stain) cells. The percentage of recovered cells (n_F) was calculated according to the the following equation:

$$n_F = \bar{x} \cdot \frac{A_{flask}}{A_{field\ of\ view}} \cdot \frac{100}{n_O}$$

Where n_O corresponds to the initial number of encapsulated cells, $\bar{x}$ is the average number of living and dead cells counted per field of view in the microscope and A correspond to the area, either of the flask (A_{flask}) or of the field of view ($A_{field\ of\ view}$).

2.5.2 Plug-based systems

2.5.2.1 Cell encapsulation

To prepare the plugs, 5 x 10^6 cells/mL (determined with a Neubauer counting chamber) were stirred at 4°C and 510 rpm within a 1.8 mL cryotube using an 8 mm magnetic stir-bar. Subsequently, 660 nL plugs of this cell suspension and perfluorinated oil (FC40, 3M) were aspirated (at 500 µL/h) into PTFE tubing (0.56 µm x 1.07 mm internal/external diameter) in an alternating fashion using a syringe pump (PHD 2000, Harvard Apparatus) (Figure 6).

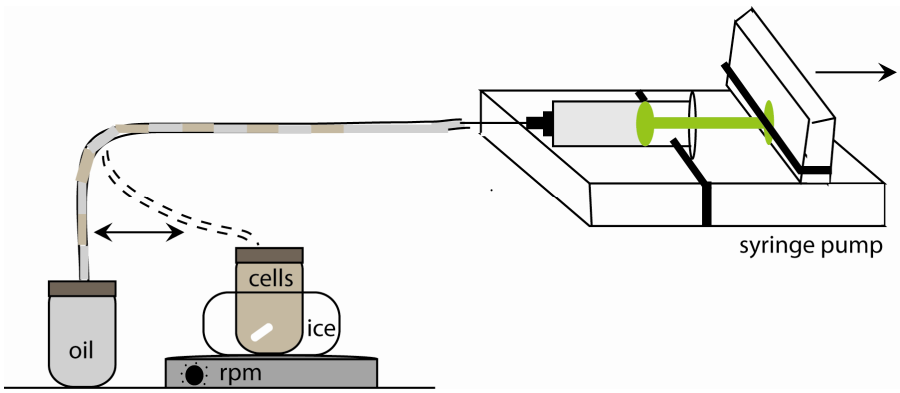

***Figure 6. Encapsulation of cells into aqueous plugs**. A syringe pump was used to aspirate oil and cells into a length of tubing in an alternating fashion. The end of the tubing was manually moved from one cryotube to the other while the cells were constantly stirred at 4°C.*

For each sample, 30 plugs of 3300 cells each were loaded before the tubing was sealed (by clamping microtubes to both ends) and incubated at 37 °C within a CO_2 incubator (5 % CO_2 atmosphere, saturated with water).

2.5.2.2 Live/dead staining of cells recovered from plugs

After incubation, the plugs were infused into a 25 cm^2 tissue-culture flask (Nunc) and the oil was extracted using a syringe. Subsequently, 4 mL live/dead staining solution (LIVE/DEAD Viability/Cytotoxicity kit for animal cells, Invitrogen Kit L-3224) was added, and the samples were incubated for 1 h at room temperature. When using adherent cells, the staining solution was additionally supplemented with 0.25 % trypsin-EDTA (GIBCO) to break up cell aggregates.

2.5.2.3 Determination of the cell recovery

The cell recovery was determined as described for droplets (see chapter *2.5.1.3*).

2.5.3 Recultivation experiments

For the recultivation of cells recovered from drops or plugs, semi-conditioned medium supplemented with 30 % FBS (GIBCO) was added to the cells instead of the staining solution. Subsequently, cells were incubated for 2 days at 37 °C in a CO_2 incubator (5 % CO_2 atmosphere, saturated with water) before imaging with bright-field microscopy was performed.

2.5.4 Encapsulation of eggs of *C. elegans*

Eggs of *C. elegans* were obtained according to the following protocol: approximately hundred worms were transferred into an eppendorf tube and subsequently lysed with 20 % alkaline hypochlorite solution. After several minutes, the worms had disintegrated and released the eggs, which are bleach resistant. Finally, the eggs were pelleted at 800 rpm for 5 min and subsequently resuspended in M9 minimal media (Sigma) supplemented with *E. coli* OP50 (10 % w/v of pelleted bacteria) in a cryotube. Plugs of the resulting suspension and perfluorinated oil (FC40, 3M) were aspirated (at 500 µl/hr) into PTFE tubing (0.56 mm x 1.07 mm internal/external diameter) in an alternating fashion using a syringe pump (PHD 2000, Harvard Apparatus). For each sample, 20 plugs were loaded before the tubing was sealed (by clamping microtubes to both ends) and incubated at room temperature.

2.6 Automated plug generation and manipulation

2.6.1 Generation of arrays of chemically-distinct plugs

Array of plugs were generated by aspirating 5 µL aqueous samples from microtiter plates and injecting them into a 300 µm inner diameter PTFE tubing (Fisher Bioblock) using a 2-position (*Load* and *Inject*) 6-port injection valve Dionex 3000 SL autosampler (Figure 7). 2.5 % (v/v) perfluoro-octanol (ABCR GmbH & Co) in fluorinated FC40 oil (3M) was used as the carrier phase and injected into the standard Valco valve by an external syringe pump (PHD 22/2000, Harvard Apparatus). Each 5 µL aqueous plugs was separated by 17.5 µL of oil. Subsequent to the loading of each plug, the whole system (excluding the target tubing) was rinsed with 20 µL of the carrier phase using the internal syringe pump.

a)

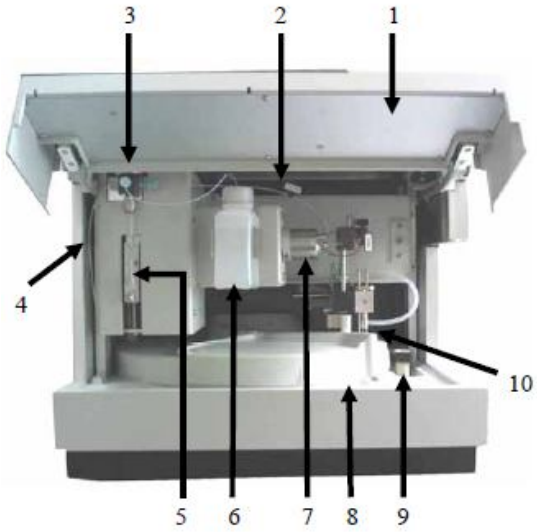

1	Front control panel
2	Buffer tubing (50 µL)
3	Syringe valve
4	Syringe waste tubing
5	Syringe (25 µL)
6	Wash liquid reservoir (125 mL)
7	Injection valve with sample loop
8	Cover for the carrousel and microtiter
9	Wash port
10	Needle tip

b)

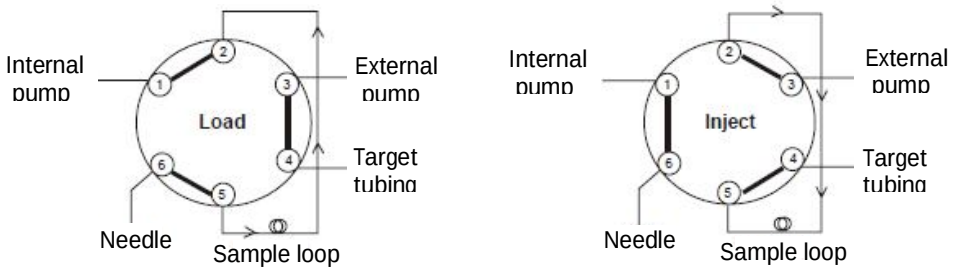

Figure 7. Working principle of the autosampler. (a) *General design.* ***(b)*** *Different valve positions. In the Load position (left), the sample is withdrawn (1), through the needle (6), into the sample loop by the external pump (5 to 2). In the Inject position (right), the sample is flushed from the sample loop (2 to 5) towards the target tubing (4) by the external pump (3), (www.dionex.com).*

2.6.2 Maintenance and cleaning of the autosampler

To minimize cross-contamination between the samples, frequent cleaning of the autosampler turned out to be crucial. Before each experiment, the system was rinsed two times with 2 mL of the following liquids (once for each position of the injection valve): PBS, ethanol, 2.5% (v/v) perfluoro-octanol in FC40.

2.6.3 Splitting of pre-formed array of plugs

For the generation of small volume copies, the parental plug arrays were injected into the splitting device at a flow rate of 800 µL·h^{-1}. Symmetric splitting was achieved by withdrawing 100 µL h^{-1} from seven of the eight outlets, respectively. The remaining outlet was connected to an open tubing thus allowing excess liquid to drain.

2.6.4 Addition of further compounds to pre-formed arrays of plugs

The on-chip addition of further substrates to each individual plug was performed in a droplet fusion device (Figure 6c). The volume (V) of added substrate was controlled by adjusting the relative aqueous flow rates (QA) according to the following equation:

$$\frac{QA_{plugs}}{QA_{drops}} = \frac{V_{plugs}}{V_{drops}}$$

The aqueous flow of an array of plugs can be calculated based on the total flow rate (Q) and the volume ratio between aqueous plugs and oil spacers:

$$QA_{plugs} = Q_{plugs} \cdot \frac{V_{plugs}}{V_{spacer} + V_{plugs}}$$

Hence the total volume of the substrate droplets added to each individual plug can be calculated according to:

$$V_{drops} = \frac{QA_{drops} \cdot (V_{plugs} + V_{spacer})}{Q_{plugs}}$$

2.7 Microfluidic devices

The microfluidic devices were fabricated by soft-litography techniques (Whitesides et al., 2001). In this process UV light (MJB3 contact mask aligner; SUSS MicroTec) was used to transfer a geometric pattern (design, Figure 8) from a photomask (Selba SA) onto a light-sensitive chemical photoresist (SU-8 2075, MicroChem Corp.) on a silicon wafer (Siltronix). The pattern was developed using SU-8 developer (MicroCHem Corp.), and subsequently an elastomeric material (Poly(dimethylsiloxane), PDMS) and a curing agent (Sylgard 184) 10:1 (w/w) were poured onto the substrate, degassed for several minutes and cross-linked in an oven at 65°C for 2 h. After that, the PDMS was peeled off the mould and inlets and outlets were made using 0.75 mm-diameter biopsy punches (Harris Uni-Core).

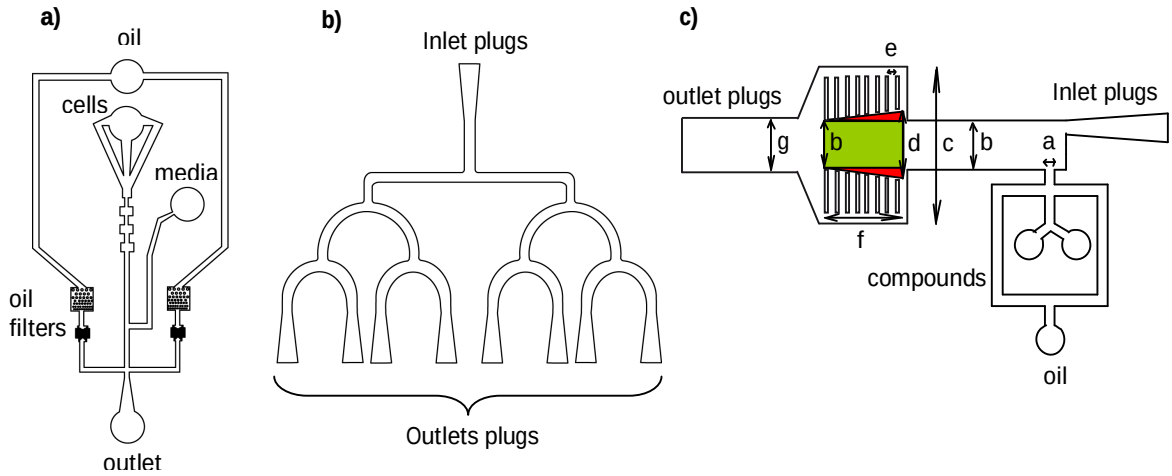

Figure 8. Microfluidic chips. (a) *Chip for the encapsulation of the cells. The device contains one oil inlet, one cell inlet to inject the cells, one media inlet to adjust the cell density during encapsulation and one outlet connected to a collection tube. The width of the channels is 100 µm, while the depth is 75 µm.* ***(b)*** *Chip for splitting array of plugs into small volume copies. The width of the channels is 250 µm, while the depth is 225 µm.* ***(c)*** *Chip for adding further compounds to pre-formed plugs. The drop maker has a width of 100 µm (a), while the fluidic channels have a width of 1000 µm (b) dilating to a total width of 3500 µm (c) in the pillar chamber (1426 µm between the pillars; d). This merging element has a length of 3225 µm (f) and consists of pillars having a width of 75 µm (with e = 75 µm) (f). The downstream channel has a width of 1800 µm (g). The total area of the chamber between the two pillar arrays can be divided into a rectangle (green colour) with an area of 3225 µm x 1000 µm and two equal triangles (red colour, up and down of the rectangle) having a total area of 3225 µm x 213 µm. For a channel depth of 225 µm, this corresponds to a chamber volume (V_c) of V_c = 225 µm x (3225 µm x 1000 µm + 3225 µm x 213 µm) = 880 nL*

The PDMS was then bound to a 50 x 75 x 1 mm glass slide (Fisher Bioblock) after activation for 3 min in an oxygen plasma (Plasma prep 2, Gala Instrumente). Finally, a hydrophobic surface coating was applied to the microfluidic channel walls by injecting Aquapel (PPG Industries), followed by nitrogen gas to purge the liquid (Squires, 2005).

2.8 Optical setup

For the on-chip detection of cells expressing fluorescein in drops, the optical setup consisted of an Axiovert 200 inverted microscope (Carl Zeiss SAS) mounted on a vibration-dampening platform (Thorlabs GmbH). A 20 mW, 488 nm diode laser (LAS, Newport-Spectraphysics) was mounted on the platform. Inside the microscope, the laser light was reflected into an LD Plan Neofluar 40x/0.6 microscope objective (OBJ; Carl Zeiss SAS) and focused onto the channel within the microfluidic device. A Phantom V4.2 high-speed digital camera (CAM; Vision Research) was mounted on the top of the microscope to capture digital images during droplet production and fluorescence measurements. Light emitted from fluorescing droplets was captured by the objective and separated from the laser beam by a dichroic mirror (DM; Semrock Inc.) before it was collected in a photomultiplier tube (PMT; Hamamatsu Photonics KK). Data acquisition (DAQ) was performed using a PCI-7831R Multifunction Intelligent DAQ card (National Instruments Corporation) executing a program written in LabView 8.2 (National Instruments Corporation). The data acquisition rate of this system was 800 Hz (Figure 9).

The optical setup for detection of fluorescence plugs consisted of a Nikon Eclipse Ti inverted microscope (Carl Zeiss SAS) mounted on a vibration-dampening platform (Thorlabs GmbH). Two diode lasers, one with a wavelength of 488 nm and the other with a wavelength of 375 nm (LAS, Newport-Spectraphysics) were mounted on the platform. Inside the microscope, the laser light was reflected into a LD Plan Neofluar 40x/0.6 microscope objective (OBJ; Carl Zeiss SAS) and focused across the channel within the microfluidic device. A Guppy F033B camera (CAM; Vision Research) was mounted on the top of the microscope to capture digital images during droplet production and fluorescence measurements.

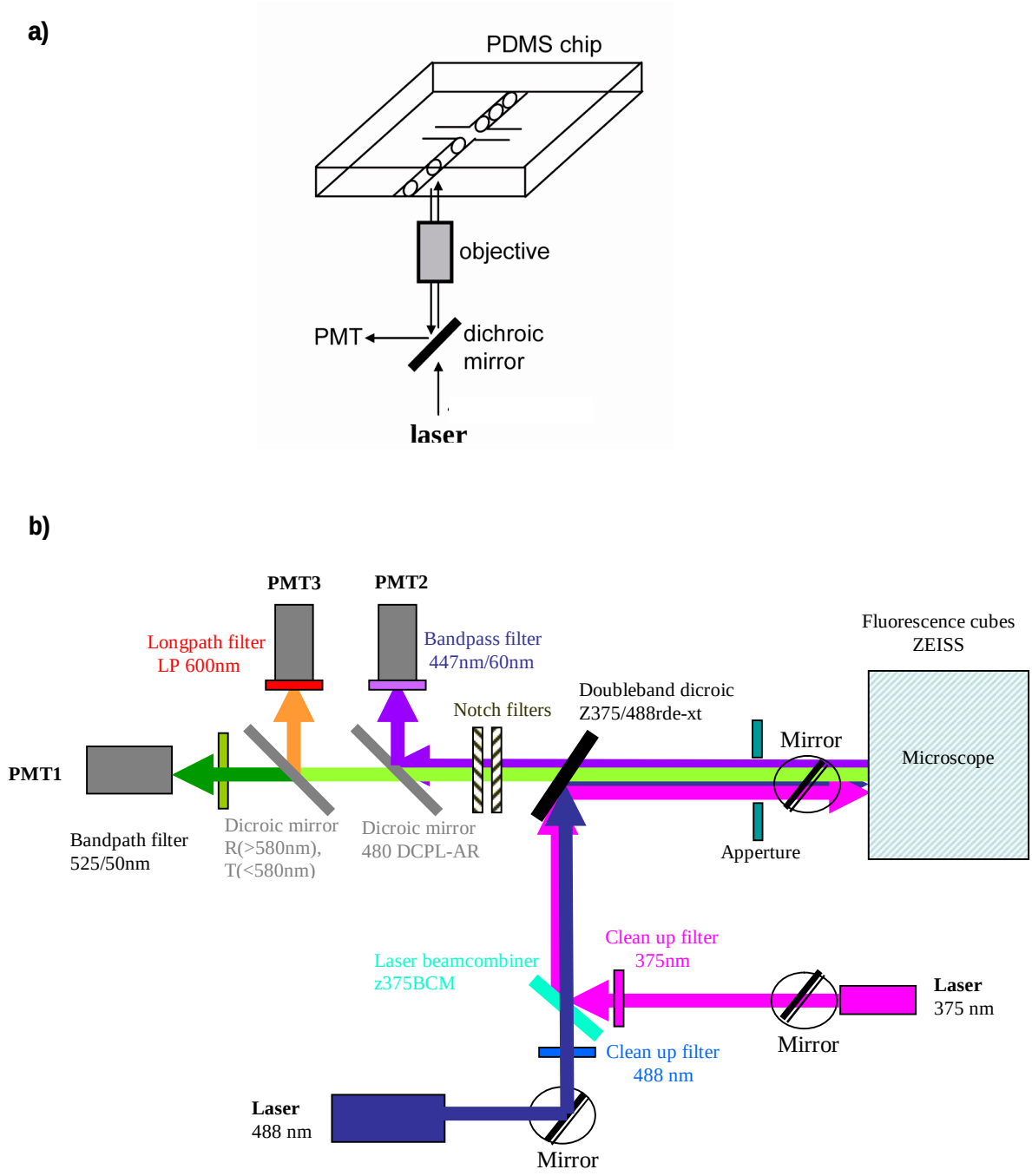

***Figure 9. Optical set up for fluorescence measurements**. **(a)** A diode laser is used to excite the fluorophores within aqueous microcompartments inside the microchannel. **(b)** Filters and beam splitters are used to direct specific wavelengths from the lasers towards the PDMS chip and from the microcompartmens (emitted light) to the photomultiplier tubes (PMTs).*

Light emitted from fluorescein and coumarin plugs was captured by the objective and separated from the laser beam by a doubleband dichroic mirror and then filtered by notch

filters. Subsequently, the emitted light from fluorescein plugs was transmitted through a dichroic mirror (T<580 nm) (DM; Semrock Inc.), filtered by a bandpath filter (525 ± 25 nm) and then collected in the photomultiplier tube #1 (PMT; Hamamatsu Photonics KK). In parallel, the emitted light from coumarin plugs was reflected by a dichroic mirror (R<480 nm), filtered by a bandpass filter (447 ± 30 nm) and then collected in the photomultiplier tube #2. Data acquisition (DAQ) was performed using a PCI-7831R Multifunction Intelligent DAQ card (National Instruments Corporation) executing a program written in LabView 8.2 (National Instruments Corporation). The data acquisition rate for this system was 40 Hz (Figure 9).

3. Results

3.1 Two-phase microfluidics platforms for the encapsulation and screening of mammalian cells and multicellular organisms

3.1.1 Droplet-based systems

3.1.1.1 Biocompatibility of surfactants

Surfactants are used to increase the stability of the drops and thus to avoid droplet coalescence. They reduce the interfacial tension between two immiscible liquids by adsorbing at the liquid-liquid interface (Stone HA, 1990). Besides, when biological samples such as human cells are encapsulated within drops, surfactants need to be biocompatible to not interfere with the assay and to not affect cell viability. In our investigations we specifically used fluorocarbon surfactants since fluorinated oils were used as the carrier phase. In particular, we synthesized several perfluoropolyether-derived surfactants (PFPE surfactants) and tested their effect on long-term cell survival (Figure 1). The surfactants differed solely in their hydrophilic head groups, which should be the only part of the molecule in contact with the encapsulated cells. The common perfluorinated tail should be dissolved in the carrier oil and thus be oriented away from the cells.

To analyze the biocompatibility, we seeded HEK293T cells on top of a layer of perfluorocarbon oil in the presence and absence of different surfactants. In the absence of any surfactant, the cells retained an intact morphology and even proliferated, whereas the ammonium salt of carboxy-perfluoropolyether (Johnston et al., 1996) and poly-L-lysine-perfluoropolyether (PLL-PFPE) mediated cell lysis. However, polyethyleneglycol-perfluoropolyether (PEG-PFPE) and dimorpholinophosphate-perfluoropolyether (DMP-PFPE) showed good biocompatibility. They did not affect the integrity of the cellular

membrane, and even allowed for cell proliferation (Figure 1). Since DMP-PFPE generated more stable emulsions than PEG-PFPE, it was used for all further experiments.

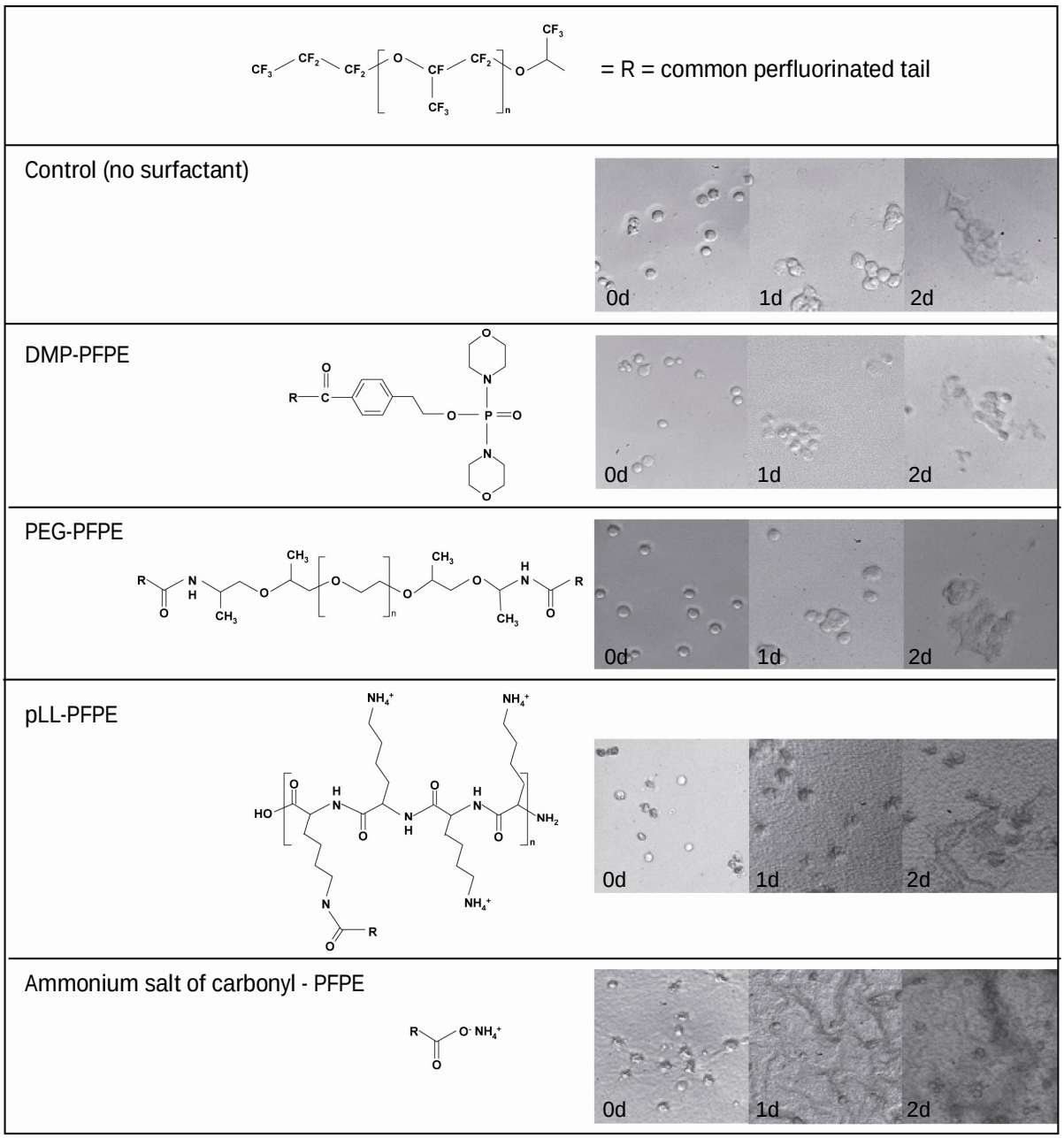

Figure 1. Biocompatibility of different fluorosurfactants*. The chemical structure of each surfactant tested is shown (left). HEK293T cells were seeded on a layer of FC40 oil in the presence or absence (control) of the indicated surfactant (0.5 % w/w) and microscopical bright-field images of the cells were taken at different time points (right).*

3.1.1.2 Cell encapsulation

To achieve the encapsulation of single cells per drop, the cell density was adjusted at the nozzle. For that purpose a suspension of Jurkat cells, with an initial density of 5 x 10^6 cells/mL, was brought together with a stream of sterile medium by co-flow (Anna SL, 2003) (Figure 2a). The relative flow rates of the cell suspension and the medium were changed using two independent syringe pumps, whereas the overall aqueous flow rate was kept constant (2000 µL/h). The number of cells per drop was determined by evaluating movies taken with a high-speed camera mounted on a microscope. For each dilution, 120 drops were analysed to determine the number of cells per drop. Subsequently, the data was fitted to a Poisson distribution (Figure 2b):

$$p_{[x=k]} = e^{-\lambda} \times \lambda^k / k!$$

using XmGrace (http://plasma-gate.weizmann.ac.il/Grace/). In this equation *k* corresponds to the number of cells per drop and λ is the average number of cells per drop. The cell density per drop for the different relative flow rates was always in good agreement with a Poisson distribution: high cell densities at the nozzle ($\geq$2.5 x 10^6 cells/mL) made the encapsulation of multiple cells per drop highly likely (p> 30 %). In contrast, cell densities of 1.25 x 10^6 cells/mL and below resulted in low probabilities (p< 7 %) for the encapsulation of more than one cell per drop (while increasing the probability of finding drops without any cells inside). At the same time, the average number of cells per drop (λ) decreased from approximately 2 (at 5 x 10^6 cells/mL) to far below 1 (at $\leq$ 1.25 x 10^6 cells/mL). Hence the number of cells per drop can easily be regulated, even allowing for the compartmentalization of single cells.

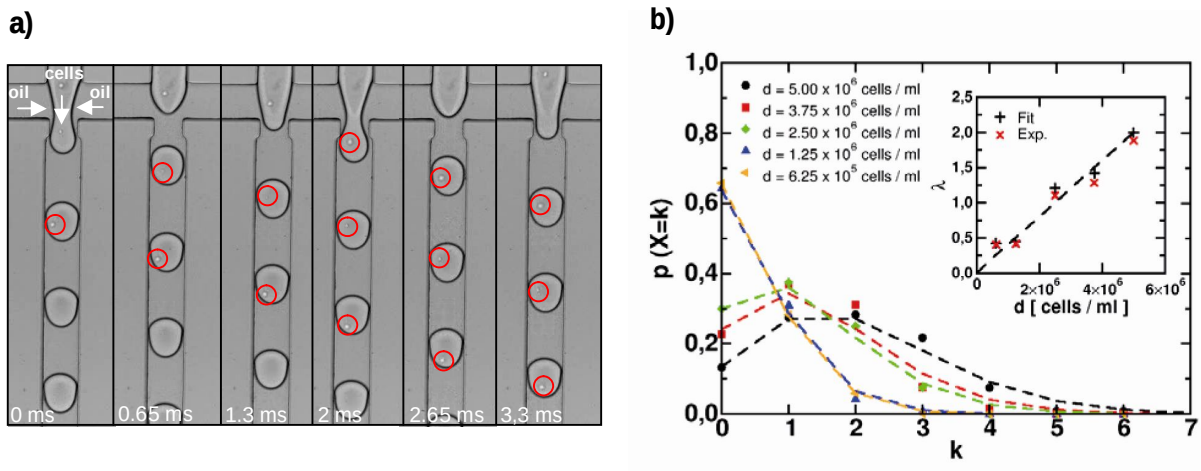

Figure 2. Encapsulations of cells into drops. (a) *Sequence of pictures taken during single cell encapsulation (cells are highlighted with a red circle). The numbers at the bottom are the time intervals between the series of pictures.* ***(b)*** *The experimentally determined probability (p, y axis) for the number of cells per drop (k, x axis) is in good agreement with a Poisson distribution (dashed lines) for various cell densities resulting from on-chip dilution. Inset: the average number of cells per drop (λ) plotted against the cell density for the experimental data (Exp.) and the Poisson distribution (Fit). The dashed line is the theoretical number of cells per drop according to the cell density only (homogeneously distributed).*

3.1.1.3 Live/dead staining of cells recovered from drops

For determining cell viability in drops, we encapsulated cells at a density corresponding to an average of less than 1 cell per 660 pL drop (1.25 x 10^6 cells/ml at the nozzle, resulting in a λ value of ~0.55 and single cells in ~31.7 % of all drops) and collected the resulting emulsions in 15 mL centrifugation tubes. After different incubation times at 37°C within a CO_2 incubator, the emulsions were broken and the cells were treated with a live/dead stain to determine the survival rate and the total number (live and dead) of recovered cells. During the first 4 days, the fraction of recovered viable Jurkat cells did not change significantly and was always in excess of 79 %. Then, the percentage of living cells decreased from 71 % after 5 days to 32 % after 6 days and finally to 1 % after 14 days of encapsulation (Figure 3a). When repeating the experiments with adherent HEK293T cells, similar results were obtained: during the first 2 days, the fraction of recovered viable cells remained constant at more than 90 % before slowly decreasing to 58 % after 5 days and 39 % after 9 days. Finally, after 14 days of encapsulation, 28 % of the recovered cells were still alive (Figure 3b).

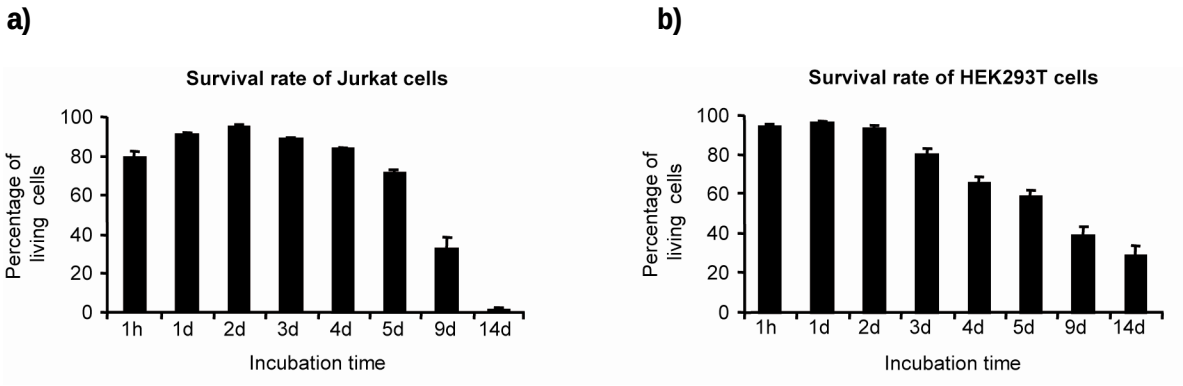

Figure 3. Cell viability of cells encapsulated in 660 pL drops. *The percentage of viable* ***(a)*** *Jurkat and* ***(b)*** *HEK293T cells recovered from emulsions after incubation for different time points was determined using a commercial live/dead stain. Error bars show the standard deviation of three independent experiments.*

In an additional experiment, we assessed the effect of the cell density on the survival rates. For this purpose, we used 5- and 10-fold higher densities of Jurkat cells than used initially. Comparison of the cell survival after 3 days showed that an increasing cell density inversely correlated with the survival rate. While almost 90 % of viable cells were recovered when using the initial cell density, only 80 % and 68 %, respectively, survived for the 5- and 10-fold increased cell density (Figure 4). Insufficient gas exchange can be ruled out, since equally dense cultures in ordinary tissue-culture flasks did not survive longer.

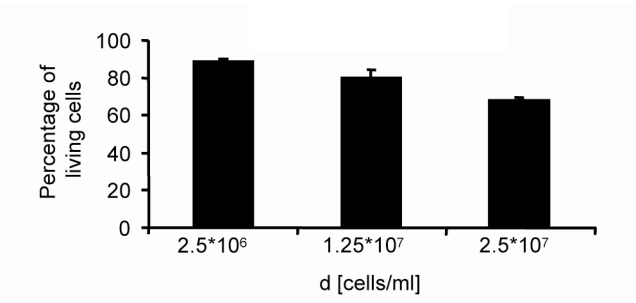

Figure 4. Survival rate of Jurkat cells after incubation in drops at different cell densities. *Percentage of viable Jurkat cells after three days of incubation within 660 pL drops at different cell densities (at the nozzle during encapsulation). Survival rates were determined using a commercial live/dead stain. Error bars show the standard deviation of three independent experiments.*

Using a density equal to 1 cell in a 660 pL drop (~1. 5 x 10^6 cells/mL), the number of viable Jurkat cells remained above 87 % for the first 2 days, before decreasing to 51 % after 4 days and 0 % after 9 days. Therefore, we concluded that the encapsulated cells most likely die due to the lack of nutrition or the accumulation of toxic metabolites, rather than compartmentalization-specific factors such as the oil and surfactant.

3.1.1.4 Determination of the cell recovery

The recovery rate ($N(\%)$) was defined as the total number of recovered cells (live and dead, N_f) divided by the number of initially encapsulated cells (N_o) (equal to the aqueous flow rate (Q_A) multiplied by the injection time ($t_{injection}$) multiplied by the cell density at the nozzle (d_{nozzle})).

$$N_o = Q_A \cdot t_{injection} \cdot d_{nozzle} \qquad N(\%) = \frac{N_f}{N_o}$$

The recovery rate of Jurkat cells increased from 29 % after 1 h to more than 55 % after 2 days. This indicates some degree of proliferation within the drops, which is also supported by the fact that after 24 h the percentage of dead cells was lower than after 1 h. During further incubation within drops, the recovery rates slowly decreased to just 14 % after 14 days (Figure 5). This decrease can be explained by the fact that dead cells ultimately disintegrate (after several days) and thus cannot be stained anymore. This effect is well known and has been analyzed in detail for bacterial cells (Villarino et al., 2000). For HEK293T cells the total recovery rate increased slightly from 20 % after 1 h to more than 32 % after 2 days. During further incubation within drops, the recovery rates slowly decreased to 23 % after 14 days (Figure 5). The longer survival of HEK293T cells compared to Jurkat cells is most likely due to the slower proliferation, resulting in slower consumption of the available nutrition.

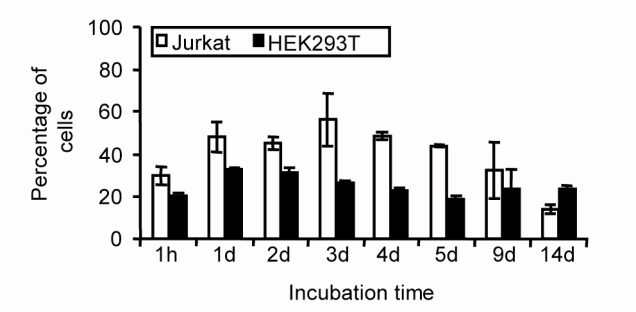

Figure 5. Recovery of cells encapsulated in 660 pL drops. *The total number of recovered living Jurkat (white bars) and HEK293T (black bars) cells relative to the number of initially encapsulated cells was obtained after incubation for different time points. Error bars show the standard deviation of three independent experiments.*

To confirm the viability of the cells after incubation for several days in drops, we recultivated them in parallel to performing live/dead stains. To do so, HEK293T cells incubated for 2 days within droplets were seeded in a T25 flask after breaking the emulsion. Subsequent to a cultivation for 48 h, microscopic analysis revealed normal cell morphology and proliferation (Figure 6).

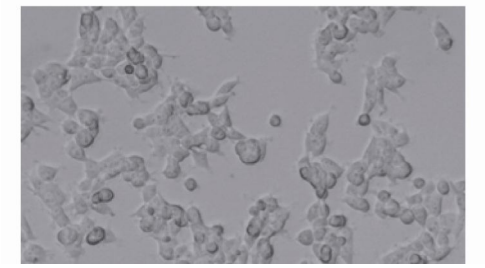

Figure 6. Recultivation of HEK293T after incubation in 660 pL drops*. The bright-field image was taken after incubating the cells for 2 days within drops and subsequent cultivation for 2 days in ordinary tissue culture flasks.*

3.1.1.5 On-chip single-cell analysis

High-throughput cell-based assays require the readout of individual samples after the incubation step (e.g. to screen the phenotype of individual cells within a heterogeneous population). For this purpose, microcompartments stored in a reservoir (off-chip) could be reinjected into a readout module after the incubation period. To prove the feasibility of

this approach, we encapsulated HEK293T cells within 660 pL drops, collected the resulting emulsions, and incubated them for 2 and 14 days. Subsequently, the emulsions were reinjected into a chip (same design as for the encapsulation step) and were analyzed microscopically. During reinjection of the emulsion after 2 days of incubation, hardly any coalescence of indivicual samples was detectable (Figure 7a). After 14 days of incubation, some degree of coalescence was observable; however, the majority of drops (>90 %) remained intact. Microscopical comparison of the drops at the time of incubation and reinjection revealed no obvious reduction of the drop size (Figure 7b). This indicates that the drops were not subjected to significant evaporation during the incubation period (within a water-saturated atmosphere).

To demonstrate that the drops can be analyzed individually after reinjection, we encapsulated a population of HEK293T cells that, 2 weeks before the experiment, had been incubated in bulk with viral particles having packaged the *lacZ* gene. The fraction of cells stably expressing the corresponding gene product (β-galactosidase) was ~13.9 %, as determined in an X-Gal assay (Stitz et al., 2001). During the drop production, a fluorogenic substrate for β-galactosidase was coencapsulated into the drops and a laser beam (488 nm wavelength) was focused onto the channel downstream of the nozzle. The emitted light was collected in a photomultiplier tube to record the fluorescence signal at t_0. This measurement was performed with the initial population of transduced HEK293T cells. At the time of encapsulation no difference in the fluorescence signals was observable, and even drops without any cell showed the same signal intensity. After incubation for 16 h at 37°C, the emulsions were reinjected into the chip together with additional fluorinated oil (separately injected into the oil inlet to space out the drops) to repeat the fluorescence measurement (at t_i; analyzing 500 drops/s). Plotting the maximum fluorescence intensity of the drops against the peak width (which corresponds to the drop size and therefore is a good indicator of coalescence) revealed different distinct populations (Figure 7e). Analysis of the peak width proved that even though populations with 2-fold and 3-fold higher volumes were observable, the majority of drops did not coalesce (>93 %). In terms of the fluorescence, two main populations with a ~35-fold difference in their intensity were obtained, as also confirmed by fluorescence microscopy in which the drops appeared to be either highly fluorescent or non-fluorescent (Figure 7c). Based on these observations, we set gates for the quantitative interpretation of the data (as routinely done in FACS analysis). Gates were set to solely analyze those

drops that had not coalesced (corresponding to the populations with the lowest peak width). Based on the way the peak width was defined, fluorescence-positive drops appeared to be bigger (Figure 7d). Nonetheless, plotting the fluorescence against the peak width enabled non-coalesced drops to be clearly distinguished from coalesced drops for both species (positives and negatives). The use of gating led to the conclusion that ~5.08 % of all non-coalesced drops were fluorescence positive in the sample with non-diluted transduced cells. This number corresponded to ~12.7 % of the corresponding cell population when taking into account that only 40 % of the drops were occupied (as determined by microscopical analysis of the drops during the encapsulation step). This value was in the same range as the fraction of positive cells determined in bulk (~13.9 %) using a conventional X-Gal assay (see chapter *2.2.4.2*). For control purposes we repeated the experiment using a dilution of the transduced cells. In particular, we mixed them in a ratio of 1:9 with fresh HEK293T cells before encapsulation. For this diluted sample, we obtained 0.63 % positive drops, corresponding to 1.8 % of the cells (34.8 % of the drops were occupied). Compared to the non-diluted sample, the negative population showed lower fluorescence intensity. This was most likely due to the fact that all drops (even the ones without cells) contained traces of soluble β-galactosidase, resulting from the few dead cells within the syringe (during the encapsulation step). Since the diluted sample contained less enzyme in total, a lower background could be expected, too. Another possible explanation was the exchange of fluorescein between the drops. However, this seemed to be unlikely, since for incubation periods of up to 24 h we never observed any significant exchange of fluorescein for any surfactants tested (including the ammonium salt of carboxy-PFPE and PEG-PFPE). The resulting 7.1-fold difference in terms of positive cells between the samples was in good agreement with the initial 1:9 dilution (an accuracy of ±10 %, when counting the cultures in a Neubauer chamber, corresponds to an effective ratio as low as 1:7.4). In summary, these results clearly demonstrated the possibility of quantitatively analyzing individual drops in a high-throughput fashion.

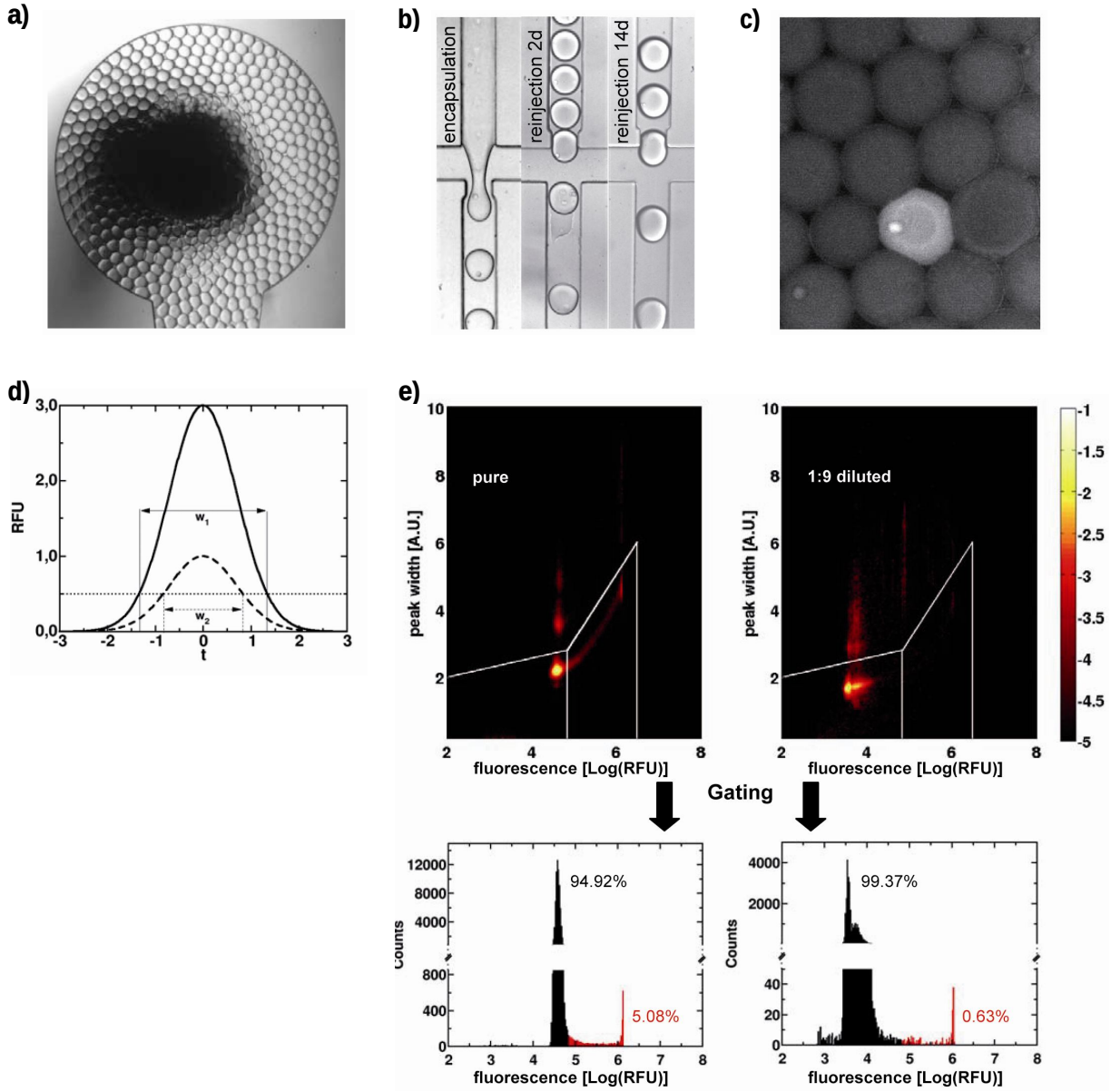

Figure 7. Reinjection and analysis of emulsions after incubation. ***(a)*** *Bright-field image of the inlet during reinjection of an emulsion (drops containing HEK293T cells) after 2 days of incubation.* ***(b)*** *Bright-field images of individual drops during encapsulation and after reinjection (off-chip incubation for 2 days and 14 days).* ***(c)*** *Fluorescence-microscopic image of drops hosting lacZ-expressing HEK293T cells (converting the fluorogenic substrate FDG) after 16 h of incubation.* ***(d)*** *Influence of the fluorescence intensity (y-axis) on the peak width (w). The peak width is defined as the time (t, x-axis) for which a fluorescent signal above a certain threshold (dotted, horizontal line) can be measured (due to a drop passing the laser beam). Different fluorescence intensities of the drops (continuous and dashed peaks) result in different apparent peak widths (w_1 and w_2).* ***(e)*** *Fluorescence signals of drops after reinjection. Upper panels: fluorescence intensity (x-axis) plotted against the peak width (y-axis) for pure (left) and 1:9 diluted (right) transduced cells. The relative frequency of all events is colour-coded according to the bar on the right (numbers corresponding to the exponent of the frequency). White gates correspond to non-coalesced drops: left gate, drops considered as negatives; right gate, drops considered as positives. Lower panel: fluorescence intensity (x-axis) plotted against the drop counts (y-axis) of all events within the gates. Positive events are depicted in red, while negative events are depicted in black.*

3.1.2 Plug-based systems

3.1.2.1 Cell encapsulation

In parallel to encapsulating cells into aqueous drops of a w/o emulsion, we established a system in which aqueous plugs spaced by immiscible oil within a piece of tubing serve as a culture vessel. This approach allows for the generation of aqueous microcompartments big enough to host small cell populations and even multicellular organisms. This cannot be achieved by simply increasing the drop size of a given emulsion. First, the maximum size of a drop generated on a microfluidic chip is limited by the channel dimensions. Second, as the size of the drops increases, they become less stable, resulting in uncontrolled sample coalescence. These problems can be circumvented by alternately aspirating aqueous plugs and immiscible oil into a holding cartridge (e.g. capillary or a piece of tubing) (Chen and Ismagilov, 2006). We used this approach to encapsulate several thousand cells into single microcompartments (see chapter *2.5.2.1* for more detailed explanations). Plugs are usually stored in tubings or microfluidic channels, where they are stably separated from each other by a spacer of oil. Hence they do not tend to fuse like the droplets of an emulsion (which are in close contact) and thus do not require the use of a surfactant.

3.1.2.2 Live/dead staining of cells recovered from drops

For determining cell viability in plugs, we encapsulated 3300 cells per 660 nL plug and stored them in a length of PTFE tubing. After different incubation times at 37 °C within a CO_2 incubator, the aqueous plugs were flushed into a T25 flask and the cells were treated with a live/dead stain to determine the survival rate and the total number (live and dead) of recovered cells. The survival rate of Jurkat cells remained at ~90 % for the first 2 days, before decreasing gradually from 69 % after 3 days, to 38 % after 5 days and finally to 6 % after 14 days (Figure 9a). When repeating the experiments with adherent HEK293T cells, slightly different results were obtained. The fraction of viable cells

remained above 80 % for the first 4 days, before slowly decreasing to 31 % after 14 days (Figure 9b).

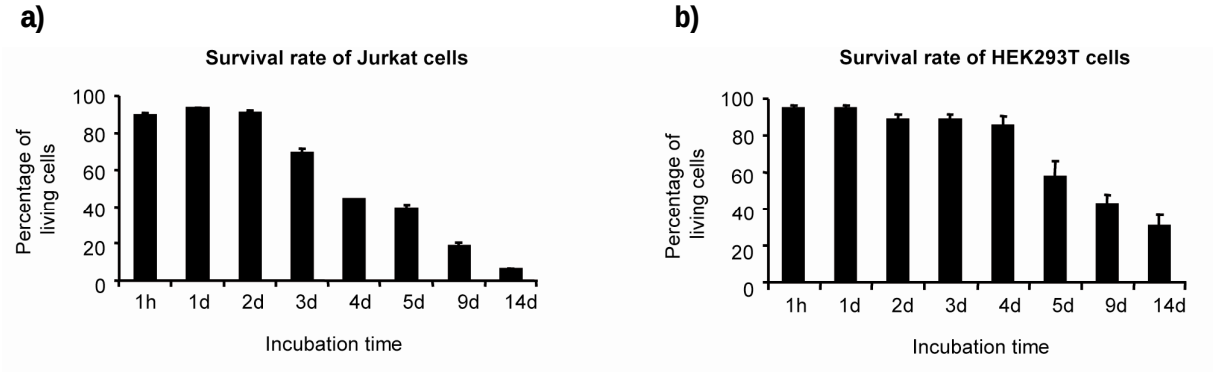

Figure 9. Cell viability of cells encapsulated in 660 nL plugs*. The percentage of viable* ***(a)*** *Jurkat and* ***(b)*** *HEK293T cells recovered from plugs after incubation for different time points were obtained. Error bars show the standard deviation of three independent experiments.*

To assess the influence of the cell density on cell survival, we also performed experiments with five- and ten- times more Jurkat cells per plug. As for the drops, we obtained an inverse correlation between cell density and survival. While ~69 % viable Jurkat cells were recovered after 3 days when using the initial cell density, only 52 % and less than 1 % survived when encapsulating five and ten times more cells per plug, respectively (Figure 10). This massive decrease in cell survival is probably due to the fact that higher cell densities directly resulted in more cells per plug (even at the lowest density, all pugs were occupied), whereas when encapsulating single cells into drops, the proportion of occupied drops was increased first (with a single cell in a drop still experiencing the same cell density).

In a last step, we assessed the influence of the material of the holding cartridge on cell survival. For this purpose, we injected 660 nL plugs (each hosting 3300 Jurkat cells) in holding cartridges of different materials. We observed that while gas-permeable PTFE tubing allowed for cell survival for several days, the use of glass capillaries and vinyl tubing (all with an inner diameter of ~0.5 mm) resulted in cell death within 24 h.

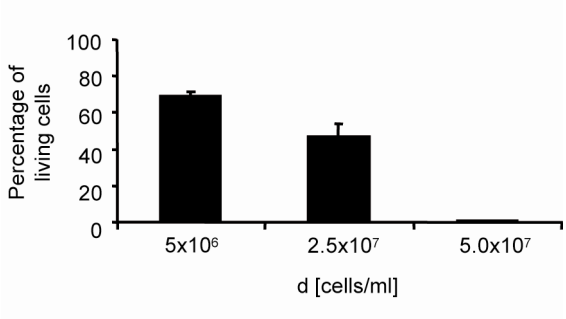

Figure 10. Survival rate of Jurkat cells at different cell densities. *The percentage of viable Jurkat cells encapsulated into 660 nL plugs at three different cell densities was determined after 3 days of incubation. Error bars show the standard deviation of three independent experiments.*

3.1.2.3 Determination of the cell recovery

We also calculated the total recovery rate for both cell lines. The total number of recovered Jurkat cells increased from 69 % after 1 h to 194 % after 5 days, indicating roughly 1-2 cell divisions, whereas during further incubation times it decreased to 80 % after 14 days (Figure 11). This decrease can be explained by the fact that dead cells ultimately disintegrate (after several days) and thus cannot be stained anymore (Villarino et al., 2000). This effect had also been observed for the experiments in drops (see chapter *3.1.1.3*). For HEK293T cells the total recovery rate increased during the first 5 days from 83 % to ~147 % (indicating some degree of proliferation) before decreasing to 35 % after 14 days.

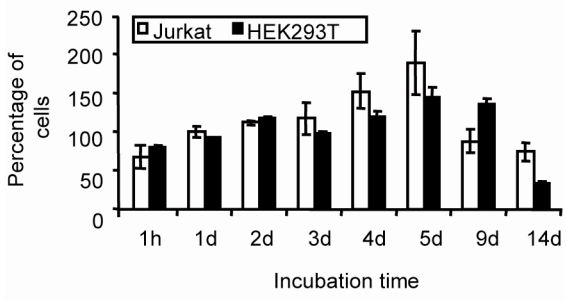

Figure 11. Recovery of cells encapsulated in 660 nL plugs. *The total number of recovered Jurkat (white bars) and HEK293T (black bars) cells relative to the number of initially encapsulated cells was determined after different incubation times. Error bars show the standard deviation of three independent experiments.*

The higher recovery rate of Jurkat cells compared to HEK293T cells is most likely explained by the slower proliferation of the adherent cells due to the lack of a solid support. In line with this, the higher survival rate of HEK293T cells can be explained by the slower consumption of the available nutrition.

To confirm the viability of the cells after incubation for several days in plugs we recultivated them in parallel to performing live/dead stains. To do so, HEK293T cells incubated for 2 days within plugs were seeded in a T25 flask. After cultivation for 48 h, microscopic analysis revealed normal cell morphology and proliferation (Figure 12).

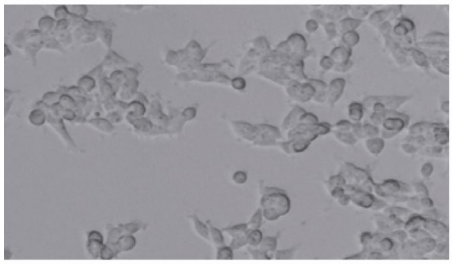

Figure 12. Recultivation of HEK293T cells after incubation in 660 nL plugs*. The bright-field image was taken after incubating the cells for 2 days within the plugs and subsequent cultivation for 2 days in ordinary tissue culture flasks.*

3.1.2.4 Encapsulation and survival of multicellular organisms

We also investigated the possibility of encapsulating multicellular organisms. For that purpose, we encapsulated eggs of the nematode *C. elegans* into plugs and analyzed them under the microscope at different time points. While after 2 days hatched worms had already reached the L2-L3 larvae stage, 4 days of encapsulation resulted in the growth of adult worms and the birth of the next generation (L1 larvae) (Figure 13a). Longer encapsulation times (7 days) resulted in plugs hosting up to 20 worms (Figure 13b), which finally died after 6-9 days. The passing of individual worms into adjacent microcompartments was never observed, even at high flow rates (up to 1000 µL/h).

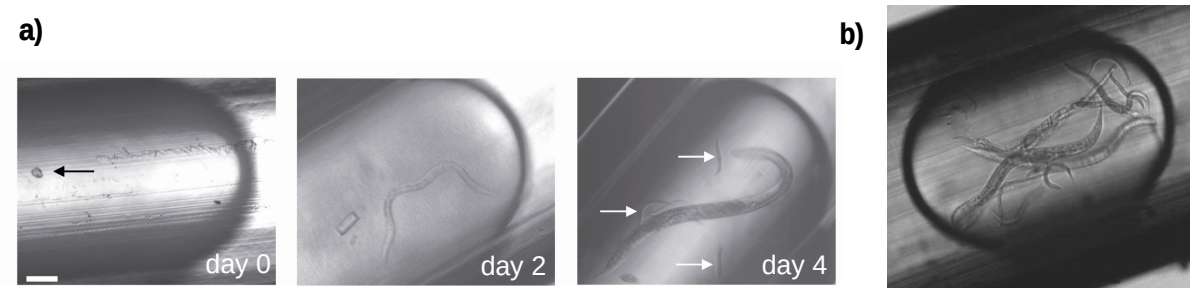

Figure 13. Growth of the nematode C. elegans within 660 nL plugs. (a) *Eggs (black arrow) were encapsulated at room temperature, and bright-field microscopical images were taken after 0, 2, and 4 days. White arrows show larvae of the second generation of encapsulated worms.* ***(b)*** *Longer encapsulation (7 days) resulted in an increased number of worms per plug. White bar = 100 µm.*

3.1.2.5 Analysis of the plug size over time

To rule out that the cell viability decreased due to evaporation of the media, and thus due to increasing concentrations of toxic metabolites released by the cells, we analyzed the plug size during a period of two weeks. In particular, we measured the mean length of 30 plugs ($\bar{l}_{plug}$) for each time point using a digital slide gauge and multiplied this mean value by the inner radio of the tube (r_{tubing}) to obtain the corresponding plug volumes (V_{plug}):

$$V_{plug} = \pi \cdot \bar{l}_{plug} \cdot r_{tubing}^2$$

When analysing the data, no significant decrease in size was observable (Figure 8), most likely due to the fact that we performed the incubation step in a water-saturated atmosphere (at 37 °C, 5 % CO_2).

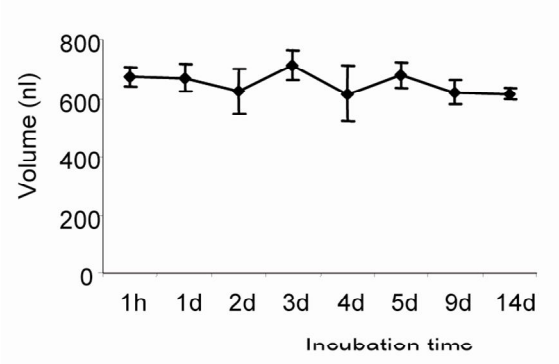

Figure 8. Plug size over time*. Mean size of plugs harbouring HEK293T cells plotted against the incubation time. Error bars show the standard deviation of three independent experiments.*

In summary, we had demonstrated that aqueous microcompartments (pL to nL volumes) can be used as miniaturized vessels for cell-based assays. Within these microcompartments human cells and even multicellular organisms (*C.elegans*) remained fully viable for several days. To exploit this technology for screening purposes, we then focused on the automated generation of chemically-distinct microcomparments (so far, all drops and plugs had the same composition).

3.2 An automated two-phase microfluidic system for the screening of compound libraries and kinetic analysis

3.2.1 Development of an automated two-phase microfluidic system to generate and manipulate chemically-distinct plugs

The ultimate goal of this study was the development of a microfluidic platform for the screening of compound libraries. For that purpose, the desired platform should allow five sample manipulation steps: first the generation of chemically-distinct plug arrays (starting from microtiter plates) using an autosampler; second, the splitting of the resulting plugs into smaller subunits; third, the addition of further compounds to each individual plug; forth, incubation and finally, the readout of fluorescence signals (Figure 14).

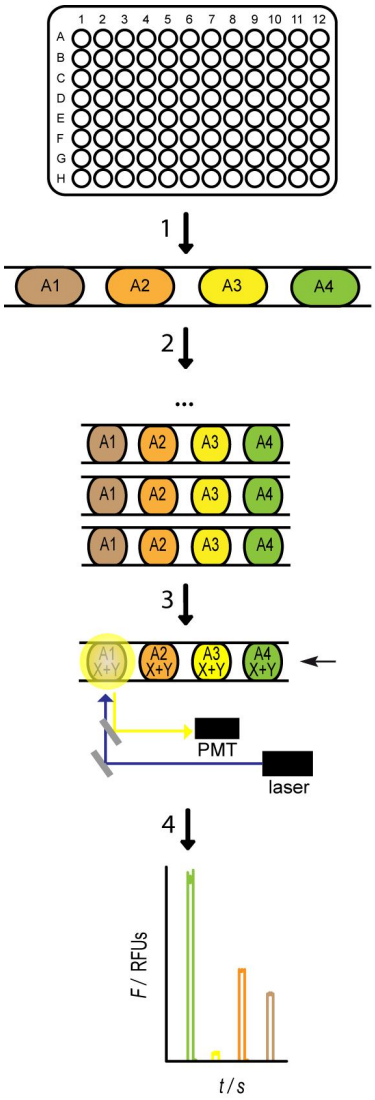

***Figure 14**. **Setup of the screening platform**. An autosampler (Dionex 3000 SL) was integrated into a microfluidic platform to aspirate samples from microtiter plates and inject them into a length of tubing in which they were separated by immiscible (fluorinated) oil (1). The resulting arrays can be split into multiple small volume copies (2) before further reagents (X and Y) can be added to each individual plug on-chip (3). Subsequently multiple fluorescence (F) readouts can be performed on-chip (by recollecting the array after each measurement and reinjecting it at further time points) (4).*

3.2.1.1 Generation and splitting of plugs

In a typical experiment for generating arrays of chemically-distinct plugs, 5 µL of each compound were loaded from 96-well plates using a Dionex 3000 SL autosampler and injected into a length of PTFE tubing (step 1 in Figure 14). To achieve stable spacing of

the samples, we used 2.5% (v/v) perfluoro-octanol in fluorinated FC40 oil as the carrier phase. The autosampler has a 2-position (*Load* and *Inject*) 6-port injection valve: in the *Load* position the internal syringe aspirates a specific volume through a needle into the sample loop.

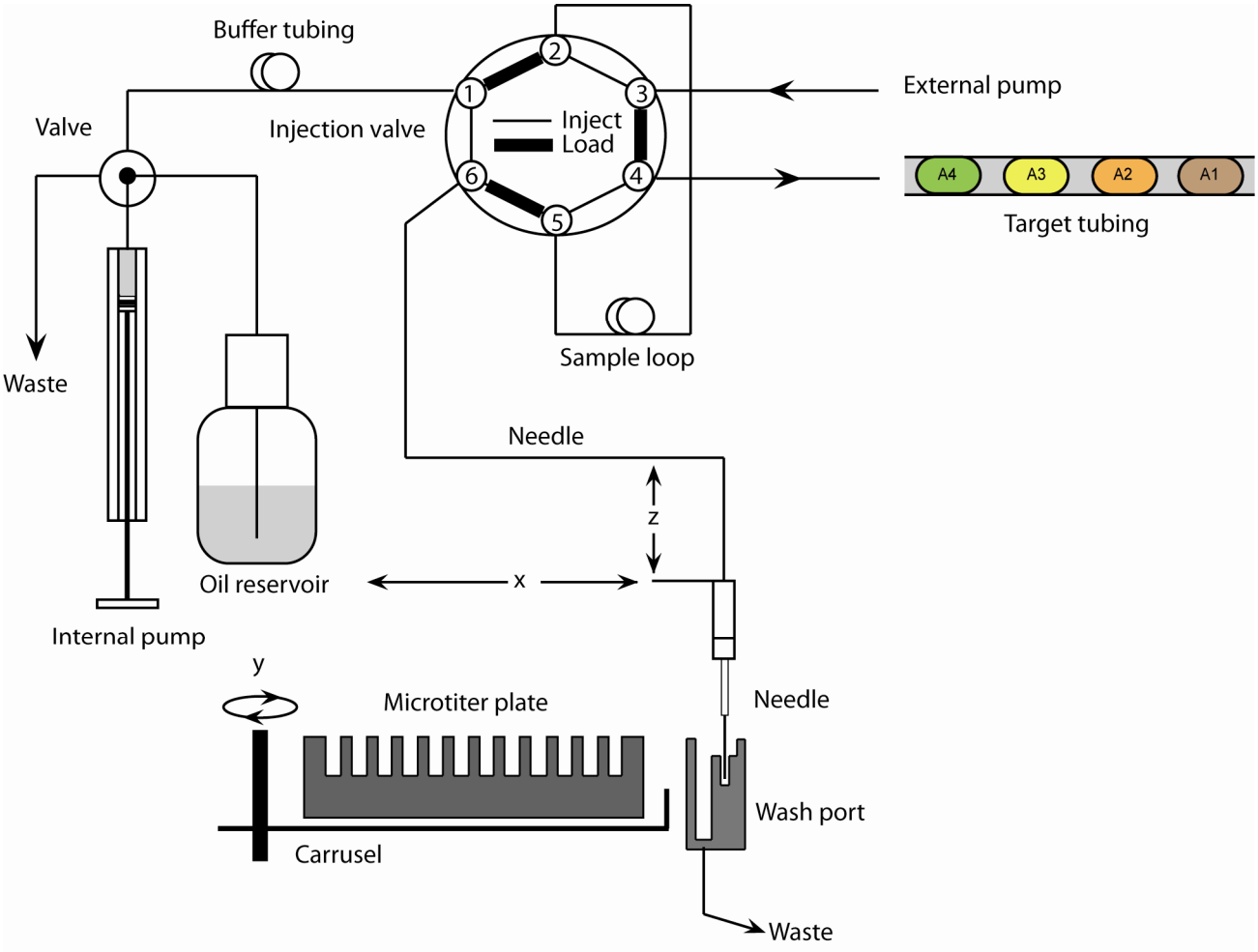

Figure 15. Setup of the autosampler to load samples from microtitre plates and convert them into assays of plugs. *In the Load position the needle tip is immersed into a well and an aqueous sample is withdrawn by the internal pump into the sample loop. The external pump is continuously injecting oil into the target tubing, thus generating an oil plug. As the next step the system switches to the Inject position, and the external pump purges the liquid from the sample loop into the target tubing, thus generating an aqueous plug. Subsequently, the needle tip is washed with oil coming from the internal pump (www.dionex.com).*

In parallel, the external pump (PHD 22/2000, Harvard Apparatus) is continuously injecting oil into the target tubing thus generating an oil plug. Subsequently, the system changes to the *Inject* position in which the external pump flushes the aqueous volume

within the sample loop into the target tubing thus generating an aqueous plug. At the same time a washing step is performed by rinsing the buffer tubing and the needle with oil from the internal syringe. As the next step, the system switches back to the *Load* position and the next sample in the microtiter plate is aspirated. Consequently, a small volume from each well of the entire microtiter plate is loaded sequentially into the target tubing in form of distinct aqueous plugs separated by immiscible oil (Figure 15).

For further processing of these plug arrays on-chip, the inlet geometry turned out to be crucial. While conventional vertical inlets caused the breaking of plugs and significant cross-contamination, horizontal inlets (in line with the channels; punched from the sides and sealed with Loctite 351 glue) allowed the injection of intact plugs into the splitting device (Figure 16).

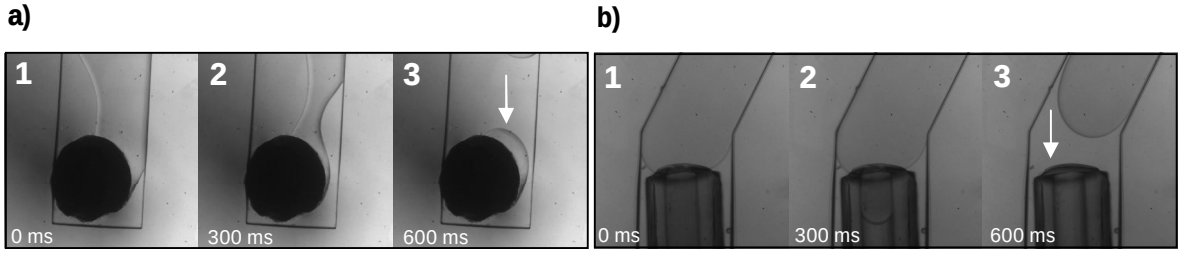

***Figure 16. Injection of an array of plugs into a microfluidic chip using vertical and horizontal inlets**. **(a)** The ports for the inlets were punched from the top, orthogonal to the channels, using a 0.75 mm-diameter Harris Uni-Core biopsy punch. **(b)** The ports for the inlets were punched from the sides (in line with the channels) using a 0.75 mm-diameter Harris Uni-Core biopsy and tubes connected with Loctite 351 glue. White arrows indicate remaining deposits from the previous plug (left) or smooth passing of the microcompartments (right). The numbers at the bottom are the time intervals between the series of pictures.*

The generation of an aqueous plug using the autosampler took about 30 s at minimum thus making the process of generating a whole array (96 aqueous plugs separated by oil) relatively slow. To further increase the throughput of our system, the parental plugs were splitted into smaller subunits thus obtaining multiple small volume copies per parental array of plugs (Figure 17). These could be used either as replicates of the same assay or for entirely different screens. For that purpose, the parental array of plugs (5 µL each plug) was flushed by the autosampler through a symmetric chip with eight branching channels of the same dimensions immediately after its generation (downstream of the autosampler) (Figure 18). The tubing at the inlet of the device was UV glued to the PDMS

and connected by an adaptor (made of PTFE) to the target tubing coming out of the autosampler. After splitting, eight small copies (625 nL each plug) of the parental array of plugs were obtained.

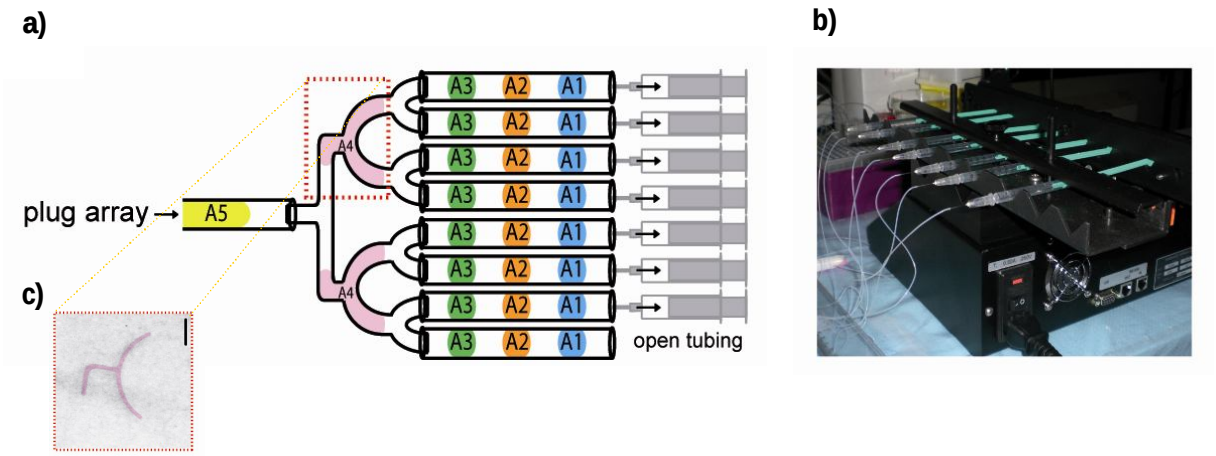

Figure 17. Splitting of plug arrays into small volume copies (step 2 in Figure 14). (a) *A parental array of plugs is injected into a device with eight branching channels. Symmetrical splitting (independently of the channel resistances) is guaranteed by withdrawing 1/8 of the total flow from seven of the eight outlets (using 7 syringes connected to a syringe pump) and connecting the remaining outlet to an open tubing.* ***(c)*** *Microscopical image of the region indicated by the red box. Scale bar = 3 mm.*

Even though this approach has been described to work reliably without any further support (Adamson et al., 2006),in our hands an additional level of flow control was absolutely necessary. To guarantee symmetric splitting of the plugs independently of the resistances of the channels and the connected tubing (which can differ due to slightly different dimensions or the generation of precipitates), we withdrew 1/8 of the total flow from seven of the eight outlets. The remaining outlet was connected to an open tubing thus allowing excess liquid to drain and avoiding the generation of negative pressures (Figure 17). This flow control-based method turned out to be highly reliable and even allowed the splitting of a given small volume copy (of an array of plugs) into even smaller subunits.

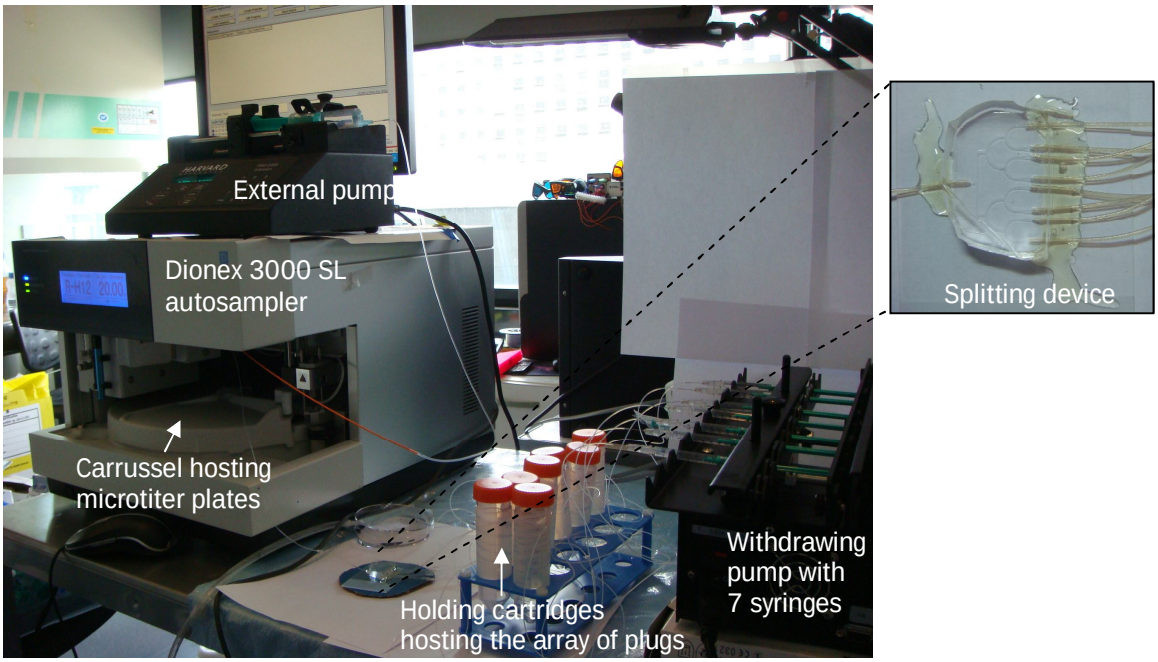

Figure 18. Setup for the generation and splitting of plug arrays. *An autosampler generates array of plugs which are subsequently splitted by flushing its contents through symmetrical branching channels (magnified in the image on the right) and withdrawing 1/8 of the total flow from 7 of the 8 outlets (one tubing is left opened to allow excess liquid to drain).*

When splitting a parental plug library two consecutive times (1:8 and 1:2), the resulting small volume copies showed highly homogenous plug sizes (coefficient of variation from the mean length = 9.38%). In order to visualize efficient splitting, the parental array consisted of alternating plugs containing trypan blue (1 mM) and methyl red (50 mM) (Figure 19a). After splitting each parental array, the resulting small volume copies were stored in PTFE tubing attached to a solid support (e.g. falcon tube) (Figure 19b). This support prevented the plugs from breaking up during their incubation and/or further manipulation.

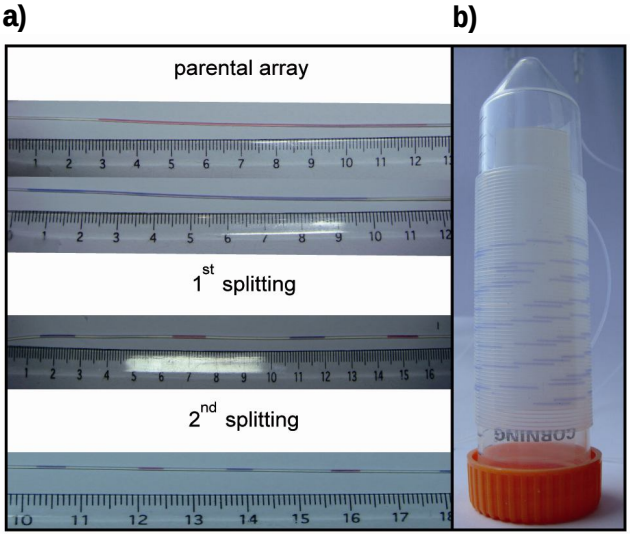

***Figure 19. Splitting and incubation of plug arrays**. **(a)** A parental array of alternating 8 µL plugs containing trypan blue (1 mM) and methyl red (50 mM) was split two consecutive times (1:8 and 1:2) to generate copies of the original plugs with a volume of 1 µL and 0.5 µL respectively. Analysis of the plug length revealed a coefficient of variation (CV) of 9.38 % after splitting. **(b)** Incubation of plugs in a length of tubing attached to a solid support.*

3.2.1.2 Addition of further compounds to plugs

3.2.1.2.1 General principle

As the next step we established a device allowing the addition of further compounds to an array of plugs. In contrast to recently described approaches based on the injection of a continuous aqueous stream into the plugs (Li et al., 2007), our design is based on droplet fusion. This way cross-contamination from one plug to the next due to the deposit of plug contents in the continuous aqueous stream (Li et al., 2007) can be ruled out completely.

Our first device for adding further compounds to plugs was based on a drop maker coupled to a dilating chamber (bubble shape) within the channel (Figure 20). In this chamber incoming drops and plugs slowed down (due to the increasing channel width) and spontaneously fused (due to the absence of surfactant). To analyze this system we generated drops containing 400 µM resorufin and fused them with alternating plugs of

PBS and 1 µM fluorescein. Subsequently, a fluorescence readout was performed and the signals were recorded. Based on the fluorescence data, we detected many non-fused droplets of resorufin (narrow orange peaks in 20b) in between two consecutive plugs.

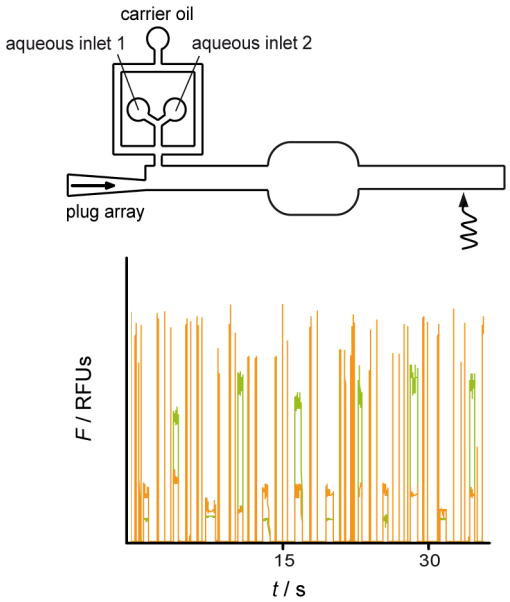

Figure 20. Addition of further reagents to a pre-formed array of plugs using the bubble-shape chamber. *Droplets containing 400 µM resorufin (orange fluorescent) were passively fused with alternating plugs containing PBS and 1 µM fluorescein (green fluorescent) respectively. Subsequently the orange and green fluorescence signal of each individual plug was determined (as indicated by the colour of the time trace). Performing the fusion step in a conventional chamber (bubble shape) results in the release of free substrate drops in between the plugs.*

Shortly afterwards, a publication describing pillar-induced droplet fusion was published (Niu et al., 2008). In a proof-of-principle experiment this approach was used to fuse two consecutive plugs by holding the first plug between pillars (allowing the carrier phase to pass by without moving the plug) until the next plug arrives and coalesces. For our purposes, we integrated an additional drop maker into this system. Consequently, drops containing further compounds (X + Y) are continuously flushed into the pillar chamber, where they are trapped due to the drainage of the carrier phase between the pillars and coalesce spontaneously due to the absence of surfactant. When a plug containing the test compound arrives in the chamber it fuses with the coalesced drops, resulting in insufficient drainage of the carrier phase between the pillars and release of the merged plug (Figure 21a). To analyse this system, we again generated drops containing 400 µM

resorufin and fused them with alternating plugs made of PBS and 1 µM fluorescein. Analysis of the fluorescence data revealed that the integration of the pillar chamber allowed highly reliable plug-drop fusion without the release of free substrate droplets (during the processing of thousands of plugs) (Figure 20b).

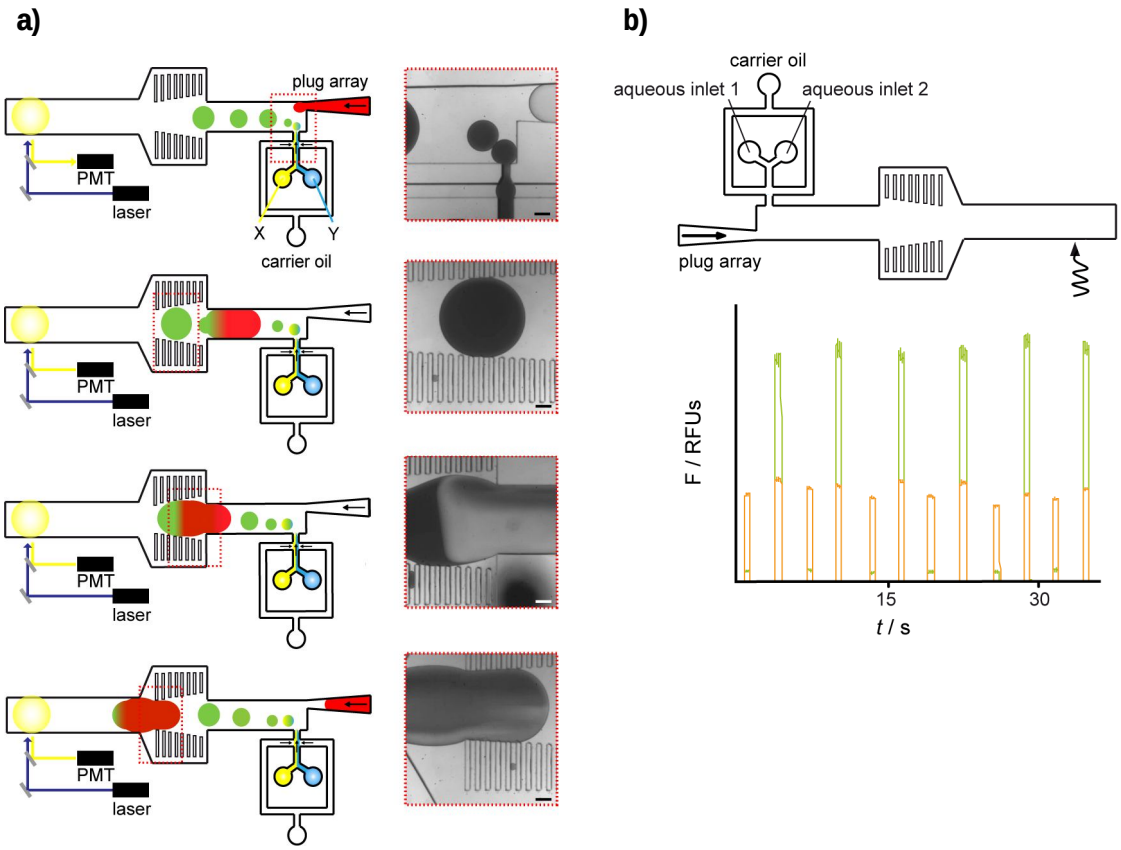

Figure 21. Addition of further reagents to a pre-formed array of plugs using the pillar-chamber (step 3 in Figure 14)*. Droplets containing assay compounds are flushed into a pillar chamber on a microfluidic chip, where they coalesce (due to the absence of surfactant) and get trapped (due to the drainage of the carrier phase). Upon fusion with the next incoming plug the chamber is filled up completely, resulting in insufficient drainage of the carrier phase and release of the substrate-plug merger which can be applied to a fluorescence measurement further downstream of the channel. Light micrographs of the regions indicated by the red boxes are on the right. Scale bar = 200 µm.* ***(b)*** *Droplets containing 400 µM resorufin (orange fluorescent) were passively fused with alternating plugs containing PBS and 1 µM fluorescein (green fluorescent) respectively. Subsequently the orange and green fluorescence signal of each individual plug was determined (as indicated by the colour of the time trace). Performing the fusion step in a pillar chamber allows the reliable fusion of all substrate drops with the passing plugs.*

3.2.1.2.2 Characterization of the device

To further characterize our pillar-based merging device, we determined the range of mixing ratios and total volumes that can be achieved. In a first step, we kept the total plug volume after the addition of substrate constant (813 nL) and changed the relative volume ratios between plugs and drops. It turned out, that the system works reliable over a wide range of ratios (approximately from 0.6:1 to 3.3:1), thus allowing significantly different amounts of a given compound to be added without requiring any change in the chip geometry/dimension. Noteworthy, even at total flow rates of up to 5000 µL/h droplets and plugs were efficiently fused without observing free substrate droplets downstream of the pillar chamber or the fusion of two consecutive plugs (Figure 22a).

In a next step, we changed the resulting plug volumes after substrate addition and determined the fusion efficiency for different overall flow rates. In theory, pillar-induced droplet fusion should work reliably as long as the final plug volume ($V_{final} = V_{plug} + V_{drops}$) is similar to the volume of the pillar chamber ($V_{chamber}$, ~880 nL for the described device). While bigger volumes ($V_{final} > V_{chamber}$) should result in a premature release of the plug (before fusion has occurred), smaller volumes ($V_{final} < V_{chamber}$) should cause the plugs to be retained for a longer time period, thus resulting in coalescence with the next consecutive plug (hosting a different compound). Indeed, our observations exactly match these expectations: the successful addition of substrate droplets was obtained for V_{final} = 500 nL – 1100 nL. Furthermore, when plotting the total volume of the plug merger against different overall flow rates we furthermore saw that very high total flow rates (>7000 µL/h) result in the release of free substrate droplets downstream of the pillar chamber. Nonetheless, efficient droplet fusion was observed for a wide range of resulting plug volumes and flow rates (Figure 22b), thus demonstrating the flexibility of our device.

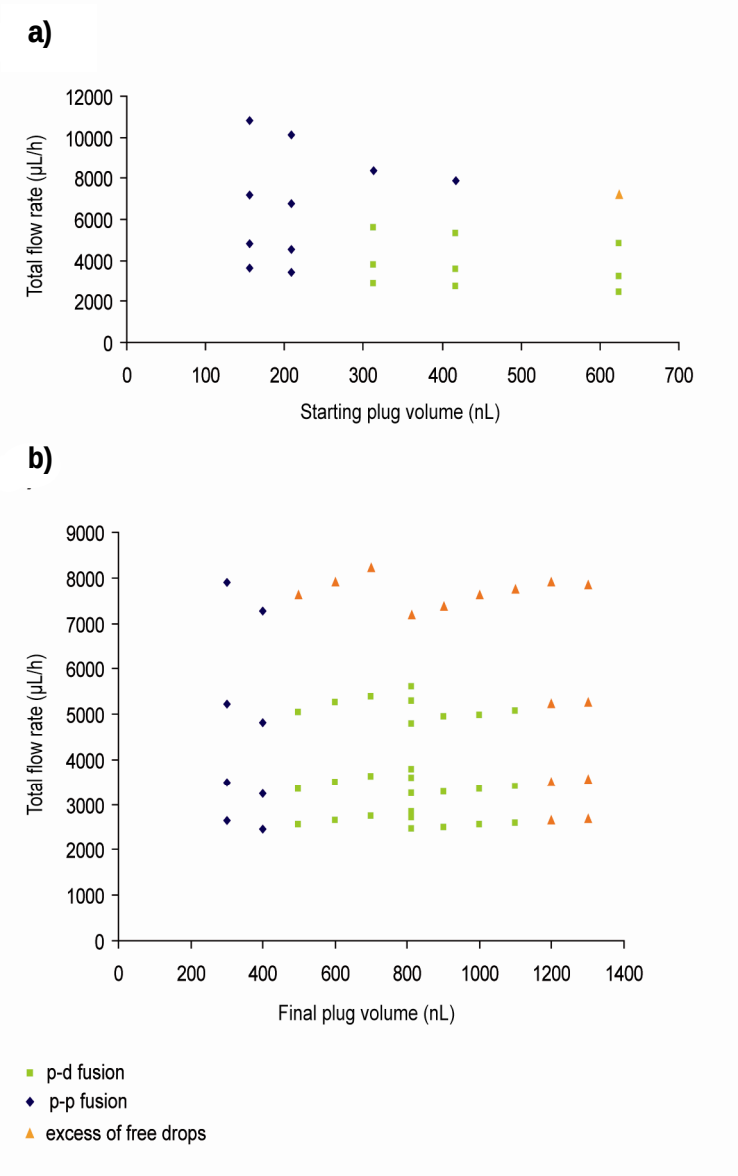

***Figure 22**. **Characterization of the merging device. (a)** Fusion efficiency for plug-drop mergers of constant final volume (V_{total}) at different total flow rates (Y-axis). Plugs of different starting volumes (X-axis) were injected into the device and the relative aqueous flow rates (QA_{plugs}:QA_{drops}) were adjusted to obtain a resulting plug-drop merger with a volume of 813 nL (see chapter 2.6.4 for details how the corresponding flow rates were obtained). The plug-drop fusion process (p-d fusion) was considered successful (indicated by green points), as long as two consecutive plugs did not fuse (p-p fusion; indicated by blue squares) and no free droplets (indicated by orange triangles) were released from the pillar chamber. **(b)** Fusion efficiency for plug-drop mergers of different final volumes (V_{total}; X-axis) plotted against the total flow rate (Y-axis). The indicated final volumes were obtained using relative volume fractions (V_{plug}:V_{drops}) for which successful plug-drop fusion had been demonstrated (green points in a)).*

3.2.1.3 Cross contamination studies

In a next step we analyzed the level of cross-contamination in our system. For this purpose we generated arrays in which the first plug contained 30 µM fluorescein followed by three plugs made of PBS and determined the carry-over (Figure 23a). In particular, we performed fluorescence measurements directly after the generation of the plugs, after splitting into small volume copies and subsequent to the addition of a further substrate (PBS) by droplet fusion. Even after such a series of manipulation steps the carry-over between the first and the second plug was just 2.5 % and decreased further to non-detectable levels in the following plugs. The generation of plug arrays by the autosampler caused only about 1 % of cross-contamination, while additional carry-over was generated by transferring the plugs from one module to the next one. Performing fluorescence measurements on-chip as well as in the transparent tubing (connecting the different modules), we could show that each time the plug array passed the outlet of a given device, the carry over increased by roughly 0.75 % (Figure 23b). Strikingly, we did not observe this effect at the inlets, probably indicating that a transition from smaller to bigger diameters is less problematic than vice versa. In general, optimization of the inlet and outlet geometry seems to be the most important for decreasing the levels of cross-contamination, as we already observed when comparing horizontally and vertically punched tube connections. Therefore, the design of three-dimensional molds (with smooth transitions of the channel depths) could be a solution. Nonetheless, the overall level of cross-contamination in our system (even without additional measures) is not significantly higher than in automated microtiter plate systems, which can show cross-contamination levels of up to a few percent (Bartsch et al., 2004; Hanson and Cartwright, 2001). Furthermore, as presented here, the carry-over between chemically distinct plugs can be reduced by additional buffer plugs in between the samples.

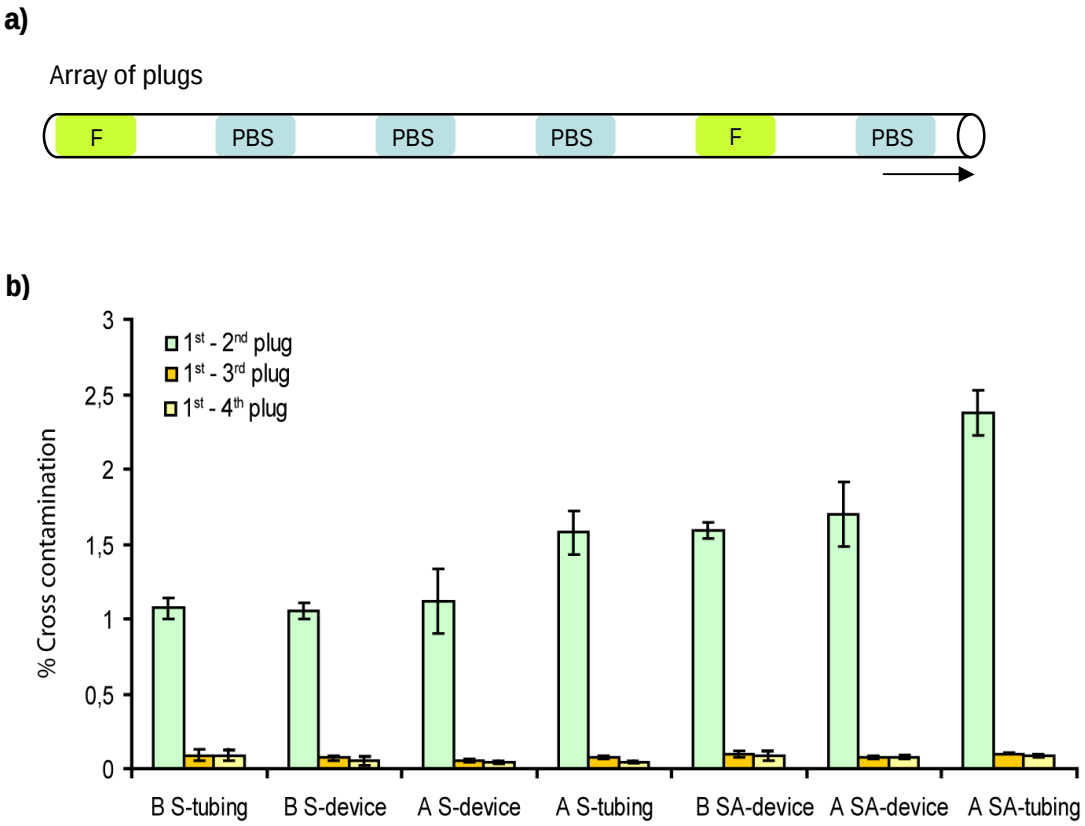

***Figure 23. Cross-contamination between plugs**. **(a)** Arrays of plugs in which the first plug contains 30 µM fluorescein in PBS followed by three plugs containing PBS alone were generated. **(b)** Subsequently, fluorescence measurements were performed before and after each manipulation step, either using transparent PFTE-tubing (tubing) or on-chip (device). B S = before splitting; A S = after splitting; B SA before substrate addition and A SA = after substrate addition. Error bars represent the mean standard deviation from six experiments.*

3.2.1.4 Analysis of the plug size after multiple manipulation steps

To further characterize the reliability of our integrated platform, we determined the coefficient of variation (CV) of the plug volumes after each manipulation step. This was achieved by analyzing the width of the fluorescence peaks for plugs containing 30 µM fluorescein. Since the flow rate of the plugs (υ_p) is known and the peak width corresponds to the time (t) required for a plug to pass the laser focus, it can be used to calculate the plug volume (V_p):

$$V_p = \upsilon_p \cdot t$$

After the automated generation of plugs, a CV of 3 % in terms of the volume was observed, which increased by an additional 4 % during the splitting step. An increase in CV of only 1.5 % was obtained during the addition of substrate droplets in the merging device (Table 1). Based on this value, the CV for the total volume of drops added to each individual plug was just 6.5 % (188 nL ± 0.015 x 813 nL). This clearly demonstrates the reliability of the droplet fusion process.

***Table 1**. Coefficient of variation of the plug length (variation of the peak width for fluorescence signals from plugs containing 30 µM fluorescein) and corresponding plug volumes after different manipulation steps.*

	Plug generation	Plug splitting	Substrate addition
Resulting plug length	7.1 ± 0.2 cm	9 ± 0.6 mm	11.5 ± 1 mm
Resulting plug volume	5 ± 0.15 µL	625 ± 44 nL	813 ± 69 nL
Coefficient of variation	3%	7%	8.5%

3.2.2 Compound screening and kinetic analysis

After having established all individual modules, we integrated the autosampler and all newly developed microfluidic chips in a single platform suitable for the screening of compounds. To characterize the resulting system we then performed a model screen of compounds inhibiting the enzyme β-Galactosidase. For this purpose we prepared a 96-well plate in which seven wells of row A and seven wells of column 6 contained the inhibitor 2-phenylethyl β-D-thiogalactoside (PETG) in increasing concentrations (160 nM - 80 µM) (Figure 25). Furthermore, even though the sample identity in our arrays is spatially encoded (meaning that the order of all plugs is fixed throughout all sample manipulation steps), we added 7-Amino-4-methylcoumarin in different concentrations (50 µM – 400 µM) to each well of column 1 to further facilitate assigning the readout signal to individual samples (Figure 24). This fluorescent marker emits at a different wavelength (450 nm, blue) from fluorescein, the product of the enzymatic assay (520 nm, green) and therefore does not interfere with the screen.

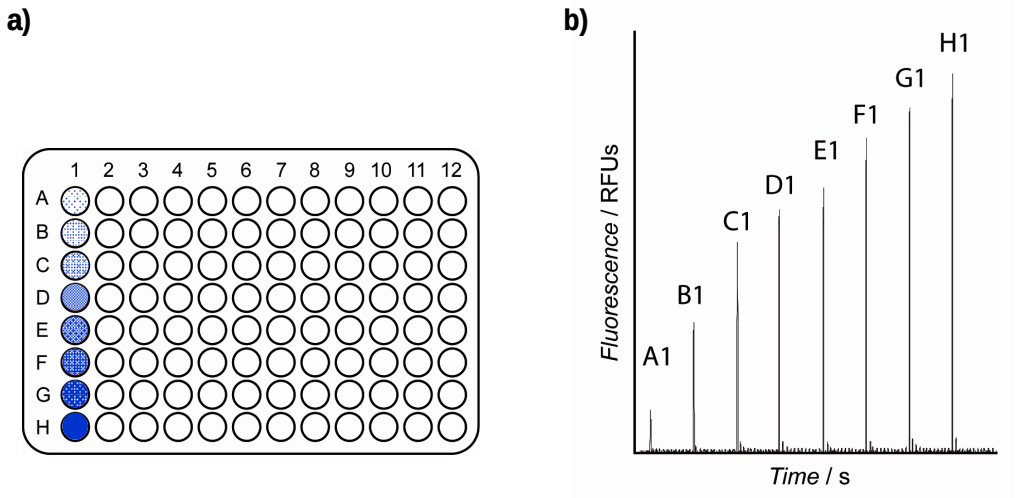

***Figure 24. Optical encoding of the plug samples**. **(a)** 7-amino-4-methylcoumarin was added at different concentrations (50 µM – 400 µM) to the first well of each row in a microtiter plate. **(b)** Every twelfth sample of the plug array showed a peak of unique intensity (at a different emission wavelength than the product of the reaction, fluorescein) thus allowing unambiguous tracking of the sample identity.*

After converting all samples of the 96-well plate into an array of plugs (loading in the order A1 to A12, then B1 to B12, etc…) and subsequent splitting into 8 small volume (625 nL) copies, we injected the plugs into the droplet fusion device. Here we added β-Galactosidase and the fluorogenic substrate fluorescein di-β-D-Galactopyranoside (FDG) in final concentrations of 1 nM and 500 µM respectively to each plug. Subsequently the fluorescence intensities were determined (t_0) before the plugs were collected in another length of tubing and reinjected/analyzed/recollected at multiple time points (t_x). In contrast to earlier studies, this approach allowed each individual plug to be monitored over time. Typically, kinetic studies in droplet-based microfluidic systems are based on the measurement of fluorescence intensities at different positions in a delay line (corresponding to different time points) (Song and Ismagilov, 2003). Even though different droplets are analyzed for each time point, kinetic data can be extracted since all samples have the same composition and need the same time until arriving at the readout point. However, while this strategy works very well for single compounds, it can obviously not be applied when screening samples of different composition. In contrast, our approach enables the recording of kinetic data for diverse compound libraries, since each individual plug can be monitored over time. Analysis of the blue fluorescence from the coumarin marker enabled unambiguous assignment of all data to specific samples since

every twelfth sample showed a blue peak of unique intensity (Figure 24b). While the fluorescence signal of all samples increased over time (due to enzymatic activity), the samples containing inhibitors showed significantly lower intensities (Figure 25).

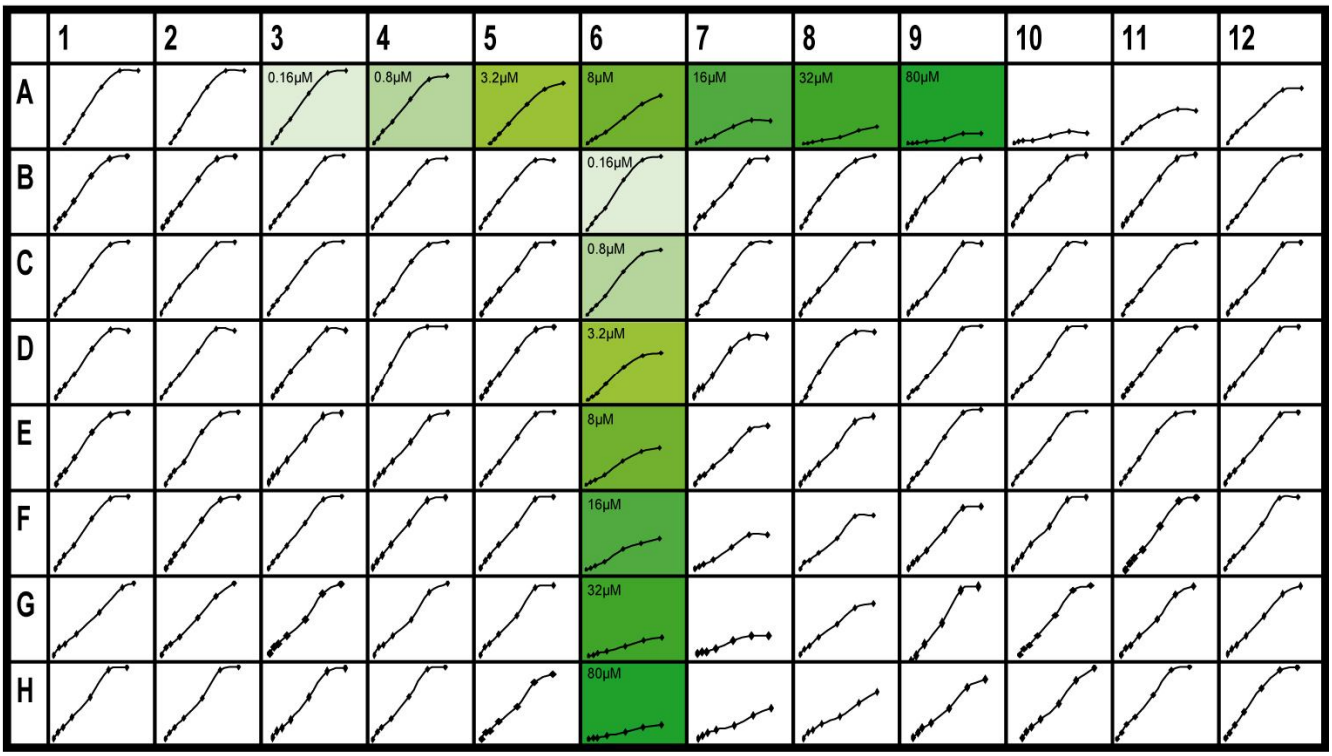

Figure 25. Screening of β-Galactosidase inhibition. *A 96-well plate containing different concentrations (as indicated) of the inhibitor 2-phenylethyl β-D-thiogalactoside (PETG) (green; dark colour indicates high concentrations) and inactive control samples (PBS; white) served as a model library. 1 nM β-Galactosidase and 500 µM FDG was added on chip and the fluorescence was determined after 0, 0.5, 1, 2, 4, 6 and 8 hours. Each curve represents the data from single plugs.*

Analysis of the initial velocities (v_0) extracted from the kinetic data of row A (using non-linear regression to fit the four parameter Hill Equation using GraphPad Prism) revealed an IC_{50} of 7.7 µM PETG (Figure 26). This is in very good agreement with other studies reporting IC_{50} values of 10±1.3 µM (S. Jambovane, 2009) and 3.1 µM (Angenendt et al., 2004) and the value of 8.4 µM which we obtained for control experiements in microtitre plates (Figure 26).

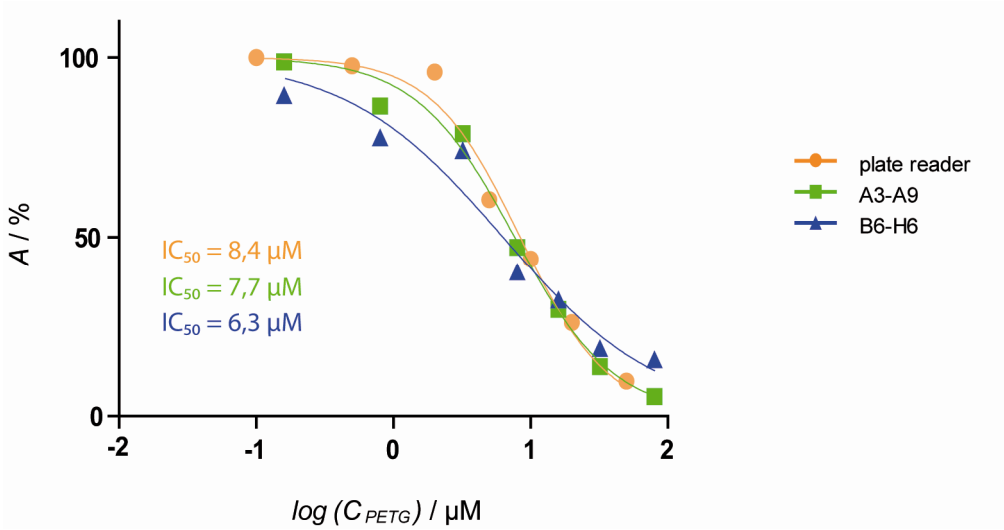

Figure 26. Concentration-response curves constructed using the initial reaction velocities from the kinetic measurements. *The data was obtained on-chip by analyzing the data from samples A3-A9 (green) and samples B6-H6 (blue), or off-chip using a microplate reader (orange). The relative enzyme activity (Y-axis, no inhibitor = 100 %) was plotted against the inhibitor concentration (X-axis, logarithmic scale) and the IC_{50} value was determined using non-linear regression to fit the four parameter Hill Equation using GraphPad Prism.*

When using high inhibitor concentrations (16 µM and above) reduced enzyme activity was also observed in the consecutive plugs. This is in good agreement with the previously determined cross contamination level of ~2.5 %, especially when keeping in mind that the critical on/off-chip transition was performed at each time point (seven times in total). This level of cross contamination does not significantly alter the IC_{50} calculated when screening each compound consecutively in increasing concentrations: indeed, the IC_{50} calculated from analysis of row A (where cross-contamination from the previous plug, which contains a lower inhibitor concentration in each case, is expected) is 7.7 µM, compared to an IC_{50} of 6.3 µM from the analysis of column 6 (where no cross-contamination from the previous plug, which contains PBS, is expected). Cross contamination could also be prevented by using additional buffer plugs in between each sample (see Figure 23b) (Chen and Ismagilov, 2006).

In summary, we have developed a fully integrated and automated screening platform allowing the generation, incubation and on-chip manipulation of chemically distinct plugs.

In a proof-of-principle experiment we successfully screened inhibitors of β-galactosidase starting from a 96-well plate.

3.3 Coupling a therapeutical effect with a positive fluorescence signal

After showing that two-phase microfluidics are compatible with cell-based assays and demonstrating the generation of chemically-distinct plugs, we focused on the development of novel fluorescence assays for drug discovery. In particular, we were interested in developing a viral inhibition assay compatible with the previously developed microfluidic systems. Hence the readout signal should be based on fluorescence and the incubation times should not exceed a few days (the time cells remain viable in the aqueous microcomparments).

3.3.1 General set up of the assays

The goal of this work was to set up an assay system coupling a positive fluorescence signal with the inhibition of viral infection. This could be achieved using engineered host cells (indicator cells) constitutively expressing a reporter gene unless infected by engineered viral particles (effector particles). To implement this idea we used HEK293T cell-derived indicator cells stably expressing a membrane-bound and HA-tagged form of the human tissue plasminogen activator (HA-tPA) (Granieri et al., 2009). This enzyme converts plasminogen into plasmin which itself allows the conversion of a non-fluororescent substrate (HDVLK-Amc) into a fluorescent product (Figure 25) (see chapter *2.3.1.3*). Furthermore, the HA-tag can be used for antibody-based stainings as an alternative readout system.

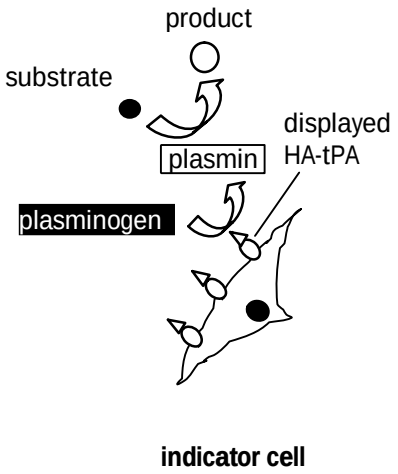

***Figure 25. Cells constitutively expressing a reporter gene unless infected effector particles**. HEK293T cell-derived indicator cells stably expressing a membrane-bound and HA-tagged form of the human tissue plasminogen activator (HA-tPA). This enzyme converts plasminogen into plasmin which itself allows the conversion of a non-fluororescent substrate (HDVLK-Amc) into a fluorescent product.*

As effector particles, we chose the murine leukemia virus. This virus seemed to be an ideal model system, since it can be pseudotyped with a variety of heterologous envelope proteins, resulting in particles with the host cell tropism of the corresponding species (Baum et al., 2006). Once established, an MLV-based system should therefore be adaptable for the screening of inhibitors against a variety of viral species. Furthermore, the use of non replication-competent pseudotype particles should allow keeping the containment level low.

To obtain effector particles capable of entering our HEK293T-derived indicator cells, we pseudotyped MLV particles with the G-protein of vesicular stomatitis virus (MLV(VSV-G Env)). Furthermore, we compared three different approaches based on RNA interference (RNAi (Ito et al., 2005)) and suicide genes for the efficient shut down of the reporter gene upon cell-entry (Figure 26a): First, we generated effector particles having packaged a vector encoding short hairpin RNA (shRNA) mediating the degradation of HA-tPA mRNA (α-tPA particles). This way, the reporter enzyme should be downregulated upon viral entry into the indicator cells. Second, we produced effector particles transducing a suicide gene (Herpes-Simplex Virus Thymidine Kinase; TK particles) which, upon addition of the

corresponding substrate (Ganciclovir), mediates cell death of the indicator cells. Consequently, the reporter gene activity should be eliminated as well as unspecific conversion of the fluorogenic substrate due to other cellular enzymes. Finally, we also generated effector particles having packaged a vector encoding shRNA abolishing the puromycin resistance of the indicator cells (α-Puro particles). Hence, in the presence of puromycin the indicator cells should be killed efficiently. In summary, all three types of effector particles should mediate a strongly decreased reporter gene signal upon cell-entry, whereas non-transduced cells should show the maximum signal intensity.

To prove this hypothesis, we incubated indicator cells with the three types of effector particles in the presence and absence of 25 µM AZT. This well-characterized inhibitor of reverse transcriptase should efficiently inhibit transduction in the corresponding samples. During the following days we then performed the fluorescence readout. For each type of effector particle, we determined the optimal time point (resulting in the highest difference of the fluorescence signal for samples with and without AZT) for the fluorescence readout and the addition of compounds (Ganciclovir or Puromycin) mediating cell death (for HSV-TK particles and α-Puro particles). Subsequently the best results for each kind of effector particles were compared to determine the most powerful assay system (Figure 26b).

While all types of particles mediated a high fluorescence signal in the presence of AZT and a low fluorescence signal in absence of AZT, the signal to background ratio (the quotient of those two values) differed significantly: Using α-tPA particles, the ratio was just 4.9, whereas for HSV-TK particles and α-Puro particles values of 9.3 and 16.5 were obtained, respectively (Figure 26c). To analyse the power of each assay system we also determined the z-factor, a statistical parameter (Zhang et al., 1999) characterizing the power of a high throughput assay. Assays having a Z-factor between 0.5 – 1 are considered as excellent assays (with 1 being the theoretical optimum). For the three different particle types we obtained Z-factors of 0.53 (α-tPA), 0.79 (HSV-TK) and 0.85 (α-Puro). Taken together this clearly showed that α-Puro particles were most suitable for the novel assay system for which reason all further experiments were performed with this particle type.

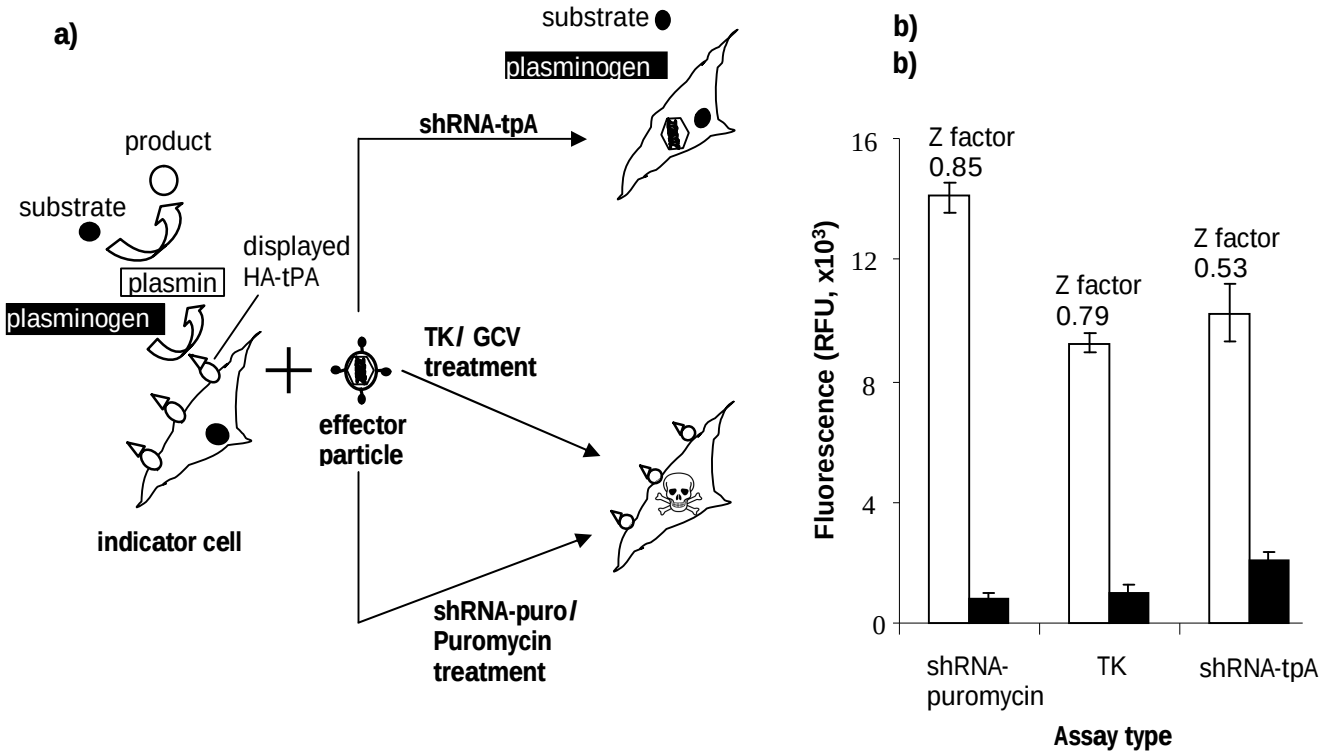

c)

Particle type	Assay type	Signal to background ratio
MLV(VSVG)	shRNA-puromycin	16.5
MLV(VSVG)	TK	9.3
MLV(VSVG)	shRNA-tpA	4.9

Figure 26. Coupling a positive fluorescence signal to the inhibition of viral cell entry. (a) *Human indicator cells displaying a membrane-bound and HA-tagged form of the tissue plasminogen activator (HA-tPA) convert plasminogen into plasmin, which in turn converts a non-fluorescent substrate into a fluorescent product. This reporter gene signal can be shut down upon viral cell-entry using three different types of effector particles. Particles having packaged a vector encoding shRNA mediating the degradation of HA-tPA mRNA (α-tPA) enter the indicator cells and decrease the expression of the reporter gene. Particles having packaged a vector encoding Herpes Simplex Virus Thimidine Kinase (HSV-TK) enter the indicator cells and mediate cell death upon the addition of Ganciclovir (GCV). Particles having packaged a vector encoding shRNA targeting the puromycin resistance of the indicator cells (α-Puro) enter the indicator cells and mediate cell death upon the addition of Puromycin.* ***(b)*** *Fluorescence signals for the three different particle types. Indicator cells were incubated with the corresponding particles in the presence (white) and absence (black) of 25 µM AZT. Subsequently, the fluorescence signals (Y-axis) were determined using a plate reader.* ***(c)*** *Signal to background ratio obtained for the different assays.*

3.3.2 Dose response experiments

To prove that the novel assay allows the screening of compounds simultaneously for inhibitory and cytotoxic properties, we incubated indicator cells and effector particles in the presence of different concentrations of AZT (10^{-8} M to 10^{-3} M). Subsequently we determined the fluorescence signals relative to those of control cells which had been incubated in absence of AZT and any viral particles (the fluorescence of these cells was considered as 1; Figure 27a). As expected, increasing concentrations of the drug correlated with increasing levels of inhibition. However, for concentrations above 25 µM, the fluorescence signal was decreasing again, most likely due to cytotoxic effects. It is well known that AZT has adverse effects on a variety of human tissues (Kline et al., 2009; Zhang et al., 2001). Hence the strongest fluorescence signal should not be obtained at maximum inhibitor concentrations but rather at concentrations exhibiting an optimal balance between viral inhibition and cytotoxicity.

To further prove that the novel assay allows cytotoxic effects to be monitored, we performed the same experiments in the presence of different concentrations of sodium azide (1.5×10^{-7} M to 1.5×10^{-2} M), a highly cytotoxic compound without specific inhibitory properties. In this case, the highest relative fluorescence signal was obtained in the complete absence of the compound (with an intensity indicating the lack of inhibitory properties), while increasing concentrations correlated with even lower fluorescence signals (Figure 27b). This clearly demonstrates that the novel assay system enables simultaneous monitoring of inhibitory and cytotoxic effects.

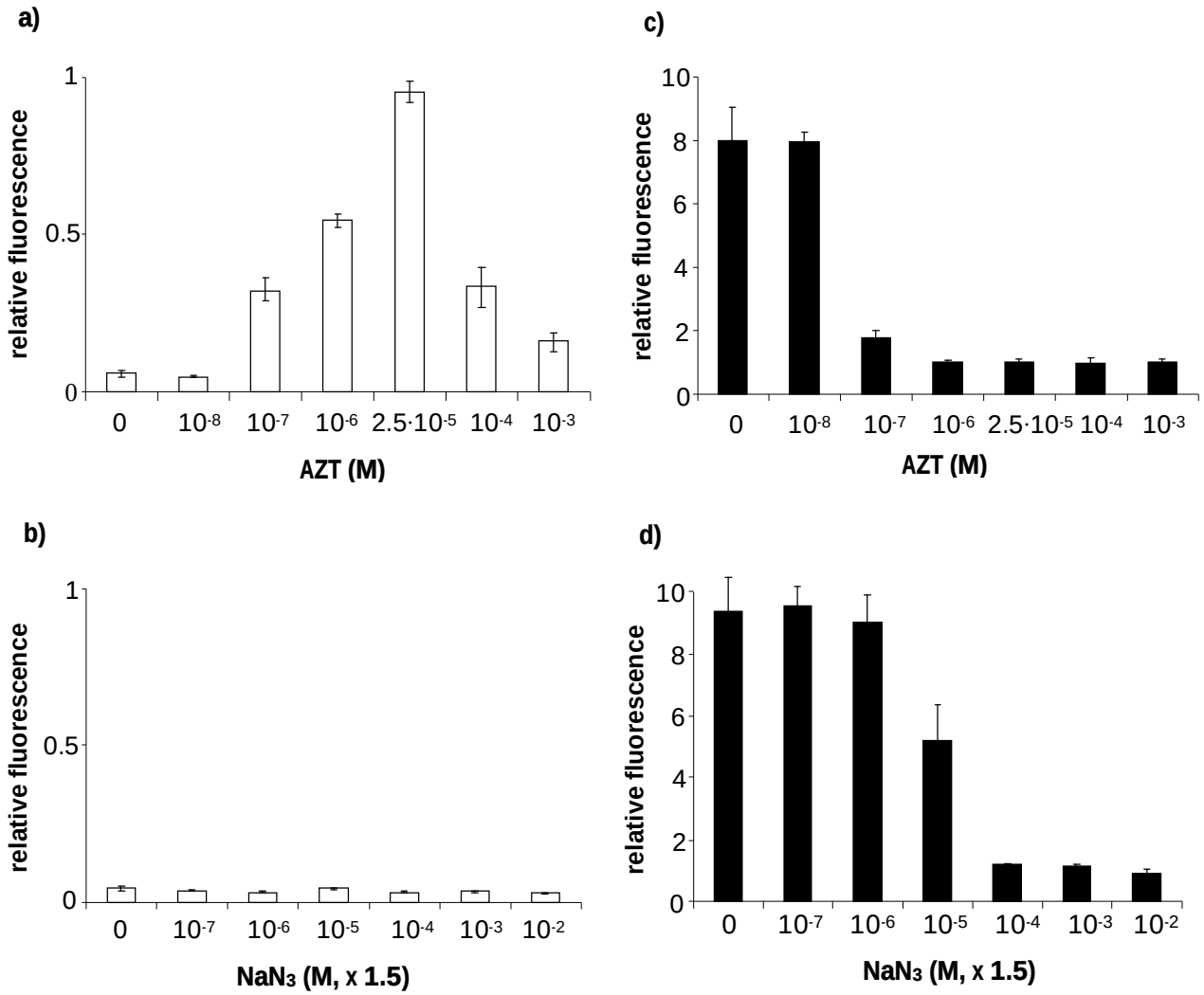

Figure 27. Coupling a positive fluorescence signal with the inhibition of viral transduction (left, white bars) or with the transduction itself (right, black bars). *Indicator cells were transduced with α-Puro effector particles in the presence of* ***(a)*** *different concentrations of the specific inhibitor AZT or* ***(b)*** *the non-specific, toxic compound NaN_3. The fluorescence signals (Y-axis) were determined after the addition of plasminogen and the fluorogenic (Plasmin) substrate HDVLK-Amc and are shown relative to those of control cells which had been incubated in absence of drugs and any viral particles (fluorescence = 1). For comparison with conventional assay systems, HEK293T cells were transduced with particles having packaged a β-Galactosidase encoding gene in presence of* ***(c)*** *different concentrations of the specific inhibitor AZT or* ***(d)*** *the non-specific, toxic compound NaN_3. The fluorescence signals (relative to the control samples without drugs and virus) were determined after the addition of the fluorogenic β-Galactosidase substrate FDG.*

For comparison with conventional assay systems we repeated the dose-response experiments using a setup coupling a positive fluorescence signal with the transduction

step itself rather than its inhibition. To do this, we incubated the indicator cells with effector particles having packaged a vector encoding β-Galactosidase (instead of α-Puro shRNA). This allowed a positive fluorescence signal to be obtained upon transduction and subsequent addition of the fluorogenic β-Galactosidase substrate Fluorescein di-ß-D-Galactopyranoside (FDG). Using this conventional setup, increasing concentrations of AZT correlated with decreasing fluorescence signals (indicating less transduction events) and does not take into account the cytotoxic effect of high concentrations of AZT (Figure 27c). When using sodium azide as a model inhibitor, this systematic error became even more obvious: Even though this compound does not mediate any specific inhibition of viral cell-entry, increasing concentrations correlated with decreasing fluorescence intensities (the readout for efficient viral inhibition; Figure 27d). Hence a system coupling a positive signal with the transduction step itself (rather than its inhibition) is not suited for the selection of specific inhibitors. In contrast, the novel assay system allowed inhibitory and cytotoxic effects to be monitored simultaneously, thus enabling the identification of highly specific compounds that do not harm human cells in the effective concentration range.

3.3.3 Reliability of the assay

To assess the reproducibility of the novel assay system, we performed two completely independent sets of experiments (Run 1 and Run 2) on two different days and compared the results. Each experiment contained triplicates of all samples for which the fluorescence was determined (using AZT concentrations of 10^{-8} M to 10^{-3} M; 21 samples per run). Subsequently, the values obtained for Run 1 were plotted against the corresponding values for Run 2. The resulting data points in the dot plot show a linear correlation, demonstrating a high degree of reproducibility for the assay (Figure 28). The fitted trend line has a coefficient of determination (R^2) of 0.95. In parallel, we determined the (mean) relative standard deviation (RSD) between the replicates in one run (intra-comparison) and between the two Runs (inter-comparison). The obtained values of 11 %

(intra-comparison) and 15 % (inter-comparison) demonstrate the reliability and robustness of the assay.

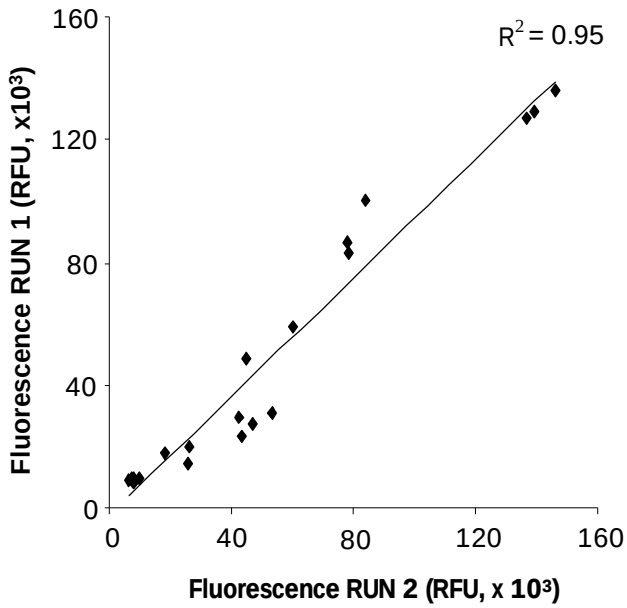

Figure 28. Reproducibility of the viral inhibition assay. *Two completely independent sets of experiments were performed on two different days (using the same sample compositions). The fluorescence signals for all samples of Run 1 were plotted against the corresponding fluorescence signals of Run 2. R^2 = determination coefficient.*

In summary, a novel assay for the screening of antivirals has successfully been developed. Since the assay is based on fluorescence and requires incubation times of no more than a few days, it should be compatible with the previously developed microfluidic platforms.

4. Discussion and Outlook

This work has been focusing on the development of a two-phase microfluidic platform for drug screening. In a first place we have established two-phase microfluidics systems generating miniaturized reaction vessels in which mammalian cells and even multicellular organism (*C. elegans*) can remain fully viable for several days. The size of the compartments (reaction vessel) can be adjusted according to the assay duration. Since cell density was found to be inversely correlated with the survival time of encapsulated cells, large compartments are hence preferential for long-term assays. Consequently, even proliferation assays (e.g. for screening cytostatic drugs) should be possible as long as the chosen volume is big enough to guarantee sufficient supply of nutrition. On the other hand, small compartments might be advantageous for obtaining high concentrations of secreted cellular factors (e.g. antibodies, (Koster et al., 2008). Besides the volume, additional factors, notably the biocompatibility of the surfactants and the gas permeability of the storage system, have a major impact on cell survival.

Surfactants can interfere with biochemical reactions carried out in the drops (e.g. mediating cell lysis, denaturating proteins), and can cause mass transfer of the aqueous phase between drops by micellar transport resulting in cross contamination. This mass transfer correlates with the surfactant concentration and the hydrophobicity of the molecules within the aqueous phase. When working with plugs, surfactants are not required for acquiring stability since they are usually stored either in a channel or a length of tubing stably separated by a spacer of immiscible oil. Hence there should not be any mass transfer, while biocompatibility is guaranteed (as long as the oil itself is inert). However, this approach has strict limitations in terms of the storage capacity. A tubing, with an inner diameter of 300 µm and a length of 100 m can host no more than 10500 aqueous plugs with a volume of 150 nL when considering that in our approach the oil spacer between two aqueous plugs is 3.5 times bigger than the plug itself. This limitation cannot be circumvented by increasing the length of the tubing indefinitely since the back pressure/resistance of the system would increase to values that cannot be handled. In contrast, droplets are usually incubated as an emulsion where they constantly get in close contact with other drops, thus requiring the use of surfactant. In the described experiments, the applied surfactant (dimorpholinophosphate-perfluoropolyether,DMP-

PFPE) turned out to be biocompatible with the cells and did not mediate significant mass transfer of the assay components during 16 h of incubation (positive and negative samples appeared as two independent populations in the fluorescence measurements). Furthermore, the storage capacity of drops off-chip is almost unlimited; for example, 10^7 drops with a volume of 660 pL correspond to a total volume of just 6.6 mL.

Long-term incubation assays also require sufficient gas exchange. This can be ensured either by using open reservoirs, or channels and tubing made of gas-permeable materials such as fluorinated polymers. Efficient gas exchange is also helped by the fact that perfluorocarbon carrier fluids can dissolve more than 20 times the amount of O_2, and 3 times the amount of CO_2, than water and have been shown to facilitate respiratory gas delivery to both prokaryotic and eukaryotic cells in culture (Lowe et al., 1998).

Furthermore, the possibility of reinjecting microcompartments into a chip after the incubation step opens the way for integrated droplet-based microfluidic systems for cell-based HTS. As we have shown here, a fluorescence-based readout for the expression of a cellular reporter gene can be performed in individual compartments at frequencies of 500 Hz. Hence, a wide range of commercially available fluorescence-based assays (Gonzalez and Negulescu, 1998; Sundberg, 2000) can potentially be performed in a high-throughput fashion. The fact that possible coalescence of individual drops does not necessarily bias the readout is noteworthy. As shown here, coalesced drops with higher volumes can easily be identified and excluded from the data analysis. In theory, the use of gates also allows for the analysis of only those compartments hosting a specific number of (fluorescent) cells. In contrast to conventional FACS analysis, the assay readout does not have to be based on fluorophores that remain in, or on the surface of the cells (e.g. GFP or fluorescent antibodies). Using compartmentalization, we have been able to measure the activity of an intracellular reporter enzyme (β-galactosidase) by using a fluorescent product that is highly membrane permeable (fluorescein).

The integration of additional microfluidic modules into the microfluidic platforms shown here should allow the application range to be expanded. Integrating a microfluidic sorting module (based on dielectrophoresis or valves) (Fu et al., 2002) could, for example, enable the screening of drug candidates. The candidates could be genetically encoded by the encapsulated cells themselves (starting with a cell library); hence, the collection of sorted positive drops would allow for the identification of hits by DNA sequencing. On the other hand, a screening of drug candidates could also be performed by encapsulating

different small molecules (e.g. libraries of drugs candidates) in each droplet. One approach might be the encapsulation of individually labelled beads displaying variants of a small molecule library (one-bead-one-compound libraries). Beads could be individually encapsulated and after the screen, depending on the labelling method, hits could be identified either on chip (e.g. using optical tags) or after sorting (e.g. using mass spectroscopy tags). However, there are some possible problems, such as the manipulation of beads in drops due to their size since standard library synthesis is done on beads of 90 to 300 µm in diameter (Brown et al., ; Liu et al., 2002), as well as the generation of large libraries of tags compatible with the screening assay (Liu et al., 2002; Pregibon et al., 2007). To overcome these problems we have worked on a second approach for the screening of drug candidates, which is the sequential encapsulation of compounds in a fixed order, thus abolishing the need for labelling and decoding. For that, we have established a fully integrated screening platform allowing the generation, incubation and on-chip manipulation of chemically-distinct plugs. Samples are loaded from 96-well plates using a Dionex 3000 SL autosampler and injected into a length of PTFE tubing. In contrast to earlier systems (Song and Ismagilov, 2003), our system does not require the immersion of the target tubing into the samples, thus making it compatible with multi-arm robots. Furthermore, the whole sample loading module can be applied to extensive washing cycles. Moreover, the platform allows performing screenings without the need for direct compound labelling and each individual plug can be monitored over time. Usually kinetic studies in droplet-based microfluidic systems are based on the generation of chemically-identical samples and subsequent measurement of fluorescence intensities at different positions in a delay line (corresponding to different time points) (Song and Ismagilov, 2003). Even though different droplets are analyzed for each time point, kinetic data can be extracted, since all samples have the same composition and experience the same delay until arriving at the readout point. However, while this strategy works extremely well for single compounds, it can obviously not be applied for the screening of diverse compound libraries. In contrast, the approach presented here allowed kinetic data to be recorded for many individual plugs of different composition. Another interesting application of our system might be integrated combinatorial synthesis on-chip.

The current limitation of the system is the time required to transform a compound library from the microtiter plate format into an array of plugs. While the loading of a single compound took at least 30 s, all downstream manipulations were performed at rates of approximately 0.33 Hz. However, due to the possibility of splitting a parental library into many small volume copies, the throughput-limiting step has to be performed only once for several screens. Further improvements could be achieved by mounting a multi-tip pipettor on the robotic arm, thus allowing to load several sample loops simultaneously (each one connected to the same target tubing via a multiway valve). In addition, each parental array of plugs could be splitted into even more copies (with smaller volumes). In our hands, plugs with a minimal volume of approximately 150 nL could be generated by splitting (smaller volumes resulted in coalescence within the tubing), which not only increases the throughput, but also decreases the cost of the assay: compared to a 96-well plate, the assay volume is roughly 1000-fold smaller. The miniaturization also facilitates the use of samples which generally cannot be obtained on the scale for HTS. For example, this system might be used for the screening of cells which are only available in small numbers, such as stem cells and primary cells. As demonstrate in this work, cells and multicellular organisms remain fully viable for several days within plugs (Clausell-Tormos et al., 2008).

Regarding the cross contamination between samples, the generation of plug arrays by the autosampler caused only about 1% of cross-contamination, while additional carry-over (1.5 %) was generated by transferring the plugs from one module to the next one. In general, optimization of the inlet and outlet geometry seems to be the key element in the reduction of cross-contamination, as we already observed when comparing horizontally and vertically punched tube connections. Hence the design of truly three-dimensional molds (with smooth transitions of the channel depths) could be beneficial. Nonetheless, even without additional measures the overall carry-over in our system is not significantly higher than in automated microtiter plate systems, which can show cross-contamination levels of up to a few percent (Bartsch et al., 2004; Hanson and Cartwright, 2001). Furthermore, as presented here, the cross-contamination between chemically distinct plugs can be reduced by additional buffer plugs in between the samples.

Recently, another approach for screening drug candidates in drop-based midrofluidcs has been described. A microtiter plate has been robotically interfaced with a drop maker, allowing automated preparation of a droplet library by loading each compound from a

microtiter plate and injecting it into a drop maker. Each compound was co-encapsulated with a unique label (a fluorescent dye of different concentrations), allowing the identification of each member of the library during screening. Ultimately, all droplets where stored in a communal reservoir from were they can be reinjected into other devices for further manipulations (Brouzes et al., 2009). However, the authors only demonstrated the encapsulation of 8 different samples; probably due to the difficulties of increasing the number of different barcodes. The optical labelling of large libraries complexes the microfluidics set up, since more lasers and PMTs have to be used. Moreover, the use of many different dyes might interfere in the assay readout (fluorescence detection) and cause spectral overlap (Pregibon et al., 2007). In addition, since the storage of the resulting emulsions requires the use of surfactants, a possible leakage of the marker dyes as well as of the library compounds cannot be ruled out. Consequently, the system has certain limitations for high-throughput screenings.

In parallel, since fluorescence is one of the most widely used readout signals in microfluidics, we were focusing on viral inhibition assays that could be performed inside the drops. For that purpose, we have developed a generic fluorescence assay coupling a positive fluorescence signal with the inhibition of viral transduction. This allows screens for viral inhibitors to be performed in which cytotoxic compounds (or concentrations thereof) are excluded, thus significantly decreasing the number of false positives. Using MLV effector particles and AZT as a model drug, we observed a 50 % reduction of the relative fluorescence signals for a concentration between 0.1 µM and 1 µM. This is in good agreement with other studies determining an IC_{50} value of 0.1 µM for amphotropic MLV on HEK293T cells (Rosenblum et al., 2001). Our assay turned out to be highly reliable (Z-factor of 0.85) and offers further advantages due to the fact that it is based on non replication-competent pseudotyped particles. First of all, the application of pseudotyped particles allows the containment level to be kept low. Second, it offers high flexibility in terms of the viral species against which inhibitors can be selected. MLV particles can be efficiently pseudotyped with a variety of heterologous envelope proteins, resulting in the host cell tropism of the corresponding species such as HIV (Siegert et al., 2005), influenza (Hatziioannou et al., 1998) and Hepatitis C (Bartosch et al., 2003). Therefore, exchanging the envelope proteins of the effector particles described here (and expressing our reporter system in cells permissive for the corresponding species) should

enable the selection of inhibitors against many clinically relevant viruses.

We found that the most efficient effector particles (α-Puro particles) had packaged the vector encoding shRNA abolishing the puromycin resistance of the indicator cells. Hence, after transduction, the indicator cells died in the presence of puromycin. A further application of these α-Puro effector particles is the controlled killing of cells. In our hands the expression of shRNA targeting the puromycin resistance mediated cell death much more efficient than the well-established suicide gene Thymidine Kinase (TK). This was not only reflected by the signal to noise ratio of the two different assays (using either TK-particles or α-Puro particles), but was also confirmed by microscopical analysis of the corresponding samples. While at the day of the assay readout TK-particles/Ganciclovir treated samples still contained a significant number of living cells, hardly any viable cells were observed in the α-Puro particles/Puromycin treated samples. Hence the α-Puro effector particles can be used for the specific selection of non-transduced cells without the need for fluorescence activated cell sorting (FACS). This could be of special interest when transducing a cell library expressing genetically-encoded inhibitors (such as peptides, antibodies, shRNAs and ribozymes). In this case the elimination of all permissive cells should result in the specific selection of potent inhibitors.

Even though the novel assay has so far been optimized for microtiter plates only, it marks an interesting starting point for the selection of antivirals using our microfluidic platform. The incubation times used in this assay are compatible with the previously demonstrated cell survival within microcompartments. Furthermore, efficient transduction has already been performed in droplets in our lab (Lieber et al., unpublished data). Therefore, future work will focus on the integration of all modules and components developed during the course of this work, thus allowing the screening of antivirals on a drastically miniaturized scale. The minimized sample volumes not only allow decreasing the assay costs, but also facilitate the use of components that can hardly be generated on a large scale, such as the recombinant effector particles required for the novel assay.

5. Thesis summary in French

Développement d'une plateforme microfluidique en système biphasique pour le criblage de médicaments

Le but de ma thèse était le développement d'une nouvelle technologie de criblage pour l'identification de nouveaux médicaments. En particulier, nous nous sommes concentrés sur le design de systèmes microfluidiques en gouttes pour réaliser des tests cellulaires. Dans ces systèmes, des gouttes aqueuses entourées d'une phase continue d'huile servent de réservoirs miniaturisés pour des réactions (les volumes vont du pL au nL). Bien que cette technologie ait été utilisée pour toute une gamme d'application en (bio)-chimie (Beer et al., 2007; Chen and Ismagilov, 2006; Martin et al., 2003; Wheeler et al., 2005), il n'existait pas de systèmes permettant de réaliser des tests cellulaires dans des gouttes quand ce projet de thèse a débuté. En particulier, la survie et la croissance de cellules humaines dans les gouttes, la lecture automatisée sur puce microfluidique de la réponse d'un système rapporteur cellulaire et l'encapsulation de divers médicaments candidats dans les gouttes n'avait pas été encore démontrés. Le but de ce projet était donc de dépasser ces limites et d'utiliser de faibles volumes de liquides pour une approche nouvelle appliquée au criblage de médicaments.

Réaliser des tests cellulaires dans des systèmes conventionnels comme les plaques de microtitration à 96, 384 ou 1536 puîts nécessite la manipulation de volumes relativement grands, ce qui rend difficile la manipulation d'échantillons précieux (comme les particules virales pseudotypées, les cellules primaires, les cellules souches, des inhibiteurs ou des substrats coûteux...). Malheureusement, il y a peu de possibilité de miniaturisation de la technologie des plaques de microtitration en raison de l'évaporation ou des phénomènes capillaires qui créent des ponts entre les puîts des plaques (Dove, 1999). Toutefois, les systèmes de microfluidiques en gouttes sont une approche prometteuse pour dépasser ces limites.

Les systèmes de microfluidique en goutte consistent en des réseaux de canaux de dimensions latérales typiques de 10 à 100 microns dans lesquels les composés sont compartimentés au sein de gouttes de phase aqueuse (utilisés comme microréacteurs) séparés par une huile non miscible à la phase aqueuse (Figure 1). Les gouttes d'eau dans l'huile (e/h) peuvent être générées jusqu'à des cadences de l'ordre de 10 kHz pour former des émulsions très monodisperses (<3% de polydispersité). Les gouttes peuvent être fusionnées ou divisées, leur contenu peut être mélangé rapidement, et elles peuvent être triées (Link et al., 2006). Les systèmes de microfluidique en goutte ont été utilisés pour différentes applications, comme la PCR sur molécule unique, l'analyse de protéome, le diagnostic clinique de fluides physiologiques humains, la cristallisation de protéines et la titration d'anticoagulants (Beer et al., 2007; Chen and Ismagilov, 2006; Martin et al., 2003; Wheeler et al., 2005).

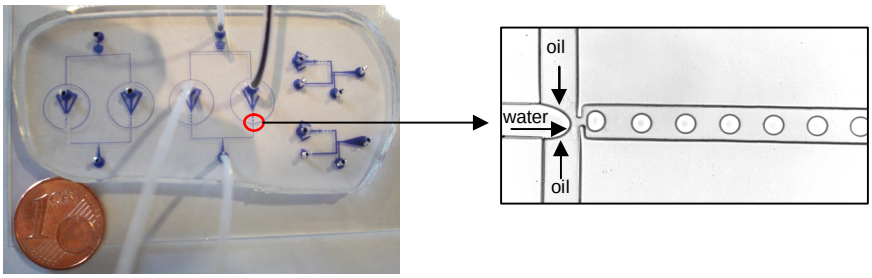

***Figure 1. Plateforme intégrée**. **(a)** Dispositif microfluidique: génération de vecteurs de microcompartiments (plugs) avec un échantillonneur automatique (à partir de plaques de microtitration) (1) Division en unités plus petites (2) addition d'un composé à chaque plug individuel et (3) incubation et lecture du signal fluorescent de chaque plug (4). **(b)** Division d'un plug en unités plus petites. **(c)** addition d'un autre composé (vert et jaune) dans chaque plug (rouge). Schéma du dispositif (gauche) et photos du dispositif expérimental avec une caméra rapide (droite). La barre d'échelle est 200 µm.*

La première étape de ce projet a été de démontrer que des cellules humaines peuvent être incubées plusieurs jours dans les gouttes et être récupérées complètement viables (jusqu'à présent la technologie n'avait jamais été utilisée pour des tests impliquant des cellules humaines) (Clausell-Tormos et al., 2008). Pour ceci, nous avons encapsulé des cellules dans des micro-compartiments de tailles différentes (660 pL to 660 nL) et analysé la survie de cellule sur 14 jours. Un test 'Live/Dead' a révélé que le taux de survie dépend principalement de la quantité de nutriments et donc de la densité de cellules

dans le compartiment. Ainsi, les gouttes de quelques centaines de nL sont préférables pour les longues incubations en raison de la grande quantité de nutriments disponibles. De plus, ces gouttes peuvent également contenir des petites populations de cellules ou même des organismes multicellulaires. Pour prouver ceci, nous avons encapsulé des oeufs de nématodes (*C. elegans*) dans des gouttes de 660 nL et observé la croissance de vers adultes et la naissance de la nouvelle génération en quatre jours.

Ensuite, nous avons démontré la possibilité d'utiliser ces systèmes microfluidiques pour détecter l'entrée virale dans les cellules à haut-débit (Clausell-Tormos et al., 2008). Dans une expérience classique (hors puce microfluidique), nous avons incubé des cellules HEK293T avec des particules virales contenant le gène encodant la β-galactosidase (lacZ). Nous avons déterminé l'efficacité de la transduction en utilisant un test standard X-Gal. En parallèle, nous avons encapsulé des cellules uniques de cette population de cellules avec un substrat fluorogénique de la β-galactosidase (FDG, fluorescein di-β-galactopyranoside). Les gouttes ont été incubées hors puce pendant 16h à 37°C. Les gouttes ont été ensuite réinjectées dans une puce microfluidique pour une mesure de la fluorescence de chaque goutte. L'analyse des données a révélé que 12.7 % des cellules était très fluorescente (exprimant le gène lacZ) ce qui était en très bon accord avec la fraction des cellules transduites déterminée avec le test X-Gal hors goutte (13.9 %). Ceci démontre la fiabilité et le potentiel de la technologie.

Ensuite, nous avons démontré la co-encapsulation de différents composés dans les gouttes, nécessaire pour le criblage de médicaments candidats. En particulier, nous avons développé un système automatisé de génération de micro-compartiments distincts. Pour ce faire, nous avons interfacé un échantillonneur automatique (Dionex SL3000 modifiée) avec notre plateforme microfluidique. Il aspire les composés depuis des plaques de microtitration et les injecte dans une portion de tuyau ou ils sont espacés par de petits volumes d'huile perfluorée dans laquelle les composés sont insolubles. Comme les composés sont encapsulés dans un ordre fixé, leur identité est connue tout au long du test ce qui contourne le problème du marquage des composés pour leur identification. Les composés compartimentés (volume = 5 µL) de manière vectorielle sont ensuite injectés au travers de 8 canaux inter-connectés pour obtenir des copies multiples du vecteur initial (625 nL chaque copie). Même si cette approche a été décrite comme

fiable sans effort supplémentaire (Adamson et al., 2006), entre nos mains, un niveau de contrôle supplémentaire a du être implémenté. Pour garantir une division symétrique des compartiments indépendamment des résistances hydrauliques des canaux et des tuyaux (qui peuvent varier légèrement à cause des variations de dimensions des tuyaux ou de la présence de précipité), nous aspirions 1/8 du débit total au niveau de 7 sorties sur les 8. La 8e sortie était laissée à pression atmosphérique pour permettre le drainage de l'excès de liquide. Cette méthode de contrôle des flots s'est avérée très fiable et a également permis la division d'un vecteur de compartiment déjà divisé, en vecteurs de compartiments encore plus petits. L'étape suivante a consisté en l'établissement d'un dispositif permettant l'addition de composés à ce vecteur de compartiments. Contrairement aux approches décrites récemment et basées sur l'injection d'une phase continue dans des microcompartiments ('plug') notre design est basé sur la fusion de goutte. Ainsi, la contamination croisée des microcompartiments liée au dépôt de leur contenu dans la phase aqueuse continue peut être éliminée. Le design est basé sur la fusion de goutte induite par un réseau de piliers. En générale, cette approche est utilisée pour fusionner des gouttes successives en retenant la première goutte entre des piliers jusqu'à ce que la suivante arrive et coalesce avec la première (Niu et al., 2008). Dans notre cas, nous avons intégré dans le système un producteur de goutte supplémentaire. Ainsi, les gouttes contenant les composés à ajouter au microcompartiment (plug) initial sont injectées en continu dans le réseau de piliers et coalescent spontanément (il n'y a pas de tensio-actifs pour stabiliser les gouttes dans ce cas, Quand un microcompartiment contenant un des composants du test arrive dans la chambre il fusionne avec les gouttes coalescées contenant l'autre composant. La goutte résultante empêche le drainage de la phase continue entre les piliers ce qui pousse la goutte hors du réseau de piliers et la libère.

Avec notre système, nous avons réalisé un criblage modèle basé sur un test enzymatique fluorogénique. Nous avons préparé une plaque 96 puîts dans laquelle 14 puîts contenait différentes concentration d'un inhibiteur de β-Galactosidase: PETG (0,16 µM à 80 µM; concentrations croissantes comme indiquée par l'intensité des couleurs croissantes). Après génération d'un vecteur de microcompartiment et division en microcompartiments plus petits, nous avons injecté les microcompartiments dans le dispositif d'addition de substrats. Ici, la β-galactosidase et la FDG, son substrat fluorogénique, ont été ajoutées à

chaque micro-compartiment et l'activité enzymatique initiale a été mesurée (t_0). Ensuite, les micro-compartiments ont été collectés dans un autre tuyau et réinjectés pour analyse à différents temps de réaction (t_X). Alors que le signal de fluorescence augmente en fonction du temps en raison de l'activité enzymatique, les échantillons contenant les inhibiteurs ont révélé une intensité significativement différente. L'analyse des vitesses initiales (v_0) extraites des données cinétiques a révélé des valeurs d'IC_{50} de 7.7 µM PETG et 6.3 µM PETG en très bon accord avec d'autres études reportant des valeurs de 10±1.3 µM et 3.1 µM (Jambovane et al., 2009; Niu et al., 2008) et la valeur de 8.4 µM obtenue en plaque de microtitration. Ainsi, nous avons développé un système de microfluidique en goutte pour le criblage de composés chimiques.

En parallèle des développements microfluidiques, nous avons établi de nouveaux tests pour la découverte de médicaments. Nous avons couplé un effet thérapeutique avec un signal fluorescent afin de les rendre compatibles avec les systèmes de détection en microfluidique.

La plupart des tests pour le criblage d'antiviraux couplent un signal positif avec l'infection elle-même et non pas avec l'inhibition (Daelemans et al., 2005). En conséquence une molécule inhibant l'expression du système rapporteur (par exemple en tuant la cellule) plutôt que l'entrée virale sera inévitablement sélectionnée comme un faux positif. Pour contourner ce problème, nous avons développé un test qui couple l'inhibition de l'entrée virale directement à un signal fluorescent. En particulier, nous avons développé des cellules indicatrices recombinantes générant un signal fluorescent fort à moins qu'elle ne soit transduite par des particules virales pseudotypée non réplicantes. Ce nouveau test utilise des cellules hôtes exprimant de manière stable une forme spécifique de la tPA (tissue Plasminogen Activator) humaine liée à la membrane et HA-tagged (tPA-HA). Celle-ci convertit le plasminogène en plasmine qui à son tour convertit un substrat non fluorescent (HDLVK) en produit fluorescent.

Comme virus modèle nous avons utilisé un virus pseudotypé non réplicant, le MLV (Murine Leukaemia Virus) avec la protéine G du VSV (Vesicular Stomatitis Virus), dans lequel est empaqueté un vecteur encodant des fragments courts d'RNA double-brin qui forment une structure en épingle à cheveux (shRNA). Ces molécules shRNA sont

impliquées dans la dégradation de mRNA de séquence identique qui conduit à la dérégulation de la protéine encodée. En conséquence, l'entrée virale dans la cellule et l'expression des shRNA dans la cellule inhibe l'expression du gène rapporteur de la tPA-HA ce qui a pour conséquence une décroissance significative de la fluorescence.

Malheureusement, le substrat est aussi convertit de manière non-spécifique par d'autres enzymes cellulaires ou d'autres facteurs dans le milieu ce qui conduit à un niveau de base de fluorescence conséquent. Ainsi, l'optimisation de ce test s'est concentrée sur la réduction de ce niveau de base. Pour ce faire, nous avons testé deux autres méthodes de transfert de gène: d'une part, un gène suicide et d'autre part, un vecteur encodant un shARN ciblant la résistance à la puromycin de la cellule. En utilisant le gène suicide HSV-TK (Herpes Simplese Virus Timidine Kinase) le test est basé sur la mort cellulaire après transduction et addition ultérieure du substrat de l'HSV-TK, le ganciclovir, qui est convertit à son tour en produit hautement cytotoxique. En utilisant un vecteur encodant un shARN ciblant la resistance à la puromycin, le test est alors basé sur la mort cellulaire après transduction et addition ultérieure de puromycin. Dans les deux cas, les cellules indicatrices meurent ce qui permet d'éviter la conversion non spécifique du substrat et élimine de fait le signal de base.

Afin de déterminer quelle stratégie donne le meilleur rapport signal sur niveau de base et le meilleur facteur Z (Zhang et al., 1999), nous avons incubé les cellules rapportrices avec des particules (MOI de 50) dans une plaque de 96 puîts en présence et en absence d'inhibiteur (25 µM d'AZT, un inhibiteur de la reverse-transcriptase). L'intensité du signal du gène rapporteur augmente avec la concentration d'inhibiteur sur deux ordres de grandeur (0,25 µM – 25 µM) avant de diminuer aux concentrations plus importantes à cause de la cytotoxicité. Ainsi, le test permet à la fois de mesurer les propriétés d'inhibition d'une molécule donnée mais également de prendre en compte les effets secondaires. Alors que le test basé sur le shARN ciblant la resistance à la puromycin donnait un rapport signal sur niveau de base de 9 et un facteur Z de 0.85 (Figure 2), le test basé sur la TK donnait un signal sur niveau de base de 9 et un Z factor de 0.79. Le test basé sur un shARN ciblant l'expression de la tPA avait un rapport signal sur niveau de bruit de 5 et un facteur Z de 0.53. D'après la littérature, des tests avec un facteur Z>0.5 sont des tests excellents; ainsi notre optimisation a été réussie.

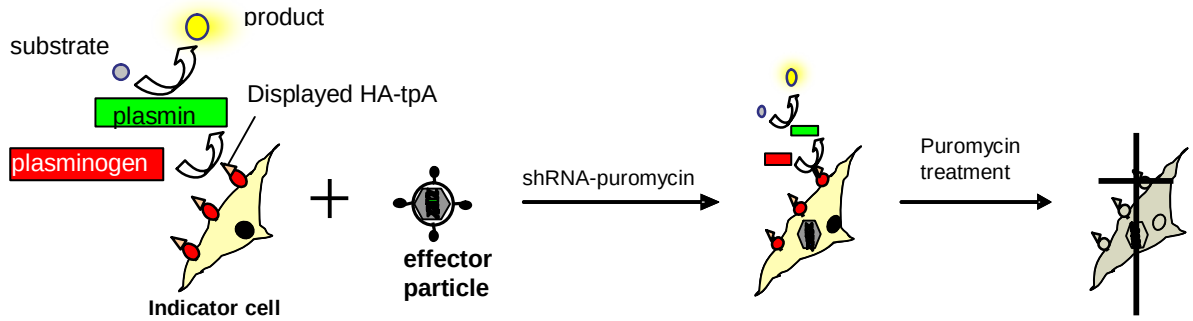

***Figure 2. Couplage d'un signal fluorescent positif avec l'inhibition de l'entrée virale**. Des cellules indicatrices humaines présentent une forme spécifique de tPA (tissue plasminogen activator), liée à la membrane et HA-tagged (HA-tPA). Ce HA-tPA convertit le plasminogène en plasmine qui convertit à son tour un substrat non fluorescent en produit fluorescent. Le signal du gène rapporteur peut être éteint avec l'entrée virale en utilisant trois types de particules virales différents. Des particules dans lesquelles est empaqueté un vecteur encodant un shRNA induisant la dégradation du HA-tPA mRNA (α-tPA) entrent dans la cellule indicatrice et diminuent l'expression du gène rapporteur. Des particules dans lesquelles est empaqueté un vecteur encodant l'HSV-TK (Herpes Simplex Virus Thimidine Kinase) entrent dans la cellule et induisent la mort cellulaire après addition de Ganciclovir (GCV). Des particules dans lesquelles est empaqueté un vecteur encodant un shRNA ciblant la résistance à la puromycin de la cellule indicatrice (α-Puro) entrent dans la cellule et induisent la mort cellulaire après addition de Puromycin.*

En général, le tropisme cellulaire d'une particule peut être altéré en pseudotypant des particules avec l'enveloppe d'autres espèces virales. Ainsi nous avons pseudotypé des particules de MLV avec la protéine Env du VIH pour combiner les propriétés efficaces d'extinction de gènes de notre virus modèle (MLV-VSV-G) avec le tropisme cellulaire du VIH. Cette approche peut ainsi permettre de cribler des inhibiteurs de l'entrée du VIH dans les cellules.

En résumé, nous avons développé une nouvelle technologie de microfluidique en goutte pour le criblage de médicaments et établi de nouveaux tests d'inhibition virale. Combiner ces réussites devrait permettre des approches nouvelles pour l'identification de médicaments antiviraux ou de cocktails d'antiviraux. La miniaturisation des tests devrait permettre non seulement une réduction massive des coûts des criblages (jusqu'à 1000 fois) mais également l'utilisation d'échantillons de très grande valeur que l'on obtient difficilement à des échelles nécessaires au criblage à haut-débit (cellules primaires,

hybridomes, particules virales pseudotypées). De plus, l'utilisation de petits volumes devrait faciliter les tests à l'échelle de la cellule unique.

6. Acknowledgements

I would like to thank Prof. Andrew Griffiths for the opportunity to do my master and phD thesis in his laboratory. This has been a great experience which I will never forget; I could say that it has changed my life. I am also very grateful to him for supporting an internship at the Imperial College London while still doing my phD. This really allowed broadening my scientific horizon. I am really happy of having done my phD in Andrew Griffiths' laboratory. I have not only learned a lot but also met many people with whom I shared great moments that I will never forget.

Furthermore, I would like to thank Dr. Christoph A. Merten for supervising my thesis. During these years, he has been extremely patient and supportive. He taught me a lot of things and I consider him a good example to follow. I am really grateful for the fact that he kindly and patiently read my phD thesis.

In addition, it is a great honour for me that Prof. Josep Esteve, Dr. Roland Marquet, Prof. Andrew de Mello and Dr. Jean-Louis Viovy accepted to participate in the evaluation of my phD thesis. I am grateful to them for the time, and effort they have dedicated to my thesis.

I would also like to thank the *Ministère de l'Enseignement Supérieur et de la Recherche* for supporting the work carried out during my phD thesis.

Moreover, I would like to say thanks to the members of "Christoph Merten's subgroup", for being the way they are. We always helped each other, on the scientific side as well as in "the real life", and we always had good times during seminars and discussions in the lab.

Last but not least I would like to thank the *LBC group members* and the staff of ISIS for being very helpful and having a good mood all the time. Working at LBC has been fun, not only during the parties but as well during working times... it will be difficult to find a group like this somewhere else. In particular I would like to thank Isabelle for all the effort she

put on helping me…she is the best secretary I have ever met. Besides, I would like to thank Linas for his help during my years in Strasbourg; he has always been a big support and I owe him a lot. I would also like to thank Shigeyoshi. He has always been very patient and kind while “being exposed” to our long and loud discussions and jokes. I also appreciate lending me his amazing Japanese photocamera every time I needed it.

7. List of abbreviations

AMC	7-amino-4-methylcoumarin
ATP	adenosine triphosphate
AZT	azidothymidine
BDE	bond dissociation energy
bp	base pair
C. elegans	*Caenorhabditis elegans*
Ca	capillary number
CA	capsid
CMC	critical micellar concentration
CPE	cytophathic effect
CV	coefficient of variation
DM	dicroic mirror
DMEM	Dulbecco's modified eagles medium
DMP	dimorpholino phosphate
DMSO	dimethylsulfoxide
DNA	Deoxyribonucleic acid
DRV	replication-defective retroviral vector
dsRNA	double stranded RNA
E. Coli	*Escherichia coli*
ECM	extracellular matrix
EDTA	ethylenediaminetetraacetic acid
Env	envelope
ER	endoplasmic reticulum
Eth-Br	ethidium bromide
EthD-1	ethidium homodimer
FACS	fluorescence-activated cell sorting
FBS	fetal bovine serum
FDG	fluorescein di-β-D-galactopyranoside
GaIV	gibbon ape leukemia virus
GFP	green fluorescent protein

HLB	hydrophobic-lipophilic balance
HBS	hepes-buffered saline
HDLVK-AMC	His-Asp-Val-Leu-Lys-(amino-4-methylcoumarin)
HEK293T	human embryonic kidney cell line
HEK293tpA	human embryonic kidney cell line displaying tPA
HIV	human immunodeficiency virus
HSCs	hematopoetic stem cells
HSV-TK	herpes simplex virus thimidine kinase
HTS	high-throughput screening
IC_{50}	half maximal inhibitory concentration
IN	integrase
IPTG	isopropyl-b-D-thiogalactopyranoside
IVC	in vitro compartmentalization
IVT	in vitro translation
Kb	kilobase pairs
LB	Luria-Bertani
LOC	lab on a chip
LTR	long terminal repeat
MA	matrix
ME	β-mercaptoethanol
MEMS	microelectromechanical systems
MLV	murine leukemia virus
mRNA	messenger RNA
NC	nucleocapsid
NDA	naphthalene-2,3-dicarboxaldehyde
NF	notch filter
nt	nucleotide
o/w	oil in water
OD	optical density (or absorbance)
PBS	phosphatase buffer saline
PCR	polymerase chain reaction
PDMS	polydimethylsiloxane
PEG	polyethylene glycol

PETG	2-phenylethyl-β-D-thyogalactosidase
PFPE	perfluoropolyether
PG	plasminogen
PL	plasmin
PLL	pol-L-lysine
PMT	photomultiplier tube
PR	protease
PTFE	polytetrafluoroethylene
RE	restriction enzyme
Re	Reynolds number
RISC	RNA-induced silencing complex
RNA	ribonucleic acid
RNAi	RNA interference
RRVs	replication-competent retroviral vector
RSD	relative standard deviation
RT	reverse transcriptase
SAMs	self-assembled monolayers
SDS	sodium dodecylsulphate
shRNA	short hairpin RNA
SU	surface unit
TAE	tris-acetat-EDTA
TG	transfer gene
THF	tetrahydrofuran
TM	transmembrane domain
tPA	tissue plasminogen activator
UTR	untranslated region
UV	ultraviolet
VSV	vesicular stomatitis virus
w/o	water in oil
YFP	yellow fluorescent protein

8. Bibliography

Adamson, D.N., Mustafi, D., Zhang, J.X., Zheng, B., and Ismagilov, R.F. (2006). Production of arrays of chemically distinct nanolitre plugs via repeated splitting in microfluidic devices. Lab on a chip *6*, 1178-1186.

Angenendt, P., Nyarsik, L., Szaflarski, W., Glokler, J., Nierhaus, K.H., Lehrach, H., Cahill, D.J., and Lueking, A. (2004). Cell-free protein expression and functional assay in nanowell chip format. Analytical chemistry *76*, 1844-1849.

Anna SL, B.N., and Stone HA (2003). Formation of dispersions using "flow focusing" in microchannels. Appl Phys Lett *82*.

Aris, R. (1956). On the Dispersion of a Solute in a Fluid Flowing through a Tube. Proceedings of the Royal Society of London Series A Mathematical and Physical Sciences *235*, 67-77.

Balagadde, F.K., You, L., Hansen, C.L., Arnold, F.H., and Quake, S.R. (2005). Long-term monitoring of bacteria undergoing programmed population control in a microchemostat. Science (New York, NY *309*, 137-140.

Baret, J.C., Miller, O.J., Taly, V., Ryckelynck, M., El-Harrak, A., Frenz, L., Rick, C., Samuels, M.L., Hutchison, J.B., Agresti, J.J., *et al.* (2009). Fluorescence-activated droplet sorting (FADS): efficient microfluidic cell sorting based on enzymatic activity. Lab on a chip *9*, 1850-1858.

Bartosch, B., Dubuisson, J., and Cosset, F.L. (2003). Infectious hepatitis C virus pseudo-particles containing functional E1-E2 envelope protein complexes. The Journal of experimental medicine *197*, 633-642.

Bartsch, J.W., Tran, H.D., Waller, A., Mammoli, A.A., Buranda, T., Sklar, L.A., and Edwards, B.S. (2004). An investigation of liquid carryover and sample residual for a high-throughput flow cytometer sample delivery system. Analytical chemistry *76*, 3810-3817.

Baum, C., Schambach, A., Bohne, J., and Galla, M. (2006). Retrovirus vectors: toward the plentivirus? Mol Ther *13*, 1050-1063.

Beer, N.R., Hindson, B.J., Wheeler, E.K., Hall, S.B., Rose, K.A., Kennedy, I.M., and Colston, B.W. (2007). On-chip, real-time, single-copy polymerase chain reaction in picoliter droplets. Analytical chemistry *79*, 8471-8475.

Berg, M., Undisz, K., Thiericke, R., Zimmermann, P., Moore, T., and Posten, C. (2001). Evaluation of liquid handling conditions in microplates. J Biomol Screen *6*, 47-56.

Berg, M., Undisz, D., Thiericke, R., Moore, T. (1999). Miniaturization of an Enzyme Assay (β-Galactosidase) in the 384- and 1536-Well Plate Format. Journal of the Association for Laboratory Automation *4*, 4.

Bergquist, J., Gilman, S.D., Ewing, A.G., and Ekman, R. (1994). Analysis of human cerebrospinal fluid by capillary electrophoresis with laser-induced fluorescence detection. Analytical chemistry *66*, 3512-3518.

Brewer, L.R., and Bianco, P.R. (2008). Laminar flow cells for single-molecule studies of DNA-protein interactions. Nature Methods *5*, 517-525.

Briscoe, B. (1999). Adv Colloid Interface Sci *81*, 17.

Brouzes, E., Medkova, M., Savenelli, N., Marran, D., Twardowski, M., Hutchison, J.B., Rothberg, J.M., Link, D.R., Perrimon, N., and Samuels, M.L. (2009). Droplet microfluidic technology for single-cell high-throughput screening. Proceedings of the National Academy of Sciences of the United States of America *106*, 14195-14200.

Brown, J.M., Hoffmann, W.D., Alvey, C.M., Wood, A.R., Verbeck, G.F., and Petros, R.A. One-bead, one-compound peptide library sequencing via high-pressure ammonia cleavage coupled to nanomanipulation/nanoelectrospray ionization mass spectrometry. Analytical biochemistry *398*, 7-14.

Burbaum, J. (1998). Miniaturization technologies in HTS: how fast, how small, how soon? . Drug discovery today *3*, 10.

Chabert, M., Dorfman, K.D., de Cremoux, P., Roeraade, J., and Viovy, J.L. (2006). Automated microdroplet platform for sample manipulation and polymerase chain reaction. Analytical chemistry *78*, 7722-7728.

Chen, D., Du, W., Liu, Y., Liu, W., Kuznetsov, A., Mendez, F.E., Philipson, L.H., and Ismagilov, R.F. (2008). The chemistrode: a droplet-based microfluidic device for stimulation and recording with high temporal, spatial, and chemical resolution. Proceedings of the National Academy of Sciences of the United States of America *105*, 16843-16848.

Chen, D.L., and Ismagilov, R.F. (2006). Microfluidic cartridges preloaded with nanoliter plugs of reagents: an alternative to 96-well plates for screening. Current opinion in chemical biology *10*, 226-231.

Chen, D.L., Li, L., Reyes, S., Adamson, D.N., and Ismagilov, R.F. (2007). Using three-phase flow of immiscible liquids to prevent coalescence of droplets in microfluidic channels: criteria to identify the third liquid and validation with protein crystallization. Langmuir *23*, 2255-2260.

Chen, D.S., and Davis, M.M. (2006). Molecular and functional analysis using live cell microarrays. Current opinion in chemical biology *10*, 28-34.

Clausell-Tormos, J., Lieber, D., Baret, J.C., El-Harrak, A., Miller, O.J., Frenz, L., Blouwolff, J., Humphry, K.J., Koster, S., Duan, H.*, et al.* (2008). Droplet-based microfluidic platforms for the encapsulation and screening of Mammalian cells and multicellular organisms. Chemistry & biology *15*, 427-437.

Cohen, H.M., Tawfik, D.S., and Griffiths, A.D. (2004). Altering the sequence specificity of HaeIII methyltransferase by directed evolution using in vitro compartmentalization. Protein Eng Des Sel *17*, 3-11.

Daelemans, D., Pannecouque, C., Pavlakis, G.N., Tabarrini, O., and De Clercq, E. (2005). A novel and efficient approach to discriminate between pre- and post-transcription HIV inhibitors. Mol Pharmacol *67*, 1574-1580.

Darst, S.A., and Edwards, A.M. (1995). Epitaxial growth of protein crystals from two-dimensional crystals on lipid layers. Current opinion in structural biology *5*, 640-644.

Dino Di Carlo, N.A., and Luke P. Lee (2006). Single-Cell Enzyme Concentrations, Kinetics, and Inhibition Analysis Using High-Density Hydrodynamic Cell Isolation Arrays. Analytical chemistry *78*, 5.

Dorner, A.J., and Coffin, J.M. (1986). Determinants for receptor interaction and cell killing on the avian retrovirus glycoprotein gp85. Cell *45*, 365-374.

Dove, A. (1999). Drug screening--beyond the bottleneck. Nat Biotechnol *17*, 859-863.

Ewing, A.G., Gavin, P.F., Hietpas, P.B., and Bullard, K.M. (1997). Continuous separations in microfabricated channels for monitoring ultrasmall biological environments. Nat Med *3*, 97-99.

Fan, F., and Wood, K.V. (2007). Bioluminescent assays for high-throughput screening. Assay and drug development technologies *5*, 127-136.

Fehse, B., Kustikova, O.S., Li, Z., Wahlers, A., Bohn, W., Beyer, W.R., Chalmers, D., Tiberghien, P., Kuhlcke, K., Zander, A.R.*, et al.* (2002). A novel 'sort-suicide' fusion gene vector for T cell manipulation. Gene therapy *9*, 1633-1638.

Frenz, L., El Harrak, A., Pauly, M., Begin-Colin, S., Griffiths, A.D., and Baret, J.C. (2008). Droplet-based microreactors for the synthesis of magnetic iron oxide nanoparticles. Angewandte Chemie (International ed *47*, 6817-6820.

Fu, A.Y., Chou, H.P., Spence, C., Arnold, F.H., and Quake, S.R. (2002). An integrated microfabricated cell sorter. Analytical chemistry *74*, 2451-2457.

Funfak, A., Brosing, A., Brand, M., and Kohler, J.M. (2007). Micro fluid segment technique for screening and development studies on Danio rerio embryos. Lab on a chip *7*, 1132-1138.

Gavrilescu, L.C., and Van Etten, R.A. (2007). Production of replication-defective retrovirus by transient transfection of 293T cells. J Vis Exp, 550.

Gonzalez, J.E., and Negulescu, P.A. (1998). Intracellular detection assays for high-throughput screening. Current opinion in biotechnology *9*, 624-631.

Graham, F.L., and van der Eb, A.J. (1973). Transformation of rat cells by DNA of human adenovirus 5. Virology *54*, 536-539.

Granieri, L., Miller, O.J., Griffiths, A.D., and Merten, C.A. (2009). A competition-based assay for the screening of species-specific antibiotics. The Journal of antimicrobial chemotherapy *64*, 62-68.

Griffin, W.C. (1949). Classification of surfac-active agents by 'HLB'. Journal of the Society of Cosmetic Chemist *1*.

Grodrian, A., Metze, J., Henkel, T., Martin, K., Roth, M., and Kohler, J.M. (2004). Segmented flow generation by chip reactors for highly parallelized cell cultivation. Biosens Bioelectron *19*, 1421-1428.

HA, S. (1994). Dynamics of drop deformation and break-up in viscous fluids. Ann Rev Fluid Mech *26*, 37.

Hann, M.M., and Oprea, T.I. (2004). Pursuing the leadlikeness concept in pharmaceutical research. Current opinion in chemical biology *8*, 255-263.

Hanson, K.L., and Cartwright, C.P. (2001). Evaluation of an automated liquid-handling system (Tecan Genesis RSP 100) in the Abbott LCx assay for Chlamydia trachomatis. Journal of clinical microbiology *39*, 1975-1977.

Hatakeyama, T., Chen, D.L., and Ismagilov, R.F. (2006). Microgram-scale testing of reaction conditions in solution using nanoliter plugs in microfluidics with detection by MALDI-MS. Journal of the American Chemical Society *128*, 2518-2519.

Hatziioannou, T., Valsesia-Wittmann, S., Russell, S.J., and Cosset, F.L. (1998). Incorporation of fowl plague virus hemagglutinin into murine leukemia virus particles and analysis of the infectivity of the pseudotyped retroviruses. Journal of virology *72*, 5313-5317.

He, M., Edgar, J.S., Jeffries, G.D., Lorenz, R.M., Shelby, J.P., and Chiu, D.T. (2005). Selective encapsulation of single cells and subcellular organelles into picoliter- and femtoliter-volume droplets. Analytical chemistry *77*, 1539-1544.

Hill, D.C. (1998). Trends in development of high-throughput screening technologies for rapid discovery of novel drugs. Curr Opin Drug Discov Devel *1*, 92-97.

Holm, K., Weclewicz, K., Hewson, R., and Suomalainen, M. (2003). Human immunodeficiency virus type 1 assembly and lipid rafts: Pr55(gag) associates with membrane domains that are largely resistant to Brij98 but sensitive to Triton X-100. Journal of virology *77*, 4805-4817.

Huang, Z.J. (1991). Kinetic fluorescence measurement of fluorescein di-beta-D-galactoside hydrolysis by beta-galactosidase: intermediate channeling in stepwise catalysis by a free single enzyme. Biochemistry *30*, 8535-8540.

Huebner, A., Srisa-Art, M., Holt, D., Abell, C., Hollfelder, F., deMello, A.J., and Edel, J.B. (2007). Quantitative detection of protein expression in single cells using droplet microfluidics. Chem Commun (Camb), 1218-1220.

Ito, M., Kawano, K., Miyagishi, M., and Taira, K. (2005). Genome-wide application of RNAi to the discovery of potential drug targets. FEBS letters *579*, 5988-5995.

Jambovane, S., Duin, E.C., Kim, S.K., and Hong, J.W. (2009). Determination of kinetic parameters, Km and kcat, with a single experiment on a chip. Analytical chemistry *81*, 3239-3245.

Johnston, K.P., Randolph, T., Bright, F., and Howdle, S. (1996). Toxicology of a PFPE Surfactant. Science (New York, NY *272*, 1726b.

Kline, E.R., Bassit, L., Hernandez-Santiago, B.I., Detorio, M.A., Liang, B., Kleinhenz, D.J., Walp, E.R., Dikalov, S., Jones, D.P., Schinazi, R.F.*, et al.* (2009). Long-term exposure to AZT, but not d4T, increases endothelial cell oxidative stress and mitochondrial dysfunction. Cardiovascular toxicology *9*, 1-12.

Kopp, M.U., Mello, A.J., and Manz, A. (1998). Chemical amplification: continuous-flow PCR on a chip. Science (New York, NY *280*, 1046-1048.

Korf, U., and Wiemann, S. (2005). Protein microarrays as a discovery tool for studying protein-protein interactions. Expert Rev Proteomics *2*, 13-26.

Koster, S., Angile, F.E., Duan, H., Agresti, J.J., Wintner, A., Schmitz, C., Rowat, A.C., Merten, C.A., Pisignano, D., Griffiths, A.D.*, et al.* (2008). Drop-based microfluidic devices for encapsulation of single cells. Lab on a chip *8*, 1110-1115.

Kreutz, J.E., Li, L., Roach, L.S., Hatakeyama, T., and Ismagilov, R.F. (2009). Laterally mobile, functionalized self-assembled monolayers at the fluorous-aqueous interface in a plug-based microfluidic system: characterization and testing with membrane protein crystallization. Journal of the American Chemical Society *131*, 6042-6043.

Kummrow, A., Theisen, J., Frankowski, M., Tuchscheerer, A., Yildirim, H., Brattke, K., Schmidt, M., and Neukammer, J. (2009). Microfluidic structures for flow cytometric analysis of hydrodynamically focussed blood cells fabricated by ultraprecision micromachining. Lab on a chip *9*, 972-981.

Li, L., Boedicker, J.Q., and Ismagilov, R.F. (2007). Using a multijunction microfluidic device to inject substrate into an array of preformed plugs without cross-contamination: comparing theory and experiments. Analytical chemistry *79*, 2756-2761.

Li, M.W., and Martin, R.S. (2008). Microchip-based integration of cell immobilization, electrophoresis, post-column derivatization, and fluorescence detection for monitoring the release of dopamine from PC 12 cells. Analyst *133*, 1358-1366.

Li, P.C., and Harrison, D.J. (1997). Transport, manipulation, and reaction of biological cells on-chip using electrokinetic effects. Analytical chemistry *69*, 1564-1568.

Linder, V., Sia, S.K., and Whitesides, G.M. (2005). Reagent-loaded cartridges for valveless and automated fluid delivery in microfluidic devices. Analytical chemistry *77*, 64-71.

Link, D.R., Anna, S.L., Weitz, D.A., and Stone, H.A. (2004). Geometrically mediated breakup of drops in microfluidic devices. Physical review letters *92*, 054503.

Link, D.R., Grasland-Mongrain, E., Duri, A., Sarrazin, F., Cheng, Z., Cristobal, G., Marquez, M., and Weitz, D.A. (2006). Electric control of droplets in microfluidic devices. Angewandte Chemie (International ed *45*, 2556-2560.

Liu, R., Marik, J., and Lam, K.S. (2002). A novel peptide-based encoding system for "one-bead one-compound" peptidomimetic and small molecule combinatorial libraries. Journal of the American Chemical Society *124*, 7678-7680.

Love, J.C., Estroff, L.A., Kriebel, J.K., Nuzzo, R.G., and Whitesides, G.M. (2005). Self-assembled monolayers of thiolates on metals as a form of nanotechnology. Chem Rev *105*, 1103-1169.

Lowe, K.C., Davey, M.R., and Power, J.B. (1998). Perfluorochemicals: their applications and benefits to cell culture. Trends Biotechnol *16*, 272-277.

Lucchetta, E.M., Lee, J.H., Fu, L.A., Patel, N.H., and Ismagilov, R.F. (2005). Dynamics of Drosophila embryonic patterning network perturbed in space and time using microfluidics. Nature *434*, 1134-1138.

Margulies, M., Egholm, M., Altman, W.E., Attiya, S., Bader, J.S., Bemben, L.A., Berka, J., Braverman, M.S., Chen, Y.J., Chen, Z.*, et al.* (2005). Genome sequencing in microfabricated high-density picolitre reactors. Nature *437*, 376-380.

Martin, K., Henkel, T., Baier, V., Grodrian, A., Schon, T., Roth, M., Michael Kohler, J., and Metze, J. (2003). Generation of larger numbers of separated microbial populations by cultivation in segmented-flow microdevices. Lab on a chip *3*, 202-207.

Mazutis, L., Araghi, A.F., Miller, O.J., Baret, J.C., Frenz, L., Janoshazi, A., Taly, V., Miller, B.J., Hutchison, J.B., Link, D.*, et al.* (2009a). Droplet-based microfluidic systems for high-throughput single DNA molecule isothermal amplification and analysis. Analytical chemistry *81*, 4813-4821.

Mazutis, L., Baret, J.C., and Griffiths, A.D. (2009b). A fast and efficient microfluidic system for highly selective one-to-one droplet fusion. Lab on a chip *9*, 2665-2672.

Meier, M., Kennedy-Darling, J., Choi, S.H., Norstrom, E.M., Sisodia, S.S., and Ismagilov, R.F. (2009). Plug-based microfluidics with defined surface chemistry to miniaturize and control aggregation of amyloidogenic peptides. Angewandte Chemie (International ed *48*, 1487-1489.

Meister, G., and Tuschl, T. (2004). Mechanisms of gene silencing by double-stranded RNA. Nature *431*, 343-349.

Merten, C.A., Stitz, J., Braun, G., Medvedovska, J., Cichutek, K., and Buchholz, C.J. (2006). Fusoselect: cell-cell fusion activity engineered by directed evolution of a retroviral glycoprotein. Nucleic acids research *34*, e41.

Niu, X., Gulati, S., Edel, J.B., and deMello, A.J. (2008). Pillar-induced droplet merging in microfluidic circuits. Lab on a chip *8*, 1837-1841.

Oldenburg, K. (1997). Microtechnologies and miniaturization: tools, techniques and novel applications for the pharmaceutical industry.

Ong, S.M., Zhang, C., Toh, Y.C., Kim, S.H., Foo, H.L., Tan, C.H., van Noort, D., Park, S., and Yu, H. (2008). A gel-free 3D microfluidic cell culture system. Biomaterials *29*, 3237-3244.

P. B. Umbanhowar, V.P., and D. A. Weitz (2000). Monodisperse Emulsion Generation via Drop Break Off in a Coflowing Stream. Langmuir *16* 4.

Paddison, P.J., Caudy, A.A., Bernstein, E., Hannon, G.J., and Conklin, D.S. (2002). Short hairpin RNAs (shRNAs) induce sequence-specific silencing in mammalian cells. Genes & development *16*, 948-958.

Pampaloni, F., Reynaud, E.G., and Stelzer, E.H. (2007). The third dimension bridges the gap between cell culture and live tissue. Nature reviews *8*, 839-845.

Peter Van Puyveldea, S.V., Paula Moldenaersc (2001). Rheology and morphology of compatibilized polymer blends. Current Opinion in Colloid & Interface Science *6*, 6.

Phizicky, E.M., and Fields, S. (1995). Protein-protein interactions: methods for detection and analysis. Microbiol Rev *59*, 94-123.

Piirma, I. (1992). Polymeric Surfactants. CRC Press.

Pregibon, D.C., Toner, M., and Doyle, P.S. (2007). Multifunctional encoded particles for high-throughput biomolecule analysis. Science (New York, NY *315*, 1393-1396.

Qu, B.Y., Wu, Z.Y., Fang, F., Bai, Z.M., Yang, D.Z., and Xu, S.K. (2008). A glass microfluidic chip for continuous blood cell sorting by a magnetic gradient without labeling. Analytical and bioanalytical chemistry *392*, 1317-1324.

Randow, F., and Sale, J.E. (2006). Retroviral transduction of DT40. Sub-cellular biochemistry *40*, 383-386.

Rosenblum, L.L., Patton, G., Grigg, A.R., Frater, A.J., Cain, D., Erlwein, O., Hill, C.L., Clarke, J.R., and McClure, M.O. (2001). Differential susceptibility of retroviruses to nucleoside analogues. Antiviral chemistry & chemotherapy *12*, 91-97.

S. Jambovane, E.C.D., S.-K. Kim, J. W. Hong (2009). Determination of kinetic parameters, Km and kcat, with a single experiment on a chip. Anal Chem *81*, 6.

Sagiv, J. (1980). Organized Monolayers by Adsorption .1. Formation and Structure of Oleophobic Mixed Monolayers on Solid-Surfaces. J Am Chem Soc *102*, 92-98.

Sakai, S., Kawabata, K., Ono, T., Ijima, H., and Kawakami, K. (2005). Higher viscous solution induces smaller droplets for cell-enclosing capsules in a co-flowing stream. Biotechnology progress *21*, 994-997.

Sanders, D.A. (2002). No false start for novel pseudotyped vectors. Curr Opin Biotechnol *13*, 437-442.

Sandy, P., Ventura, A., and Jacks, T. (2005). Mammalian RNAi: a practical guide. Biotechniques *39*, 215-224.

Schaerli, Y., Wootton, R.C., Robinson, T., Stein, V., Dunsby, C., Neil, M.A., French, P.M., Demello, A.J., Abell, C., and Hollfelder, F. (2009). Continuous-flow polymerase chain reaction of single-copy DNA in microfluidic microdroplets. Analytical chemistry *81*, 302-306.

Schmitz, C.H., Rowat, A.C., Koster, S., and Weitz, D.A. (2009). Dropspots: a picoliter array in a microfluidic device. Lab on a chip *9*, 44-49.

Scott, R.L. (1948). The solubility of fluorocarbons. Journal of the American Chemical Society *70*, 4090-4093.

Sidwell, R.W., and Huffman, J.H. (1971). Use of disposable micro tissue culture plates for antiviral and interferon induction studies. Appl Microbiol *22*, 797-801.

Sidwell, R.W., and Smee, D.F. (2000). In vitro and in vivo assay systems for study of influenza virus inhibitors. Antiviral Res *48*, 1-16.

Siegert, S., Thaler, S., Wagner, R., and Schnierle, B.S. (2005). Assessment of HIV-1 entry inhibitors by MLV/HIV-1 pseudotyped vectors. AIDS research and therapy *2*, 7.

Song, H., Bringer, M.R., Tice, J.D., Gerdts, C.J., and Ismagilov, R.F. (2003a). Experimental test of scaling of mixing by chaotic advection in droplets moving through microfluidic channels. Applied physics letters *83*, 4664-4666.

Song, H., and Ismagilov, R.F. (2003). Millisecond kinetics on a microfluidic chip using nanoliters of reagents. J Am Chem Soc *125*, 14613-14619.

Song, H., Li, H.W., Munson, M.S., Van Ha, T.G., and Ismagilov, R.F. (2006). On-chip titration of an anticoagulant argatroban and determination of the clotting time within whole blood or plasma using a plug-based microfluidic system. Analytical chemistry *78*, 4839-4849.

Song, H., Tice, J.D., and Ismagilov, R.F. (2003b). A microfluidic system for controlling reaction networks in time. Angewandte Chemie (International ed *42*, 768-772.

Squires, T.a.Q., SR (2005). microfluidics: fluid physics at the nanoliter scale. REVIEWS OF MODERN PHYSICS *77*.

Srinivasan, V., Pamula, V.K., and Fair, R.B. (2004). An integrated digital microfluidic lab-on-a-chip for clinical diagnostics on human physiological fluids. Lab on a chip *4*, 310-315.

Stitz, J., Muhlebach, M.D., Blomer, U., Scherr, M., Selbert, M., Wehner, P., Steidl, S., Schmitt, I., Konig, R., Schweizer, M.*, et al.* (2001). A novel lentivirus vector derived from apathogenic simian immunodeficiency virus. Virology *291*, 191-197.

Stone HA, L.L. (1990). The effects of surfactants on drop
deformation and breakup. J Fluid Mech *220*, 25.

Studer, A., Hadida, S., Ferritto, R., Kim, S.Y., Jeger, P., Wipf, P., and Curran, D.P. (1997). Fluorous synthesis: a fluorous-phase strategy for improving separation efficiency in organic synthesis. Science (New York, NY *275*, 823-826.

Stylli, H. (1997). Emerging technologies for drug discovery: developing and positioning multidisciplinary approaches to optimize drug discovery.

Sundberg, S.A. (2000). High-throughput and ultra-high-throughput screening: solution- and cell-based approaches. Current opinion in biotechnology *11*, 47-53.

Sung, V.M., and Lai, M.M. (2002). Murine retroviral pseudotype virus containing hepatitis B virus large and small surface antigens confers specific tropism for primary human hepatocytes: a potential liver-specific targeting system. Journal of virology *76*, 912-917.

Tadros, T. (2005). Applied Surfactants-Principles and Applications. Wiley-VCH Verlag CMBH & Co.

Takayama, S., Ostuni, E., LeDuc, P., Naruse, K., Ingber, D.E., and Whitesides, G.M. (2001). Subcellular positioning of small molecules. Nature *411*, 1016.

Tawfik, D.S., and Griffiths, A.D. (1998). Man-made cell-like compartments for molecular evolution. Nat Biotechnol *16*, 652-656.

Taylor, G. (1953). Dispersion of Soluble Matter in Solvent Flowing Slowly through a Tube. Proceedings of the Royal Society of London Series A Mathematical and Physical Sciences *219*, 186-203.

Teh, S.Y., Lin, R., Hung, L.H., and Lee, A.P. (2008). Droplet microfluidics. Lab on a chip *8*, 198-220.

Thompson, D.M., King, K.R., Wieder, K.J., Toner, M., Yarmush, M.L., and Jayaraman, A. (2004). Dynamic gene expression profiling using a microfabricated living cell array. Analytical chemistry *76*, 4098-4103.

Thorsen, T., Roberts, R.W., Arnold, F.H., and Quake, S.R. (2001). Dynamic pattern formation in a vesicle-generating microfluidic device. Physical review letters *86*, 4163-4166.

Trajcevski, S., Solly, S.K., Frisen, C., Trenado, A., Cosset, F.L., and Klatzmann, D. (2005). Characterization of a semi-replicative gene delivery system allowing propagation of complementary defective retroviral vectors. J Gene Med *7*, 276-287.

Villarino, A., Bouvet, O.M., Regnault, B., Martin-Delautre, S., and Grimont, P.A.D. (2000). Exploring the frontier between life and death in Escherichia coli: evaluation of different viability markers in live and heat- or UV-killed cells. Research in microbiology *151*, 755-768.

von Kalle, C., Kiem, H.P., Goehle, S., Darovsky, B., Heimfeld, S., Torok-Storb, B., Storb, R., and Schuening, F.G. (1994). Increased gene transfer into human hematopoietic progenitor cells by extended in vitro exposure to a pseudotyped retroviral vector. Blood *84*, 2890-2897.

Weber, M., Muthusubramaniam, L., Murray, J., Hudak, E., Kornienko, O., Johnson, E.N., Strulovici, B., and Kunapuli, P. (2007). Ultra-high-throughput screening for antagonists of a Gi-coupled receptor in a 2.2-microl 3,456-well plate format cyclicAMP assay. Assay Drug Dev Technol *5*, 117-125.

Westby, M., Nakayama, G.R., Butler, S.L., and Blair, W.S. (2005). Cell-based and biochemical screening approaches for the discovery of novel HIV-1 inhibitors. Antiviral Res *67*, 121-140.

Wheeler, A.R., Moon, H., Bird, C.A., Loo, R.R., Kim, C.J., Loo, J.A., and Garrell, R.L. (2005). Digital microfluidics with in-line sample purification for proteomics analyses with MALDI-MS. Analytical chemistry *77*, 534-540.

Whitesides, G.M., Ostuni, E., Takayama, S., Jiang, X., and Ingber, D.E. (2001). Soft lithography in biology and biochemistry. Annu Rev Biomed Eng *3*, 335-373.

Ye, N., Qin, J., Shi, W., Liu, X., and Lin, B. (2007). Cell-based high content screening using an integrated microfluidic device. Lab on a chip *7*, 1696-1704.

Zhang, J., Balestrieri, E., Grelli, S., Matteucci, C., Pagnini, V., D'Agostini, C., Mastino, A., and Macchi, B. (2001). Efficacy of 3'-azido 3'deoxythymidine (AZT) in preventing HTLV-1 transmission to human cord blood mononuclear cells. Virus research *78*, 67-78.

Zhang, J.H., Chung, T.D., and Oldenburg, K.R. (1999). A Simple Statistical Parameter for Use in Evaluation and Validation of High Throughput Screening Assays. J Biomol Screen *4*, 67-73.

Zheng, B., Tice, J.D., and Ismagilov, R.F. (2004). Formation of droplets of alternating composition in microfluidic channels and applications to indexing of concentrations in droplet-based assays. Analytical chemistry *76*, 4977-4982.